DEPARTMENT OF PHYSICS

RESEARCH REPORT NUMBER 68-1

BASIC RESEARCH IN SEMICONDUCTOR DETECTOR-DOSIMETER CHARACTERISTICS

Edited
by

GEORGE W. CRAWFORD

Sponsored by

National Aeronautics and Space Administration
Research Grant NsG 708 / NAR-44-007-007

Principal Investigator: George W. Crawford
Report Period: June 1, 1964 through August 31, 1968

August, 1968

SOUTHERN METHODIST UNIVERSITY
DALLAS, TEXAS 75222

SOUTHERN METHODIST UNIVERSITY

DEPARTMENT OF PHYSICS

RESEARCH REPORT NUMBER 68-1

BASIC RESEARCH IN SEMICONDUCTOR DETECTOR-DOSIMETER CHARACTERISTICS

CONTENTS

CHAPTER 1
INTRODUCTION
by George W. Crawford

The research reported here is a study of the basic characteristics of semiconductor detectors. In Chapter 2 is given a detailed account of the theory of the silicon lithium-drifted detector. The basic theory is extended to apply to very large volume detectors in Chapter 3.

Complete instructions for the fabrication of lithium-drifted silicon detectors is given in Chapter 2 with further instructions for large detector fabrication given in Chapter 3. Some 70 different detectors have been incorporated into this study. They represent a family of various sized devices ranging in size from 1 x 1 x 1 mm to 7 x 7 x 150 mm. Long detectors, i.e., having proton path lengths in silicon of 10, 20, 30, 50, 70, 100, 120, 130 and 150mm, were used to totally absorb high energy protons. These studies are reported in Chapter 6. New techniques of fabrication, mounting and encapsulation were developed to obtain specific configurations. Combinations of detectors were developed to permit simultaneous measurements of dE/dx and E with identification of both mass and energy of the incident particle. A separate study (not supported by NASA) was made to determine the charge collection characteristics of the detectors in a magnetic field. The basic research has been accomplished to permit fabrication of configurations of detectors operating within a magnetic field which will produce the data required in the PROPER 3 B Monte Carlo Transport Program (see volume 2 of this report) to identify charge, mass and energy of an unknown ionizing radiation of the meson, baryon or heavier class.

The charge response of many detectors have been measured as a function of the incident energy of the proton over the energy range from 8 to 186.6 MeV. The results for the studies where the length of the detector path was short as compared to the range of the incident proton in silicon are given in Chapter 5. The studies which involved total absorption of the proton in the intrinsic region of the detector are reported in Chapter 6. The average energy required to produce an electron-hole pair in silicon has been measured for each case. These data are required to translate the charge (current) from each detector produced by a known radiation flux and stored in a calibrated condenser into dose, i.e., the total energy absorbed per unit mass of silicon.

The detector life-time behavior studies are reported in Chapter 7. In addition to the normal usuage study, a study was also made of the detectors under high degree of stress. The stress factors included temperature, high magnetic fields, high radiation flux and time.

In order to obtain data covering the range of proton energies from 8 through 187 MeV, it was necessary to make field trips to six different laboratories. We wish to express our deep appreciation to each of the following for their support of this research and for their invaluable assistance.

Gustaf Werner Institute, The University of Uppsala, Uppsala, Sweden. (187 MeV).

Professor The Svedberg
Dr. Borje Larsson
Dr. Bo Jung

Cyclotron Laboratory, Harvard University, Cambridge, Massachusetts. (160 MeV).

Dr. A. M. Koehler

Foster Radiation Laboratory, McGill University, Montreal, Canada. (100 MeV).

Dr. R. E. Bell
Dr. R. B. Moore
Dr. P. M. Portner

Oak Ridge National Laboratories, Oak Ridge, Tennessee. (36 MeV).

Dr. Alexander Zucker, Electronuclear Division
Dr. J. A. Auxier, Health Physics Division

Linear Accelerator Group, University of Southern California, Los Angeles, California. (18 - 24 MeV).

Dr. Hans Bichsel

Accelerator Laboratory, The University of Texas, Austin, Texas. (8 - 14 MeV).

Dr. B. B. Kinsey
Dr. R. N. Little
Mr. J. W. Jagger

This work was supported by grants of accelerator time at each laboratory. It is with pleasure that we express our thanks for these grants.

The team working at Uppsala was made up of: G. W. Crawford, Bo Jung, S. M. Curry, D. R. Dixon, B. D. Snow and C. Warren (of NASA). The research was carried out at Harvard by the team of G. W. Crawford, D. R. Dixon and P. H. Hunt. At McGill University, the experimental work was carried out by G. W. Crawford, P. H. Hunt, P. N. Kehler, D. R. Dixon, and S. M. Curry with support from Bob Richmond (of NASA). Data was taken at ORNL by G. W. Crawford and D. C. Nipper. At the University of Southern California, G. W. Crawford, with the collaboration of Hans Bichsel, made the measurements. The data was taken at the University of Texas by the team of G. W. Crawford, D. C. Nipper, F. E. Corlett and J. Cummins. Mr. E. K. Helwig and Miss. C. A. Wheeler assisted members of the team in analyzing the data, using the computor programs described in the second and third volumes of this report. R. J. Holt and D. R. Dixon participated in the life-time behavior studies of the detectors.

CHAPTER 2

PREPARATION OF LITHIUM-DRIFTED SEMICONDUCTOR NUCLEAR PARTICLE DETECTORS

By Bobby Darrell Snow

The process for preparing lithium drifted "p-i-n" detectors was conceived and developed by E. M. Pell[1] of General Electric Research Laboratory in 1959. Lithium was diffused into "p" type silicon to form an "n-p" junction diode. A reverse bias was applied to this diode which was held at a sufficiently elevated temperature to give the lithium donor ions appreciable mobility but low enough to prevent flooding.[2,3] While in this condition the lithium ions drifted under the influence of the electric field and diffusion current to compensate the boron ions in the "p" region.[4] Thus, this region became depleted of free carriers and the depletion continued to spread as long as the temperature and biasing voltage were maintained.[5] Depletion widths as wide as 5 mm were formed. This compensated region was intrinsic in the sense that the electron and hole concentration were equal. Consequently, an "n-i-p" formation was accomplished with the width of the intrinsic region depending upon the drift parameters.[6]

During detector operation a bias, positive from "n" to

"p," depleted the free carriers from the compensated region. The resulting intrinsic region became the sensitive region for particle detection. This depleted layer was, in effect, a layer of extremely high resistance material separating opposite electric charges. An appreciable capacitance resulted which varied with depletion width and, consequently, voltage.[7]

A particle incident on the sensitive region of the biased detector transferred its energy to the silicon by forming electron-hole pairs. These carriers were swept out of the intrinsic layer by the strong electric field and collected by the "plates" of the diode capacitor. The flow of electrons and holes were additive to constitute an electric current. A voltage pulse was produced when this current passed through a load resistor in the applicable circuitry. Each pulse was stored in electronic equipment to give a measure of the energy lost by the incident particle.[8]

For meaningful resolution of data similar to these above, a low noise to signal (pulse) ratio must be maintained. A detector capable of completely absorbing 200 Mev protons with a very low noise to signal ratio and good charge collection properties was required for the research project of which the work reported here was a part.

THEORY

The theory associated with the preparation of lithium drifted silicon detectors may be divided into five parts: (1) Theory of basic material; (2) Theory of diffusions; (3) Theory of "p-n" junctions; (4) Theory of drift; and (5) Theory of operation.

Theory of Basic Material

A semiconductor is defined by an electrical conductivity that is intermediate between that of an insulator and that of a metal. The classification is as follows:

Insulators: 10^{-22} to 10^{-14} mho-cm^{-1}

Semiconductors: 10^{-9} to 10^{2} mho-cm^{-1}

Conductors: 10^{5} mho-cm^{-1} and greater

When free electrons are perturbed by a periodic potential arising from the periodic crystal lattice, it is shown by second order degenerate perturbation theory that there is a "gap" between adjacent energy levels.[9,10] There can exist N energy levels, where N is the number of unit cells in a crystal, in each energy band. But two electrons can occupy each level if their spins are anti-parallel. Thus, each energy band can hold 2 N electrons.[10]

In general elements with an even number of electrons/unit cell will not be conductors since the energy bands would be full and additional energy would be required to excite them into the next available energy band. Similarly, elements with an odd number of electrons/unit cell would be conductors. However, not all elements with an even number of electrons/unit cell are poor conductors because of band overlap.

Silicon has four conduction electrons and the energy gap, E_G, is intermediate between conductors and insulators classifying it as a semiconductor. The energy level diagram for silicon is shown in Figure 1 with E_G = 1.21 ev at 0°K and conductivity σ = 3.3 x 10^{-6} mho cm^{-1}. [11]

The Fermi-Dirac distribution function, f(E), which gives the probability that a quantum state with energy E is occupied by an electron, is given by the formula [10]

$$f(E) = \frac{1}{1 + e^{(E - E_F)/kT}} \qquad (1)$$

where E_F is the Fermi energy or band and is the energy at which the probability of a state being filled is one-half, [11] k is Boltzmann's constant and T is the absolute temperature. Using free electron theory the temperature dependency of E_F is given approximately by [10]

$$E_F \approx E_F(0)\left[1 - \frac{\pi^2}{12}\left(\frac{kT}{E_F(0)}\right)^2\right] \qquad (2)$$

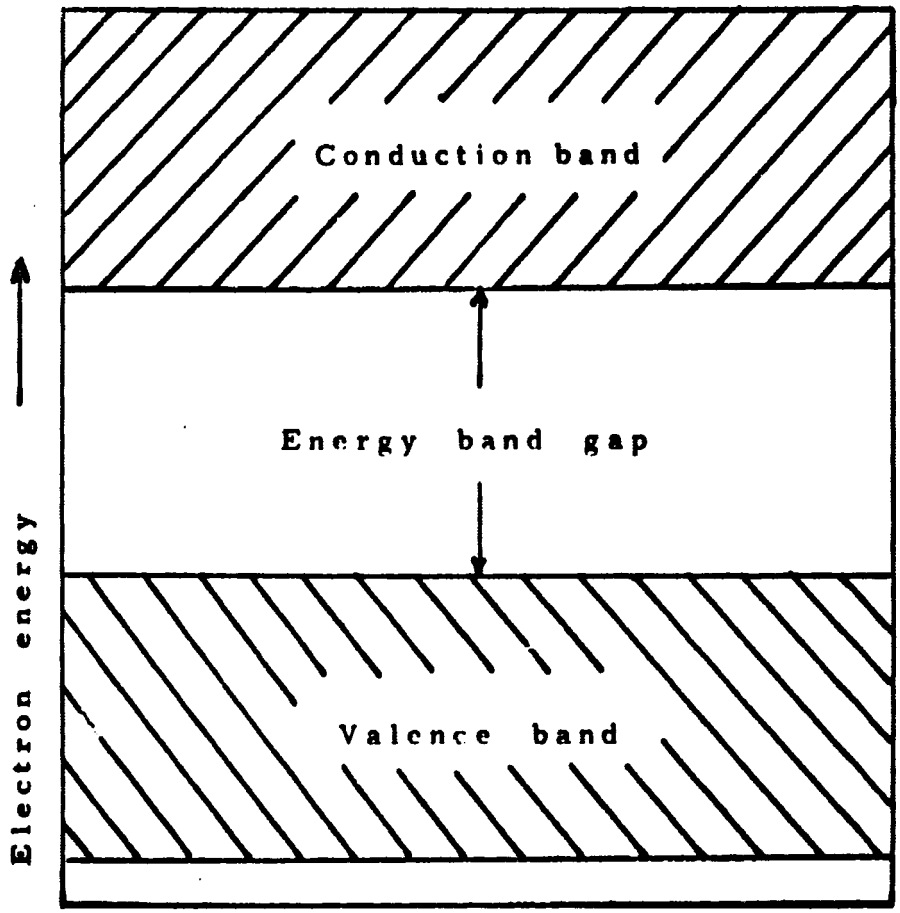

Fig. 1. Energy-level diagram for Silicon

where $E_F^{(0)}$, the Fermi energy at $0^\circ K$, is

$$E_F^{(0)} = \frac{\pi^2}{2m}(3\pi^2 n^{(0)})^{2/3}. \qquad (3)$$

$n^{(0)}$ is the charge carrier concentration at $0^\circ K$. Diagrams of the Fermi-Dirac distribution functions superimposed on energy-band diagrams are shown in Figure II.[11]

The value of kT at $T = 300^\circ K$ is 0.026 ev and the value of E_G at $300^\circ K$ is 1.1 ev.[11] The energy difference between the conduction band and the Fermi level $(E_C - E_F)$ is 0.55 ev. For this situation, where $E - E_F \gg kT$, $f(E)$ may be expressed as

$$f(E) \approx e^{-(E-E_F)/kT}. \qquad (4)$$

Equation (4) gives the value of that fraction of the quantum states at energies E occupied by an electron. Hence, $1 - f(E)$ corresponds to the fraction of states left vacant when the electron enters the conduction band that leaves behind a hole. From Equation (1)

$$1 - f(E) = 1 - \frac{1}{1 + e^{(E-E_F)/kT}} \qquad (5)$$

$$1 - f(E) = \frac{1 + e^{(E-E_F)/kT} - 1}{1 + e^{(E-E_F)/kT}} \qquad (6)$$

$$1 - f(E) = \frac{e^{(E-E_F)/kT}}{1 + e^{(E-E_F)/kT}} \qquad (7)$$

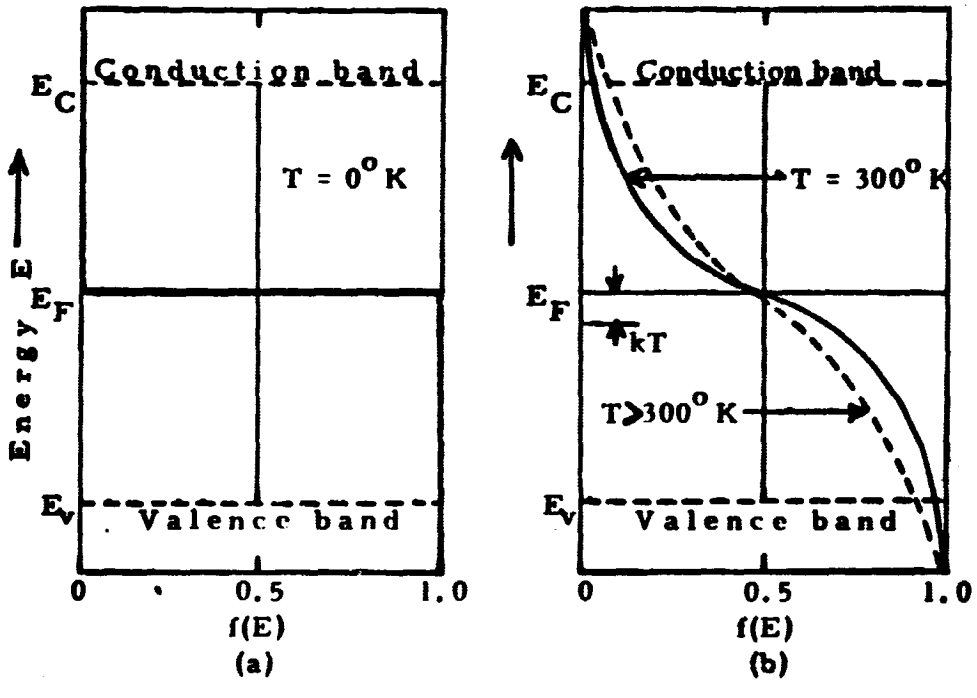

Fig. II. Fermi-Dirac distribution functions superimposed on energy-band diagrams.

$$1 - f(E) = \frac{1}{\frac{1}{e^{(E-E_F)/kT}} + 1} \tag{8}$$

$$1 - f(E) = \frac{1}{1 + e^{(E - E_F)/kT}} \tag{9}$$

making the same approximation as in Equation (4); i.e., $E_F - E_V \gg kT$ yields

$$1 - f(E) \approx e^{-(E_F - E)/kT}. \tag{10}$$

Defining $g(E)$ as the number of quantum states per unit energy per unit volume of the crystal, the density of states N in a particular energy range $E + dE$ would be

$$N = g(E)\, dE. \tag{11}$$

Therefore, the density of free carriers would be given by

$$n = \int_{E_1}^{E_2} f(E)\, g(E)\, dE. \tag{12}$$

By Brillouin-Zone analysis, the derived expression for $g(E)$ is[9]

$$g(E) = \frac{1}{2\pi^2}\left(\frac{2m_e}{\hbar^2}\right)^{3/2} (E - E_1)^{1/2} \tag{13}$$

The density of electrons in the conduction band is then

$$n = \int_{E_C}^{\infty} e^{-(E - E_F)/kT} \frac{1}{2\pi^2}\left(\frac{2m_e}{\hbar^2}\right)^{3/2} (E - E_C)^{1/2} dE. \tag{14}$$

Integrating beyond the top of the conduction band causes very little error.

Letting $E_1 = E - E_C$,

$$n = e^{-(E_C - E_F)/kT} \frac{1}{2\pi^2}\left(\frac{2m_e}{\hbar^2}\right)^{3/2} \int_o^\infty E_1^{1/2} e^{-\frac{E_1}{kT}} dE_1, \quad (15)$$

which yields

$$n = 2\left(\frac{2\pi m_e kT}{h^2}\right)^{3/2} e^{-(E_C - E_F)/kT}. \quad (16)$$

Defining

$$N_C = 2\left(\frac{2\pi m_e kT}{h^2}\right)^{3/2}, \quad (17)$$

$$n = N_C e^{-(E_C - E_F)/kT}. \quad (18)$$

Similarly

$$p = 2\left(\frac{2\pi m_h kT}{h^2}\right)^{3/2} e^{-(E_F - E_V)/kT}. \quad (19)$$

Defining

$$N_V = 2\left(\frac{2\pi m_h kT}{h^2}\right)^{3/2}, \quad (20)$$

$$p = N_V e^{-(E_F - E_V)/kT}. \quad (21)$$

Multiplying (18) by (21) yields

$$np = 4\left(\frac{2\pi kT}{h^2}\right)^3 (m_e m_h)^{3/2} e^{-\frac{E_g}{kT}}, \qquad (22)$$

where

$$E_g = E_C - E_V. \qquad (23)$$

It is therefore evident that the product, np, is independent of the Fermi level, E_F. Furthermore, it is dependent only on temperature and is a constant for any given temperature. Experimental measurements of high-quality silicon crystals have yielded the following empirical expression.[12, 13]

$$np = 15 \times 10^{32} T^3 e^{-1.21/kT} \qquad (24)$$

In intrinsic silicon carriers are due to thermal excitation and n = p. Therefore,

$$n_i^2 = p_i^2 = np \qquad (25)$$

When electrons became thermally excited and enter the conduction band, an equal number of holes are left in the valence band for conduction. Hence, conductivity increases until the carrier population is great enough for lattice vibrations to impede movement of the carriers. The conductivity due to thermally generated holes and electrons in intrinsic silicon is termed intrinsic conduction.

A two dimensional picture of a silicon crystal showing only

the valence covalent bonding electrons is shown in Figure III. The Fermi-Dirac distribution function superimposed on the energy-band diagrams for this crystal is given in Fig. II.

Suppose now a group III impurity is introduced and displaces one of the silicon atoms. There will be an electron deficiency or a "hole" which acts like a positive charge to readily accept a free electron from the crystal. Consequently, group III impurities are called acceptor impurities.

If a silicon atom is displaced by a group V atom four of the five valence electrons will satisfy the covalent bonding structure. However, the fifth electron is relatively free to migrate through the crystal. For this reason group V atoms are termed donor impurities.

Each of the above "doping" atoms, as they are called, are defined as displacement atoms. An atom may be positioned interstitually, that is, in the space between lattice atoms. They are, therefore, called interstitial atoms. Lithium is such an atom [4, 14] and "gives up" an electron to the silicon crystal to act as a donor impurity.

The presence of impurities will modify slightly the distribution of quantum states within the crystal. At very low temperatures, where the excess electrons are bound to the donor atoms, each donor atom will remove a state from the conduction band and

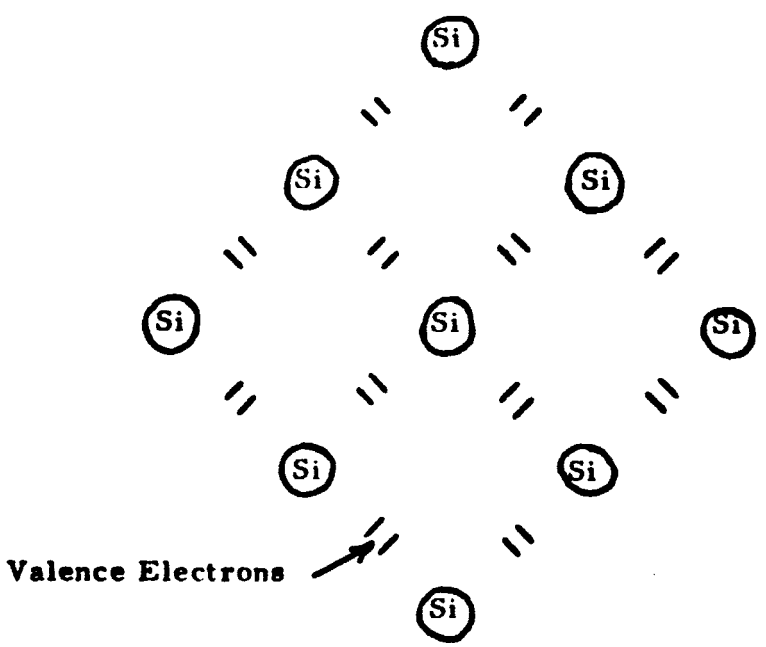

Fig. III. Two dimensional covalent bonding picture of a Silicon crystal.

establish it as an allowed state of lower energy. This lower energy level is referred to as the donor impurity energy level, E_D, and is below the bottom of the conduction band by an amount equal to the donor ionization energy. Similarly, for an acceptor impurity, each atom elevates a state from the valence band to an acceptor impurity energy level, E_A, just equal to the acceptor ionization energy.[9] These energy levels are illustrated in Fig. IV.

Material with an excess of donor impurities ($N_D > N_A$) is called "n" type because conduction is due to negative charge carriers or electrons in the conduction band. Similarly, material with an excess of acceptor impurities ($N_A > N_D$) is called "p" type because conduction is due to an excess of hole carriers in the valence band acting like positive charges. If $N_D = N_A$, the conduction is intrinsic, and the crystal is said to be compensated. In an "n" type semiconductor, the electrons are called majority carriers and holes minority carriers. Likewise, in "p" type material, the holes are the majority carriers and electrons minority carriers. Conduction due to added impurities is termed extrinsic conduction.

When $N_D > N_A$ at room temperature there is a high occupancy of the allowed states in the conduction band and a low occupancy of holes in the valence band. The conduction where $N_A > N_D$ has opposite effects. It is clear that the Fermi level, which is a

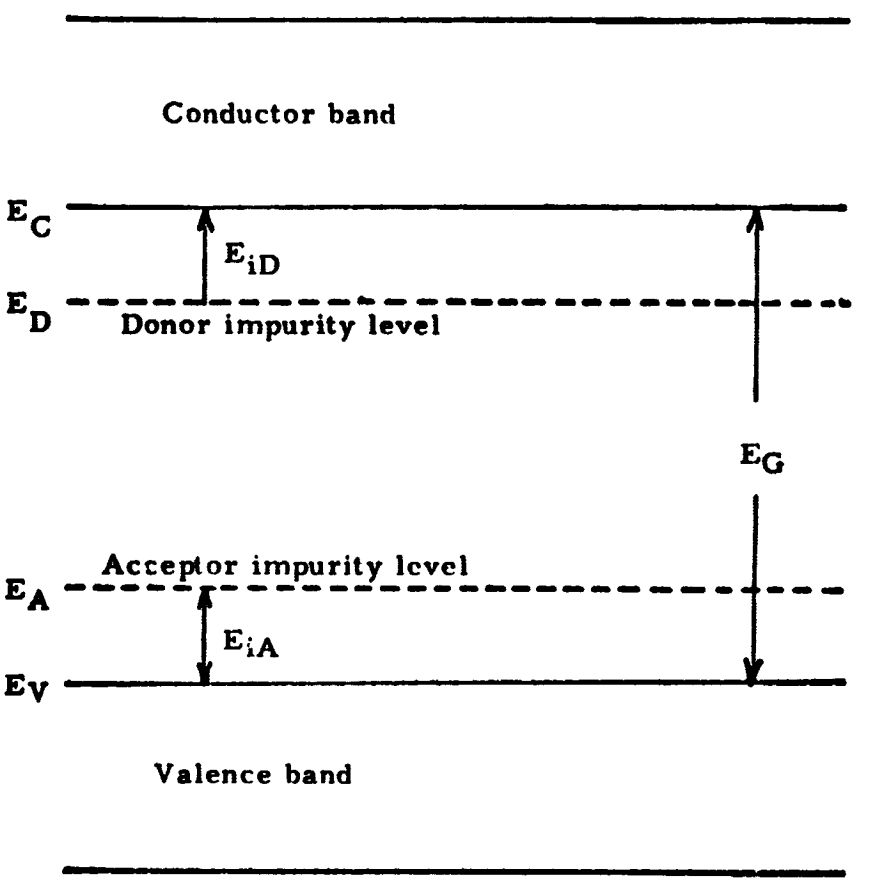

Fig. IV. Energy-level diagram for impurity semiconductor.

measure of the probability of occupancy of the allowed states, [9] will be affected. The positions of the Fermi level for impurity semiconductors are shown in Fig. V.

It has been theorized, and demonstrated by experiment, that certain allowed energy states can and do exist in the region of the forbidden-energy band. These states are called recombination centers and are attributed to foreign impurities or perhaps structural defects in the crystal. A state of this nature may exist anywhere in the forbidden region dependent on the impurity. The action of the center is to capture either a free electron from the conduction band or an electron from the valence band, leaving a hole behind. Likewise, the filled center may be emptied by capturing a hole or releasing its electron back to the conduction band. Recombination occurs when the center captures a free electron and holds it until emptied by capturing a hole. Thus, the recombination center may be considered a "stepping stone" in the gap between the bands. If the imperfection that creates the centers happens to be a foreign metal such as nickel or copper, the position of the center in the band gap would depend on the allowed energy level for the impurity in question. This is similar to the situation of the donor and acceptor impurities, except that the energy states for most metals are deeper in the band gap. The energy levels for some of the common metals of interest in silicon are given in

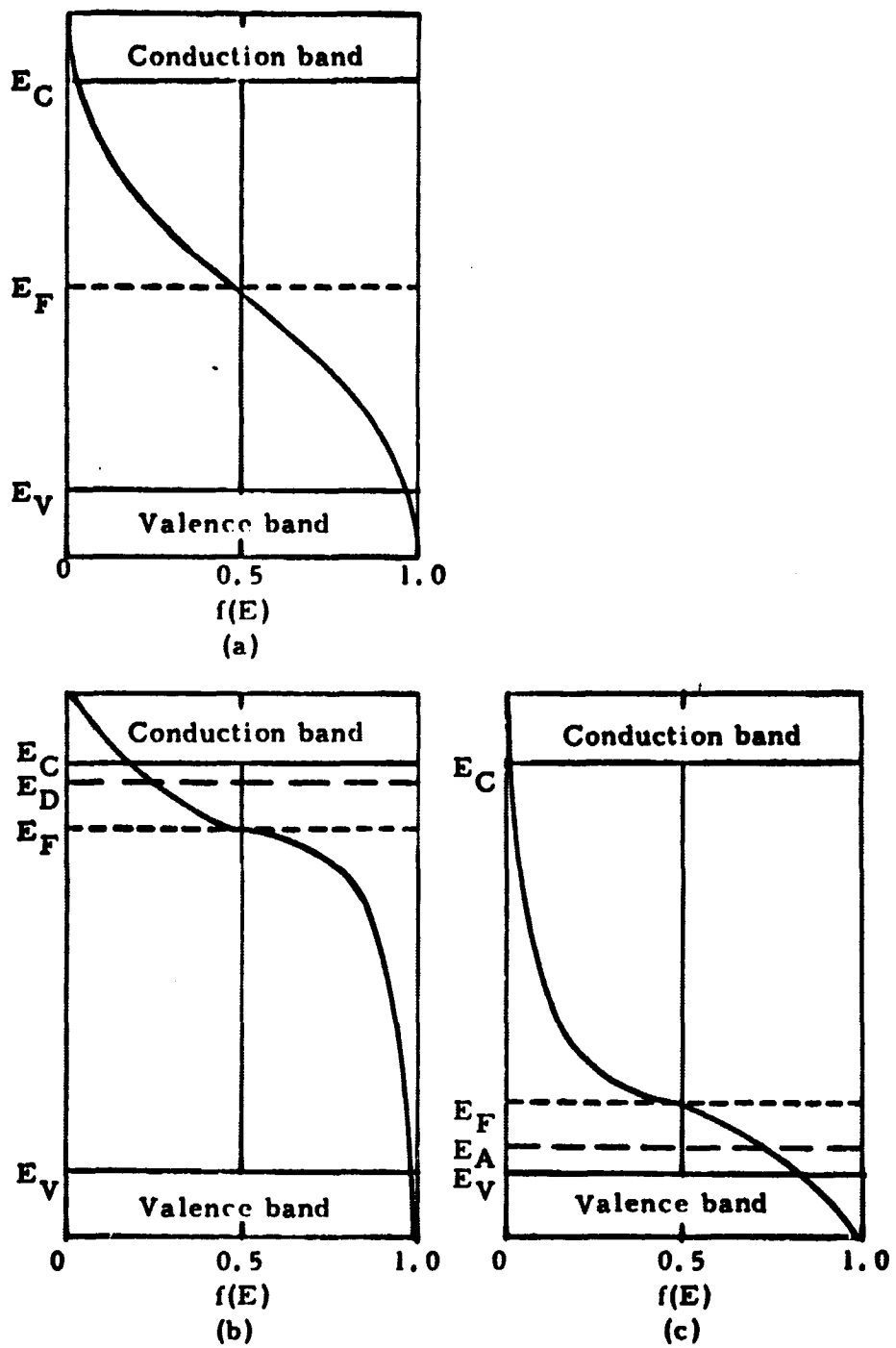

Fig. V. Positions of Fermi level for impurity semiconductors. (a) Intrinsic; (b) n type; (c) p type.

Fig. VI.[15]

It is apparent that several factors determine the probability of carrier recombination at a recombination center. They are[11] (1) the concentration of recombination centers in the crystal, (2) the concentration of the free carrier in question, which is related to resistivity, (3) the capture probability of the centers, and (4) the concentration of centers that are normally filled under equilibrium conditions. The last factor is dependent on the position of the centers in the band gap with respect to the Fermi level, since this would determine the degree of occupancy of the centers.

The beginning material for solid state radiation detectors is "p" type with boron as the acceptor impurity. Fig. V (c) corresponds qualitatively to the Fermi level for this crystal. It is obvious that the actual position of the Fermi level is dependent on the boron concentration. The activation energy of boron is 4.5×10^{-2} ev[16] establishing the acceptor energy level just above the valence band.

It has been established above that extrinsic conduction is the result of added impurities to an intrinsic silicon crystal. A larger concentration of an impurity causes more conduction states to be filled and enhances the conduction of the crystal. A graph showing resistivity as a function of acceptor and donor impurity concentration is shown in Figure VII.

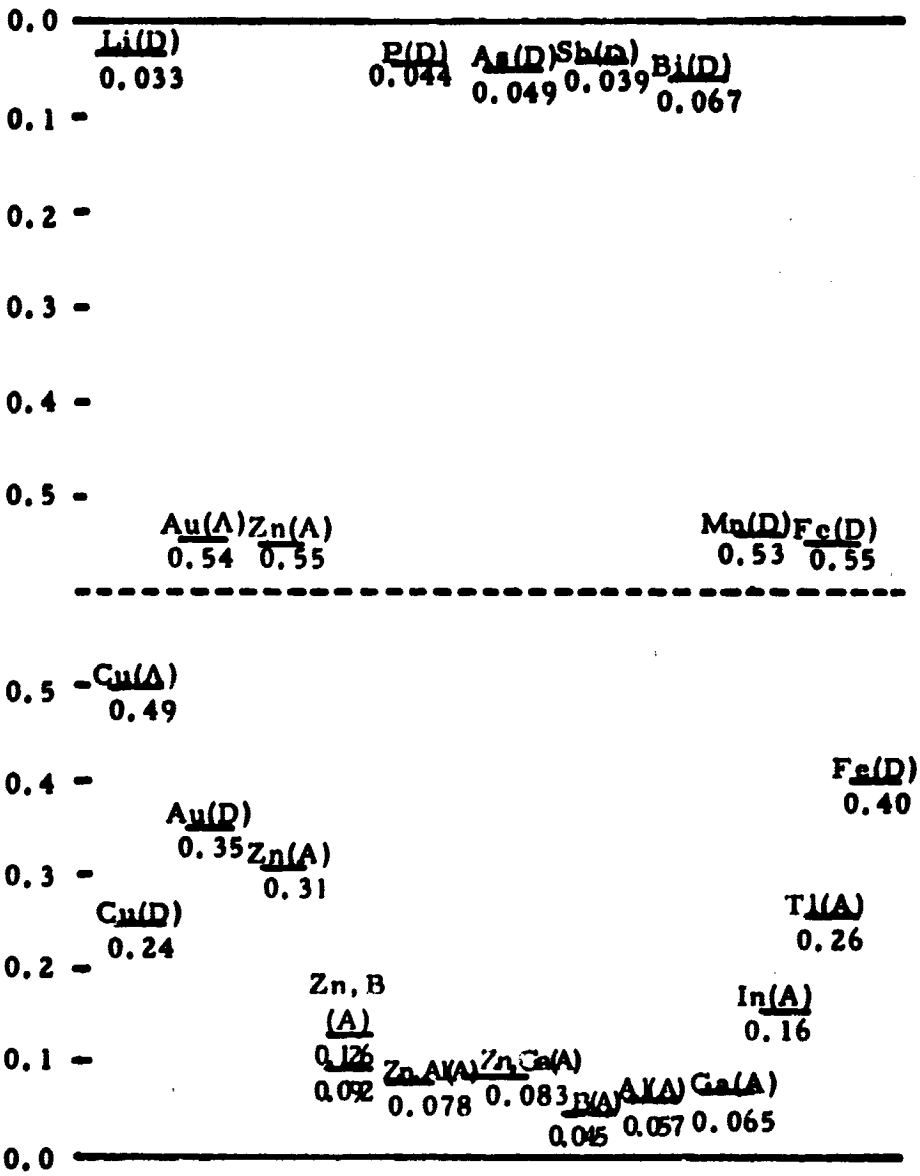

Fig. VI. Energy levels of impurities in silicon.

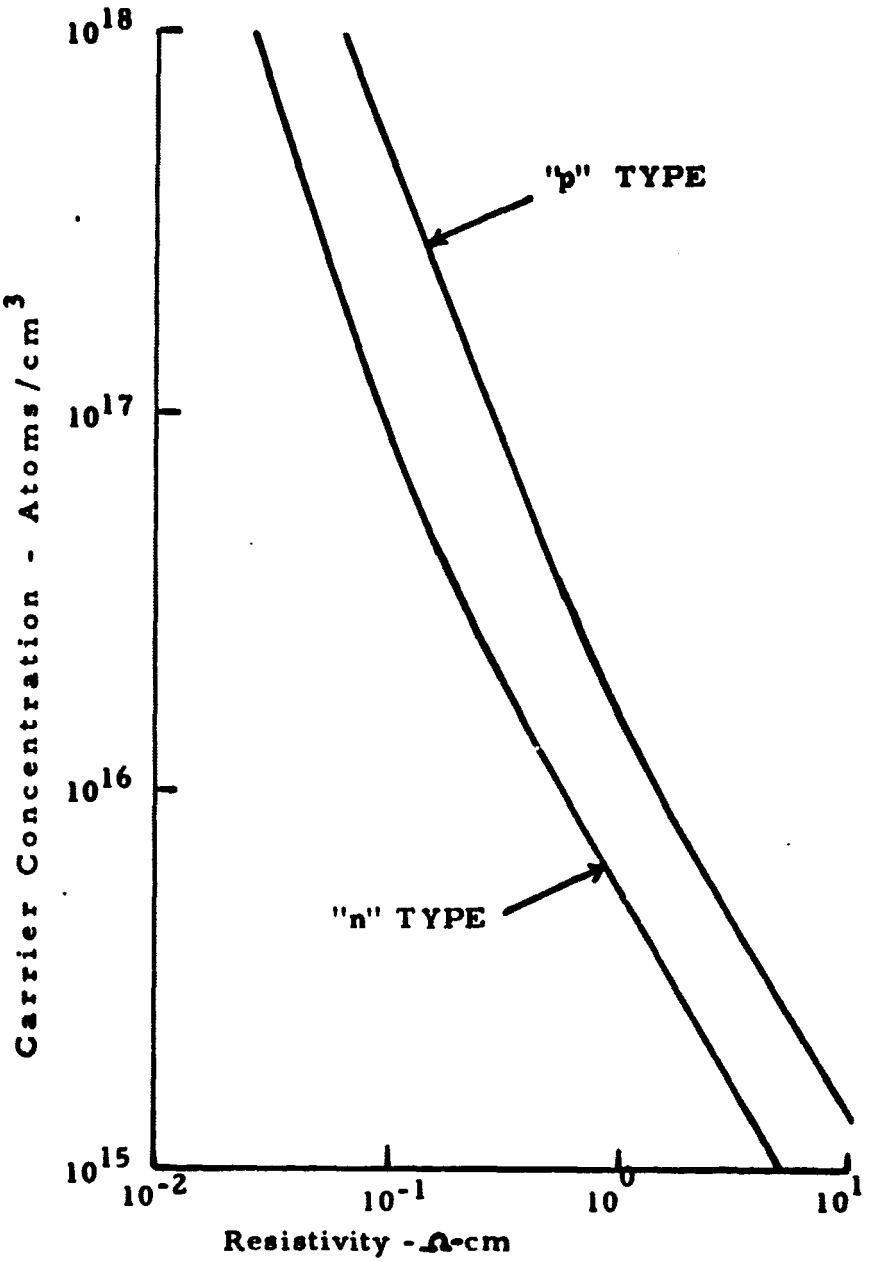

Fig. VII (a). Resistivity (10^{-2} - 10^{1} Ω-cm) as a function of carrier concentration in silicon.

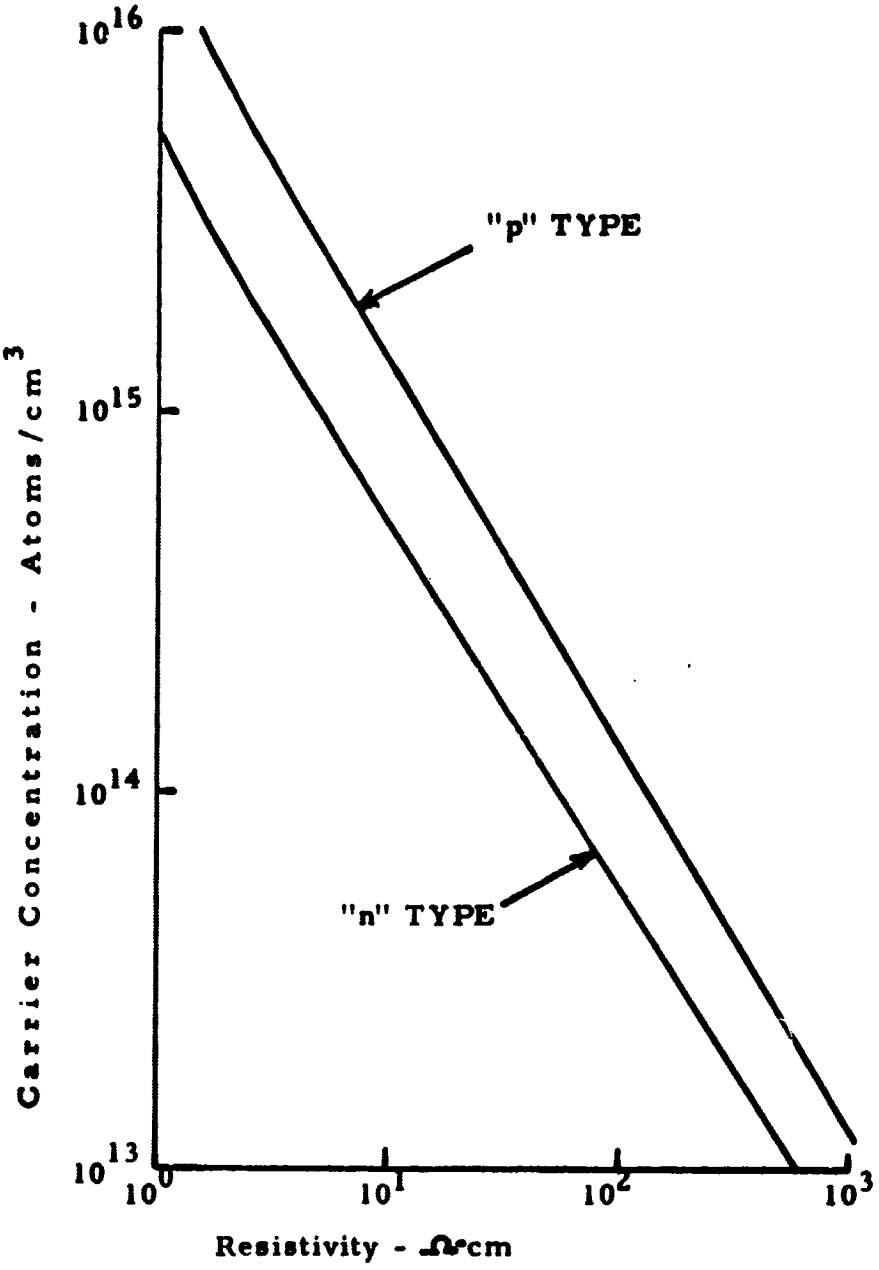

Fig. VII (b). Resistivity (10^0 - 10^3 Ω-cm) as a function of carrier concentration in silicon.

Obviously the movement of carriers is temperature dependent. A relationship can be derived beginning with the force equation

$$F = qE, \text{ and since } F = ma, \tag{26}$$

$$a = \frac{qE}{m}, \tag{27}$$

The average velocity of carriers through a crystal under the influence of an electric field is given by

$$V_D = a\,t, \text{ where } V_D \text{ is the drift velocity.} \tag{28}$$

Substituting (27) into (28) yields

$$V_D = \left(\frac{qt}{m}\right) E = \mu E \text{ cm/sec}, \tag{29}$$

where

$$\mu = \frac{qt}{m} \text{ is termed drift mobility.} \tag{30}$$

It is apparent that as the number of carrier collisions per unit time increases the drift mobility will decrease. The drift mobilities are influenced by the two principal collision mechanisms, (1) impurity-atom scattering and (2) lattice-vibration scattering. If μ_I is designated as the mobility due to impurities alone, and μ_L is lattice mobility, it is a fair approximation to write [13]

$$\frac{1}{\mu} = \frac{1}{\mu_I} + \frac{1}{\mu_L}. \tag{31}$$

The theory of impurity scattering mobility was investigated by Conwell and Weisskopf and their analysis gives the following formula: [17,18]

$$\mu_I = \frac{8\sqrt{2}\,K^2\,(kT)^{3/2}}{\pi^{3/2} N_I\, q^3\, m_{eff}^{1/2}\, \ln\left(1 + \frac{3KkT^2}{q^2 N_I^{1/3}}\right)} \qquad (32)$$

where K = dielectric constant,

T = temperature ^{o}K,

N_I = total density of all ionized impurities,

m_{eff} = effective mass of electron or hole.

Actual measurements of drift mobility in high-quality crystals of silicon, where the impurity concentrations were so small that only lattice mobility would be predominant, give the following relationships for lattice mobility: [19]

$$\mu_{L_n} = 2.1 \times 10^9\, T^{-2.5} \qquad (33)$$

$$\mu_{L_p} = 2.3 \times 10^9\, T^{-2.7}$$

The composite effects of both impurity and lattice mobilities are shown in the curves of Fig. VIII. [20, 21, 22] These curves give the values of minority carrier drift mobility as a function of impurity concentration at room temperature for silicon. As is seen, the effect of impurity scattering becomes predominant at impurity

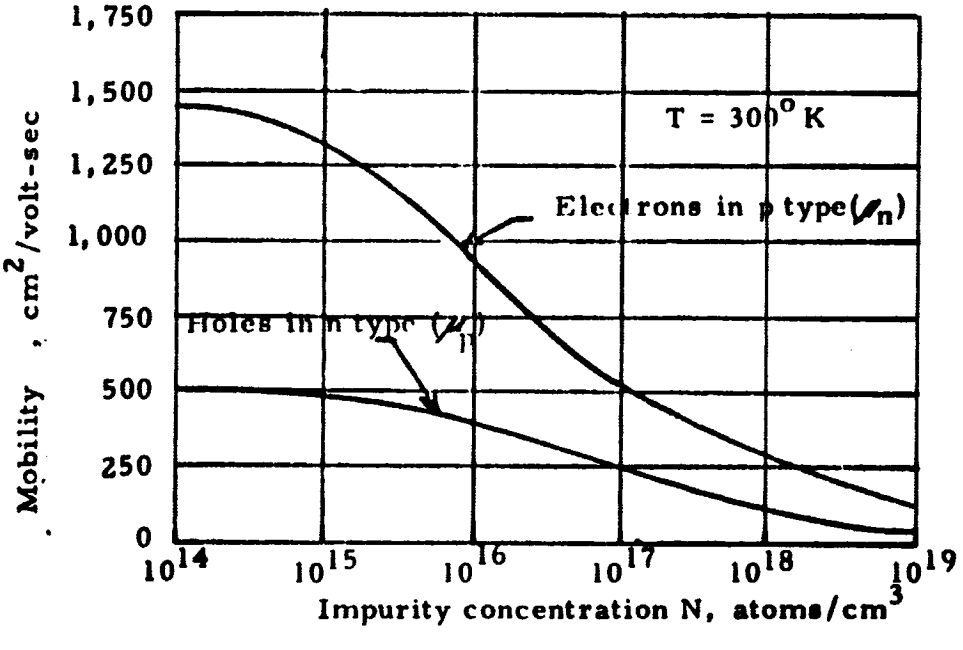

Fig. VIII. Drift mobilities in silicon.

concentrations of 10^{15} cm^{-3} or more. The mobilities have been reported by Dunlap[11] to vary as

$$\mu_n = 4.0 \times 10^9 \, T^{-2.6} \, cm^2/volt\ sec \text{ and} \qquad (34)$$

$$\mu_p = 2.5 \times 10^8 \, T^{-2.3} \, cm^2/volt\ sec .$$

Pearson and Bardeen found a $T^{-3/2}$ law dependence of mobility upon temperature.[11] Regardless of which is correct, it is seen that the constant b defined as μ_n/μ_p approaches 3 in high resistivity silicon.[23]

Electric current is defined as the flow of a total amount of charge per unit time within an electric field. If a voltage is impressed on a semiconductor of length l and cross-sectional area A, the current density J for electrons would be

$$J_n = \frac{I_n}{A} = -qnV_{D_n} \quad amps/cm^2 . \qquad (35)$$

The current density for holes would likewise be

$$J_p = \frac{I_p}{A} = qpV_{D_p} \quad amps/cm^2 , \qquad (36)$$

where in (35) and (36) "n" and "p" are the electron and hole concentrations, respectively. Since the two in a crystal are additive,

$$J = J_n + J_p = -qnV_{D_n} + qpV_{D_p} . \qquad (36a)$$

Substituting (29) into (36a)

$$J = -qn(-\mu_n E) + qp\mu_p E. \tag{37}$$

$$J = Eq(\mu_n n + \mu_p p) \tag{38}$$

Setting $E = V/l$,

$$I = \frac{VA}{l} q(\mu_n n + \mu_p p). \tag{39}$$

Using Ohm's law,

$$R = \frac{V}{I} = \frac{l}{A} \frac{1}{q(\mu_n n + \mu_p p)} \tag{40}$$

Since this is the form of $R = \rho \frac{l}{A}$, where ρ is the resistivity,

$$\rho = \frac{1}{q(\mu_n n + \mu_p p)} \text{ ohm-cm}, \tag{41}$$

or, letting σ be the conductivity,

$$\sigma = \frac{1}{\rho} = q(\mu_n n + \mu_p p) \text{ mho-cm}^{-1}. \tag{42}$$

The curves in Figure VII show resistivity as a function of impurity concentration.

The treatment of semiconductor crystals would be partly incomplete without discussing the surface. It has been well established without adequate understanding that the electrical properties of a semiconductor surface differ from those of the bulk

interior. An abrupt boundary exists for the layer of surface atoms which will disrupt the orderly energy distribution in the region. Also the surfaces are never perfect. The atoms are very active in air and form oxide layers readily. Chemical ions, water atoms, and gas atoms, dependent on the ambient, may be absorbed by these layers. Considerable experimental work has shown this to be true. Also the surface exhibits a recombination rate for carriers which is usually different from the lifetime of the bulk material.

It is generally accepted from the early work of J. Bardeen, that at the surface there exist a number of surface energy states leaving energies that fall within the forbidden band gap of the semiconductor.[24,25] These states have been categorized into two types: (1) layer states and, (2) interface states. The layer states are generally believed to be due to the characteristics of the oxide layer arising from absorbed ions and are very sensitive to the ambient which the surface is exposed to. The interface states, as originally suggested by Brattain and Bardeen[26] act very similar to the recombination centers of the Shockley-Read-Hall theory.[27, 28, 29, 30] These states are found to be independent of ambient, but dependent on the quality of the initial surface treatment by chemical etches before oxide formation. The number of layer states is usually greater than interface states.

Suppose the total ionic charge absorbed by the oxide layer on high resistivity "p" type material giving rise to layer states is positive. To maintain charge neutrality, electrons are attracted to the surface. This added concentration of electrons in the bulk region adjacent to the interface affects the Fermi level. It is customary to keep the Fermi energy as a constant reference and let the energy bands bend. Figure IX illustrates that the Fermi level is now closer to the conduction band, indicating that the conductivity of the surface reverses from "p" type to "n" type. The amount of the energy bands bend is a function of the density and energy distribution of the layer states, which is directly affected by the ambient. This conductivity reversal is called inversion and the layers thus formed are called inversion layers.

Since the density of interface states is smaller than that of the layer states, they do not appreciably affect inversion. However, the interface states have capture probabilities many orders of magnitude greater than the layer states.[26] Therefore, any observed recombination of carriers at the surface is attributed mainly to recombination at the interface centers. Surface recombination is expressed in terms of a surface recombination velocity, S, in centimeters per second. This is defined as the number of carriers recombining per second per unit area divided by the excess concentration over the equilibrium value at the surface.

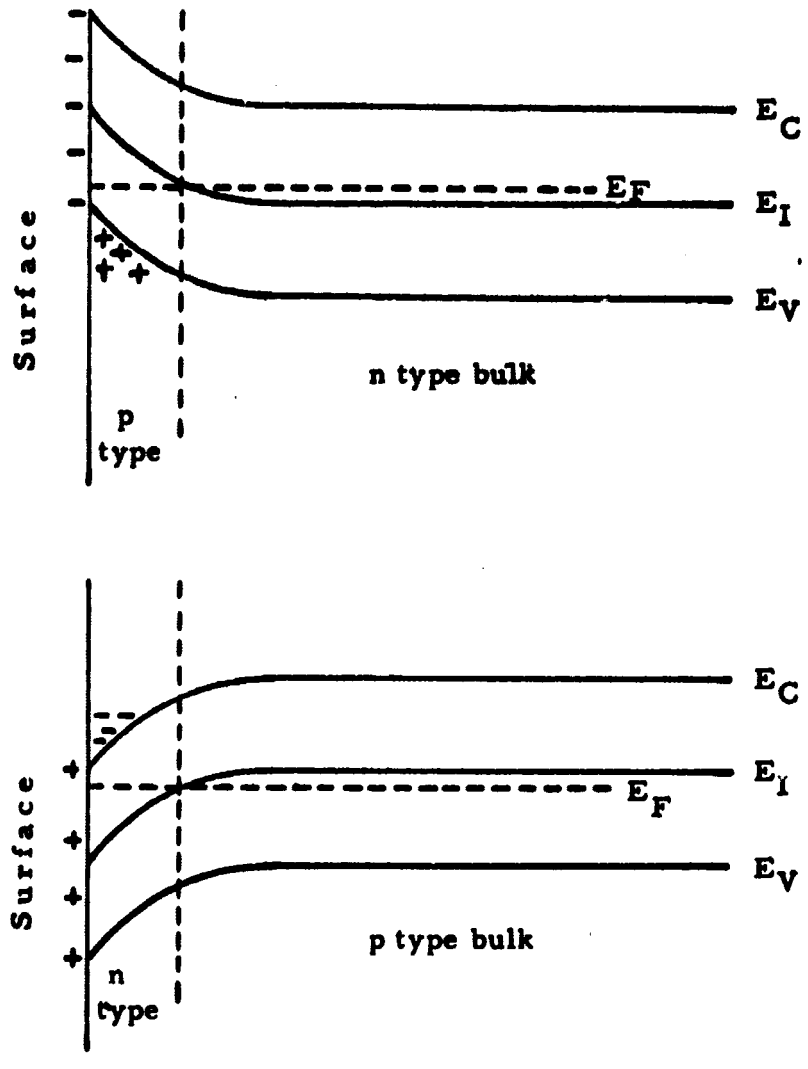

Fig. IX. Inversion layers in semiconductors.

It can be stated in conclusion that the density and energy levels of the interface states are determined by the method of initial surface treatment and are independent of any ambient effects. The ambient affects the nature of the ionic charge in the oxide layer states, which in turn alters the conductivity and type of the bulk layer just beneath the surface. Interface layers have the effect of lowering the effective crystal lifetime according to

$$\frac{1}{\tau_{eff}} = \frac{1}{\tau_{bulk}} + \frac{1}{\tau_{interface}} . \qquad (43)$$

Theory of Diffusions

In addition to motion by drift in an electric field, carriers may drift in a semiconductor crystal by diffusion in the absence of an electric field. This may be visualized by the consideration of an excess of holes or electrons in a localized region of a crystal at equilibrium. A spreading or diffusion in all directions would be observed. The rate of diffusion would be dependent on the concentration gradient. An analogy can be made to the flow of heat in a rod with a temperature gradient between the two ends. If an electric field is also applied, a drift motion is superimposed on the diffusion.[31]

For simplicity consider a one dimensional case of

diffusion.* Let the distribution of injected electron concentration be given by

$$n = n(x). \tag{44}$$

The concentration gradient is then $\frac{dn}{dx}$. It may, thus, be written

$$J_n = -c\frac{dn}{dx}, \tag{45}$$

where c is a constant. Consequently, c must include the electron charge -q. Therefore,

$$J_n = qD_n\frac{dn}{dx}, \tag{46}$$

where D_n is the diffusion constant for electrons in p-type material in cm^2/sec. Also,

$$J_p = -qD_p\frac{dp}{dx}. \tag{47}$$

Equations (46) and (47) form Fick's first law of diffusion,[32] or,

$$\vec{J_n} = -qD\vec{\nabla}n.$$

Substituting (46) and (47) into (36) yields

$$J = q\left(D_n\frac{dn}{dx} - D_p\frac{dp}{dx}\right). \tag{48}$$

---

*In a cubic lattice, such as silicon, symmetry requires an isotropic rate of diffusion making the diffusion rate a scalar. See, for instance, Kittel, Chapter I.

In three dimensions this becomes

$$\vec{J} = q(D_n \vec{\nabla} n - D_p \vec{\nabla} p) . \tag{49}$$

The diffusion constants are related to the mobility by the Einstein relationship[11]

$$D = \mu \frac{kT}{q} \text{ cm}^2/\text{sec} , \tag{50}$$

where

k = Boltzmann's constant,

T = absolute temperature.

An important property of carriers, related to lifetime,* is diffusion length which is defined by the equation[33]

$$L = \sqrt{D\tau} \tag{51}$$

where τ is the carrier lifetime. When a small density of carriers is injected into a semiconductor, the density will decrease proportionally as $e^{-\frac{t}{\tau}}$. When $t = \tau$, the density has decreased to 1/e of the original value. Therefore, the lifetime τ is a measure of the recombination rate. Shockley[13] showed that lifetime due to

*The lifetime of a carrier is the average time between generation and recombination. It should not be confused with the mean free time associated with mobilities, since a carrier may experience many collisions before it recombines.

carrier concentrations only is given by

$$\tau_c = \frac{n_i^2}{e(p+n)} , \qquad (52)$$

where e is the rate of thermal emission of carriers. The effect of the recombination centers on the carrier lifetimes is given by the Shockley-Read-Hall[27, 28, 29, 30] theory based on probability considerations employing Fermi-Dirac statistics. By their analysis it was shown that lifetime depends inversely on the recombination center concentration. Substituting Equation (50) into (51) yields

$$L^2 = \frac{kT\mu}{q} \tau . \qquad (53)$$

By comparing Equation (53) with the published values for mobility, it is seen that the diffusion length varies inversely with temperature.

The diffusion coefficient varies with temperature as[3]

$$D = D_o e^{-\frac{\Delta E_a}{kT}} , \qquad (54)$$

where

ΔE_a = energy of activation

D_o = apparent value of D at infinite temperature.

The diffusion coefficient determined experimentally for lithium in "p" type silicon [34, 35, 6] is

$$D = 2.30 \times 10^{-3} \exp\left(-\frac{0.72 \text{ ev}}{kT}\right) \text{cm}^2/\text{sec} \qquad (55)$$

for a temperature range of 0° C to 877° C. A curve showing D as a function of T is shown in Fig. X.[23]

The process of diffusion of holes and electrons is described by the differential equations (one-dimensional case)

$$D_p \frac{\partial^2 p}{\partial x^2} = \frac{\partial p}{\partial t} \qquad (56)$$

and

$$D_n \frac{\partial^2 n}{\partial x^2} = \frac{\partial n}{\partial t} \qquad (57)$$

assuming the diffusion coefficient not to be a function of concentration. Equations (56) and (57) form Fick's second law of diffusions.

If an "n" type dopant such as lithium, which dopes interstitually, is deposited on the surface of "p" type material such that the source may be considered infinite or constant, the solution to equation (57) is[36]

$$N(x) = N_o \operatorname{erfc}\left(x / 2\sqrt{Dt}\right)$$

where

N_o = surface concentration

$N(x)$ = concentration at a depth x

t = time

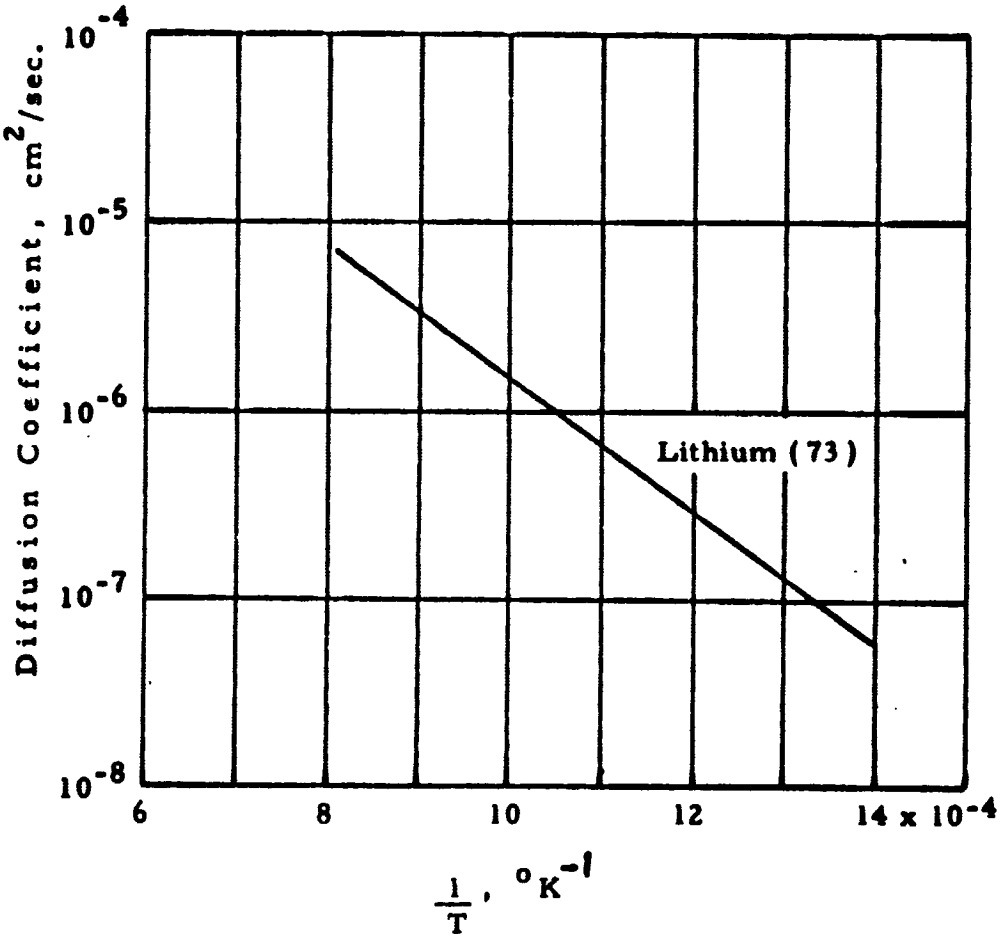

Fig. X. Diffusion coefficient of lithium in silicon as a function of temperature

and

$$\operatorname{erfc} u \equiv \frac{2}{\sqrt{\pi}} \int_u^{\infty} e^{-y^2}\, dy.$$

Theory of "P-N" Junctions

Assuming the donor concentration N_D is greater than the acceptor concentration N_A ($N_D > N_A$), there will be two regions with different type conduction. Thus, a "p-n" junction is formed.[58] A typical impurity profile and energy diagram[59] for a graded junction are shown in Fig. XI.

At the transition region the holes in the "p" region will diffuse, because of the impurity gradient, across the junction into the "n" region where the hole concentration is small. Likewise, electrons from the "n" region will diffuse into the "p" region where the electron concentration is small. Since the impurity ions are fixed in the lattice and are not free to move, as a result of the diffusion, there will be regions of unneutralized charge on both sides of the junction. Since the bare charge on each side of the junction is opposite in polarity an electric field is established which, at equilibrium, prevents majority carrier diffusion. The depleted layer is very similar to a parallel plate capacitor and will have a capacitance.

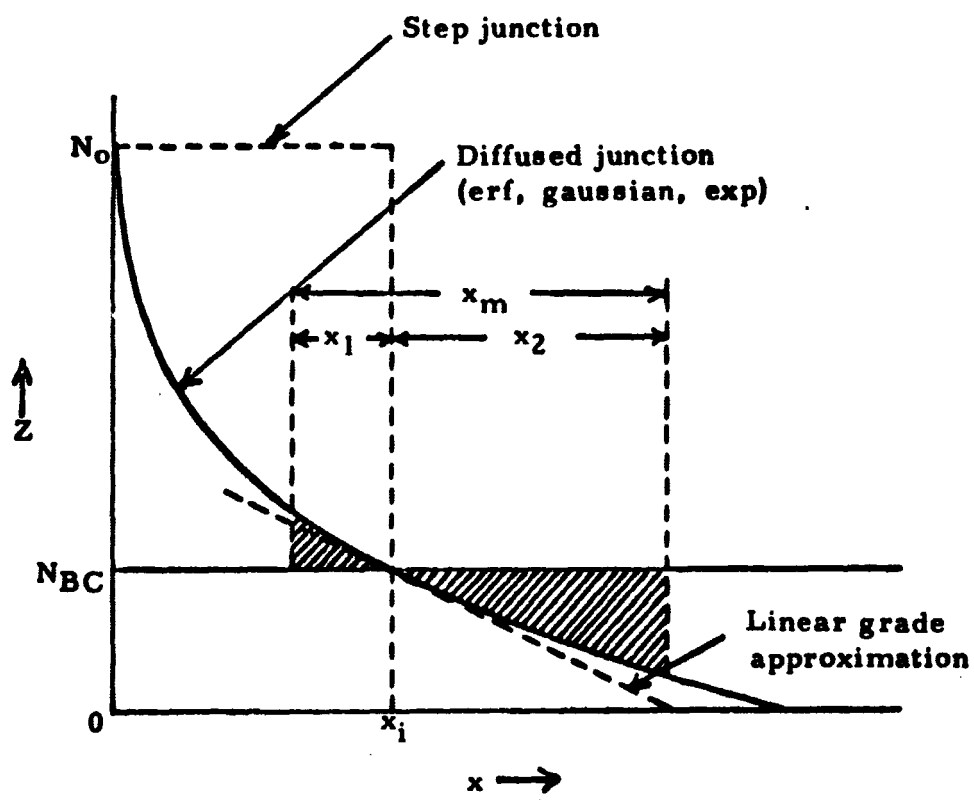

Fig. XI (a). Impurity profile and depletion-layer characteristics for diffused junctions.

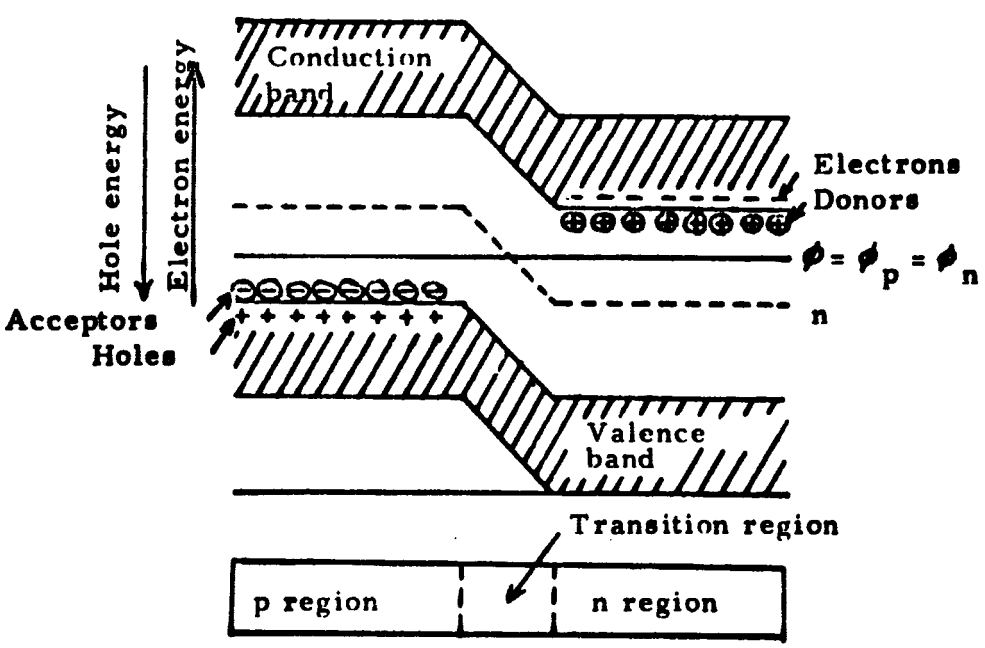

Fig. XI(b). Energy diagram for a p-n junction in equilibrium illustrating constant Fermi level.

If a supporting electric field, reverse bias, is applied to this "n-p" junction the depletion layer will widen. In the reverse biased condition there will be a small reverse current due to the minority carriers within one diffusion length of the junction that will diffuse to the transition region and drift across because of the electric field. This current remains fairly constant with an increase in voltage until the carriers acquire sufficient energy to break additional valence bonds upon collision.[37] This results in further generation of electron-hole pairs, causing the reverse current to multiply. If this voltage is increased slightly, the process becomes so cumulative that an avalanche occurs and the junction "breaks down" completely.[38]

An opposing field, forward bias, will cause the depletion layer to become narrow until the internal field is exceeded. There is then no potential "barrier" and a further increase in voltage causes a large flow of current.

Junctions formed by diffusion methods are graded since the diffused region establishes a gradual transition from one impurity type to the other. In the depletion region it is a good approximation to assume the grade to be linear. Therefore,

$$N(x) = ax \tag{59}$$

where a is the grade constant in atoms/cm^4. Because of the linear

grade of the impurities, the net charge density will also be a linear function, or

$$\rho(x) = qax. \tag{60}$$

For a distance x on either side of x = 0, the areas are equal, which indicates that the depletion spreads equally in both directions. The total depletion is then x_m. From Poisson's equation,

$$\frac{d^2V}{dx^2} = -\frac{\rho(x)}{k\epsilon_o}, \tag{61}$$

it is shown in the appendix that

$$x_m = \left(\frac{12k\epsilon_o V}{qa}\right)^{1/3} \text{ cm} \tag{62}$$

and

$$C_T = \left(\frac{(k\epsilon_o)^2 qa}{12V}\right)^{1/3} \text{ farads/cm}^2. \tag{63}$$

Similar calculations for a step junction where

$$\rho(x) = -qN \tag{64}$$

results in

$$x_m = \left(\frac{2k\epsilon_o V}{qN_A}\right)^{1/2} \text{ cm for "p" type} \tag{65}$$

and

$$C_T = \left(\frac{q k \epsilon_o N_A}{2 V}\right)^{1/2} \text{ farads/cm}^2 \text{ for "p" type.} \quad (66)$$

k for silicon is 12. Actual experimental measurements of capacitance indicate that diffused junctions do exhibit a $V^{-1/3}$ dependence at low voltages.[38] At higher voltages, the dependency becomes $V^{-1/2}$.[40] Extensive study of capacitance calculations have been made by Lawrence and Warner.[40]

Theory of Drift

As previously stated lithium diffuses interstitually. When held at an elevated temperature, the probability of a lithium atom migrating through a silicon crystal becomes higher. If an electric field is superimposed on this system, the lithium ions will drift in the direction of the electric field and effect a very high degree of boron ion compensation in the depletion region.[41] provided that the temperature is not high enough for the intrinsic "n" concentration to cause flooding.* As a result of this compensation, the depletion region must spread more into the "p" region. Assuming sufficient lithium, this process will continue during the length of voltage

*Flooding is the term describing the condition of thermally generated carriers being equal to or greater than the diffused carriers.

and temperature application. The width of the compensated region is given by[42]

$$W = (2\mu V)^{1/2} t^{1/2} \qquad (67)$$

where $2\mu V$ is defined as the drift parameter and t is time. A lithium drift parameter nomograph for oxygen-free silicon and a family of curves for drift depth as a function of time for various drift parameters are given by Blankenship and Barkowski.[42]

The minimum surface concentration of lithium atoms needed to compensate the drifted region is given by [42]

$$N_S (\text{atoms/cm}^2) = N_H \cdot W \qquad (68)$$

where N_H is the hole concentration in the starting silicon.

Theory of Operation

When a reverse bias is applied to a compensated diode, the depletion layer spreads very rapidly through the compensated region to make it intrinsic. The resulting device is "N-I-P" in structure. Any form of radiation incident on the device will form electron-hole pairs in the silicon by absorbing 3.6 ev [33] of energy per electron-hole pair. The carriers in the intrinsic region will be swept away by the electric field. This movement of charge constitutes an electric current which when passed through the circuit shown in Figure XII

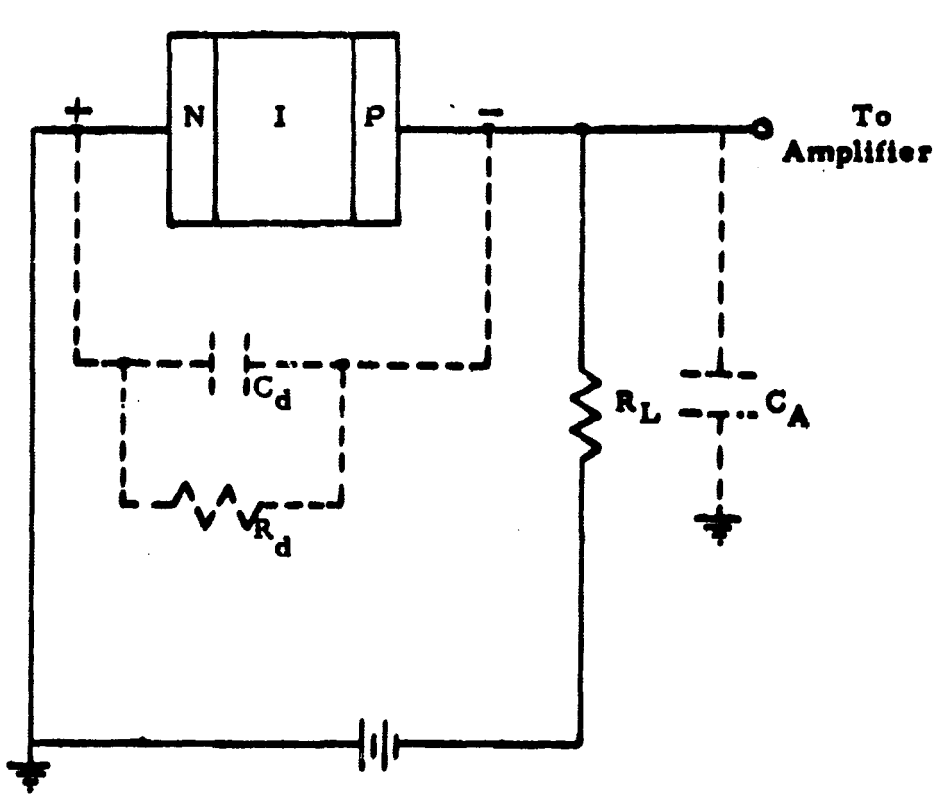

Fig. XII. Applicable circuit for nuclear particle detector.

develops a voltage pulse. Appropriate analysis of this amplified pulse gives a measure of the incident radiation energy.

In the absence of radiation, there will be a small "reverse current" under reverse biased conditions. This current has three components:[43]

(1) The drift current due to diffusion of minority carriers into the depletion region;

(2) The carrier generation current, due to carriers produced by thermal generation in the depletion region;

(3) The surface leakage.

In practice the former two components are usually negligible compared with the surface leakage. This leakage current is a source of diode noise[43] and is the predominant noise generator. Causes of this charge flow include ionic charges on the surface, conducting films on the detector, conducting ambients and inversion layers across the diode surface.

Extensive studies[44] made of electrical noise in semiconductor devices show that there are three types:

(1) Thermal noise, often called Johnson noise, due to fluctuations in the spatial distribution of carriers arising from thermal diffusion;

(2) Current noise, often called shot noise, due to statistical fluctuations in the number of carriers leading to changes in conductivity;

(3) Flicker noise, often called 1/f noise, believed to originate at the surface and is dependent on surface leakage and contact resistance.

Good detector performance demands that the noise to signal ratio be low so that the resolution is not limited.

PREPARATION OF DETECTOR

The beginning material selected was Lopex* "p" type boron doped silicon with the following specifications:

Lifetime	>	100 μsec
Dislocation density	<	3,000/cm^2
Oxygen concentration	<	10^{15} atoms/cm^3
Resistivity		300-500 Ω cm

Lopex material, rather than melt grown or float zone, was chosen because it offers the advantages of low oxygen concentration and dislocation density. Melt grown silicon has extremely low dislocation density but high oxygen content. Float zone material has very low oxygen content but high dislocation density.

A minimum lifetime specification was imposed to insure the highest possible carrier mobility. As discussed in the theory section, this is extremely important for good charge collection properties of the resulting detector. In an implicit manner this limit also imposes a heavy metal concentration maximum. This is because the metals would effect a high recombination probability and, thus, limit the lifetime.

---

*Lopex is Texas Instrument's tradename for specially processed silicon crystals to achieve extremely low, less than 10^{15} atoms/cm^3, oxygen content and low dislocation density.

The maximum dislocation density was specified to lessen the number of spikes* during diffusion, to lower the resulting device noise, and to increase the lifetime. This limit may have been quite unnecessary with the chosen material. However, some process abnormality may have existed during its growth causing a flaw in the material. Without this specification the flaw may not be detected.

From elementary chemistry it is known that lithium and oxygen react with extreme ease t .orm lithium oxide. This was the primary reason for specifying a maximum oxygen content in the silicon crystal. The reaction could have caused very poor compensation during the following drift process. It is also widely known that oxygen has a very unpredictable effect on the crystal resistivity during heat treatments. One hundred per cent changes in resistivity are not uncommon when a high concentration of oxygen is present.

The 300-500 Ωcm resistivity range was a compromise between the resulting diode avalanche breakdown and leakage. It was shown in the theory section that the "np" product is a constant for a given temperature. Also, the diode leakage is dependent on the

---

*A spike is caused by an impurity diffusing in a localized area with a much higher diffusion coefficient than in the rest of the material. This causes a much deeper penetration in this area than elsewhere. Junctions of this nature usually exhibit extremely low avalanche breakdowns.

minority carrier concentration. Lower resistivity "p" type material would have lower "n" type concentration and, consequently, lower diode leakage. This was desirable since detector noise is caused by the leakage current. However, it was also desirable to have the avalanche breakdown high enough to allow 1500 volt operation of the prepared detector. The chosen resistivity allows the realization of both of these parameters.

13 cm x 2 cm x 1 cm slabs were sawed from the grown crystals. The 13 cm length was necessary to stop 200 Mev protons. The 2 cm width and 1 cm thickness were helpful in achieving a 1 cm^2 cross sectional area.

After sawing, the slabs were cleaned by ultrasonic vibration in trichloroethylene. The vibration freed loose impurity particles lodged in the silicon surface during the sawing operation. Organic compounds on the surface were partially dissolved by the trichloroethylene. This type cleaning process is considered an excellent one by the semiconductor industry. Its use removes many particles not removable by any other known method. From this point extreme caution was exercised to not expose the bars to a contaminated atmosphere.

Many detector fabricators etch the silicon at this point in Bell 39A* or some similar etch to polish the surface. This process

---

*Bell 39A is a silicon etch developed by Bell Laboratories consisting of hydrofluoric, nitric, and acetic acid.

is advantageous if the lithium in the following diffusion step is deposited from a vapor state or is evaporated onto the surface. With the type lithium deposition used in this work, difficulty was encountered in achieving uniform impurity concentrations with polished surfaces. In order that the above etching step could be eliminated, the most elaborate cleaning techniques known had to be used.

The slabs were immersed in 150° C concentrated sulfuric acid for fifteen minutes to oxidize and remove any organics remaining on the surface. If the acid became discolored, this step was repeated. This operation is presently suspected of inducing "strange" surface states in the silicon. No conclusive literature has yet been published on this subject. A fifteen-minute immersion in 150° C nitric acid was then employed to dissolve any heavy metals remaining on the surface. As before, this step was repeated if the acid became discolored. Two fifteen-minute deionized water boils followed to remove the ions remaining from the acid cleans.

Lithium diffusion followed immediately before the slices could be contaminated with impurities that would diffuse into the silicon. Three parts of a viscous solution of five parts piecin wax, three parts bees wax and benzene were mixed with five parts of a lithium in oil suspension. The thick crust of lithium formed by letting a lithium in oil suspension sit overnight was used for the five parts lithium. The paste thus formed was spread on the slab

surfaces by continuous circular motion of some clean wooden applicator. A larger area than the desired junction area was coated. It was very necessary that the surface be thoroughly wetted with the paste. Lithium was then diffused into the silicon for five minutes in a dry nitrogen atmosphere on a hot plate previously stabilized at 400° C. A nitrogen atmosphere, or any inert one, was necessary to prevent oxidation of the lithium. The slabs were then slow cooled, also in a dry nitrogen atmosphere, on a piece of quartz. This helped to increase the carrier lifetime in the bulk silicon.

Removal of the resulting lithium crust was accomplished by immersing the slab in benzene. Trichloroethylene swabbing was then used to thoroughly clean the surface. A ten-second etch in a three parts nitric to one part hydrofluoric acid solution was employed to remove part of the damaged surface. This damage was caused by the lithium alloying into the silicon. It was possible to determine the quality of the diffusion by the uniformity of this damage. If it was felt that a poor diffusion, more accurately determined by a four point probe, was achieved, the slab was lapped with 1800 abrasive to remove the lithium and reprocessed.

A viscous solution of five parts piecin wax and three parts bees wax dissolved in benzene was used to mask an area of the lithium diffused face 1.5 cm wide and 13 cm long. This masking process was performed under a heat lamp to boil off the benzene and

make the acid resistant coating adhere to the surface better. Much care was taken to mask an area inside the preceeding lithium diffused area. The unprotected sides and face were etched twice for two minute intervals in a clean solution of three parts nitric and one part hydrofluoric acid. The slabs were quenched in clean room temperature deionized water or dilute nitric acid to prevent staining. Boiling trichloroethylene was used to remove the wax coating. Two fifteen minute clean deionized water boils followed immediately to remove the remaining acid ions.

By this manner, a mesa was formed which produces a clean well defined "n-p" junction. It was necessary to have a large enough volume of etch to prevent overheating of the solution. The etch rate was dependent on the etch temperature. Consequently, if the solution became hotter, the etching would progress at a much higher rate. Utmost caution was exercised to protect this exposed junction from any impurities that would cause junction leakage during the following drift process.

At this point the junction leakage was measured while reverse biased with 300 volts. All reverse currents were less than 10 micro amperes. This current was indicative of the junction quality.

Approximately 100 angstroms of pure aluminum were evaporated onto the back side and a 1.0 cm x 11.0 cm stripe inside the topside junction area of the slab to give good ohmic contact during

the drift procedure. No aluminum was allowed to overlap onto the sides and across the "n-p" junction to form a leakage path.

The drift procedure was performed on a hot plate previously stabilized at 135° C in an air atmosphere. A reverse bias of 400 volts was maintained with the current limited to 100 milliamperes with a constant current power supply. An aluminum chamber was used in an attempt to attain a constant temperature. It was necessary to stop the drift once, when the leakage current became excessive, and reetch the mesa. The increased current was caused by surface inversion when the silicon oxidized. Much literature has been published showing that the segregation coefficient of boron in silicon and silicon dioxide favors silicon dioxide. Thus, as silicon dioxide was grown, the boron was depleted from the silicon surface. Since very high resistivity material, low boron concentration, was used the surface inverted to "n" type very easily. This resulted in a thin conducting layer on the surface for leakage current to flow. A short etch removed this layer and again extended the "n-p" junction to the surface. Many detector fabricators drift in a silicone oil bath to prevent the growth of silicon dioxide and to produce a constant temperature. This is a much better process than the one used here. However, expensive equipment is necessary which could not be justified for small volumes. By using the precautions mentioned above excellent detectors of various geometries were produced.

Using the nomograph of Blankenship and Barkowski, a drift parameter ($2\mu V$) of 6×10^{-7} cm^2/sec was determined for V = 400 V and T = 135° C. The calculated time, by equation (67), for a 4 mm. drift depth was seventy-four hours. It was verified by earlier work where full slice drift was performed that the equations derived by Blankenship and Barkowski were extremely accurate. Consequently, the drift was allowed to proceed for forty-eight hours, at the above conditions and ninety hours at 250 V and 130° C. This was the nearest convenient time to the one calculated.

Again, the mesa was masked and the sides and aluminum back were etched for two two-minute intervals in clean etch solutions. Two clean water rinses followed before the wax was removed by boiling trichloroethylene and swabbing. The slabs were then cleaned with two fifteen-minute water boils and dried with methyl alcohol. Since this was the final cleaning process, every possible precaution was exercised to keep from introducing any impurities.

The detector was then passivated by coating all of the silicon except a 0.5 cm wide strip on the "n" and "p" faces with Dow Corning 1440 varnish. Care was taken to thickly and evenly coat the surfaces immediately after the final clean to achieve the best possible passivation. A twenty-four hour curing followed in a dry dust free atmosphere at 25° C. Its purpose was to allow the varnish to dry with very little ionic contamination.

A conducting epoxy* was used to mount the completed detector on a 1 cm x 12 cm brass strip. A thin layer of the epoxy was spread over the entire "p" face and placed down flat on the strip. This also formed contact to the "p" material. The 0.5 cm wide opening on the lithium face was then coated with the epoxy. One end of a 10 cm length of 8 mil copper wire was inserted in the coating. The whole system was allowed to dry for twenty-four hours. After this period the brass strip was mounted on the top, ground side, of a B&C connector. The copper wire was connected to the positive terminal with conducting epoxy. A twenty-four hour drying cycle followed before the detector assembly was handled. Figure XIII shows a photograph of the finished assembled detector.

*E-Soldier 3021 Silver Epoxy manufactured by: Epoxy Products, Inc., of Irvinton, New Jersey, was used.

APPENDIX

From equation (61)

$$\frac{d^2V}{dx^2} = -\frac{\rho(x)}{k\epsilon_o} \quad . \tag{1}$$

From equation (60)

$$\rho(x) = -qax. \tag{2}$$

Substituting (60) into (61) yields

$$\frac{d^2V}{dx^2} = \frac{qax}{k\epsilon_o} \quad . \tag{3}$$

Integration yields

$$\frac{dV}{dx} = \frac{qax^2}{2k\epsilon_o} - K_1 \tag{4}$$

Integrating again, the voltage equation is obtained.

$$V = \frac{qax^3}{6k\epsilon_o} + K_1 x + K_2 \tag{5}$$

To evaluate the constant K_1, we make use of the assumption that all the applied voltage is dropped across the depletion region. In

other words, the electric field is zero outside the junction. Therefore, with the boundary conditions that $E = 0$ at $x = -x_m/2$ and $x = +x_m/2$ inserted into (4), K_1 becomes

$$K_1 = -\frac{q a x_m^2}{8 k \epsilon_o} , \qquad (6)$$

or

$$\frac{dV}{dx} = E = \frac{q a x^2}{2 k \epsilon_o} - \frac{q a x_m^2}{8 k \epsilon_o} \qquad \frac{-x_m}{2} \leq x \leq \frac{x_m}{2} . \qquad (7)$$

Equation (7) represents the way the electric field varies with distance through the depletion layer. Note that the field is maximum at $x = 0$.

$$E_{max} = \frac{-q a x_m^2}{8 k \epsilon_o} . \qquad (8)$$

The applied voltage V is equal to the potential V_n at $-x_m/2$ less the potential V_p at $x_m/2$.

$$V = V_n - V_p \qquad (9)$$

Evaluating equation (5) at the appropriate boundaries to obtain V_n and V_p yields

$$V\left(-\frac{x_m}{2}\right) = V_n = -\frac{q a x_m^3}{48 k \epsilon_o} - K_1 \frac{x_m}{2} + K_2 \qquad (10)$$

and

$$V\left(\frac{x_m}{2}\right) = V_p = \frac{q a x_m^3}{48 k \epsilon_o} + K_1 \frac{x_m}{2} + K_2 . \qquad (11)$$

Substituting equations (10) and (11) into (9) results in

$$V = - \frac{q a x_m^3}{24 k \epsilon_o} - K_1 x_m . \qquad (12)$$

Substituting equation (6) into equation (12) yields

$$V = \frac{q a x_m^3}{12 k \epsilon_o} . \qquad (13)$$

Solving for x_m,

$$x_m = \left[\frac{12 k \epsilon_o V}{q a} \right]^{1/3} \qquad (14)$$

For this same linear geometry, the capacitance per unit area is derived by utilizing

$$C = \frac{k \epsilon_o}{x_m} , \qquad (15)$$

which is the expression for the parallel-plate equivalent capacitance. Substituting equation (14) into equation (15) yields

$$C_T = \left[\frac{(k\epsilon_o)^2 q}{12} \right]^{1/3} \left(\frac{a}{V}\right)^{1/3} . \qquad (16)$$

BIBLIOGRAPHY

1. E. M. Pell, J. Appl. Phys. 31 (2), 291 (1960).
2. F. J. Morin and J. P. Maita, Phys. Rev. 96, 28 (1954).
3. C. S. Fuller and J. C. Severiens, Phys. Rev. 96 (1), 21 (1954).
4. H. Reiss, C. S. Fuller and F. J. Morin, The Bell Sys. Tech. J. 35 (3), 535 (1956).
5. J. H. Elliot, Nucl. Inst. and Meth. 12 (1), 60 (1961).
6. E. M. Pell, Phys. Rev. 119, 1222 (1960).
7. H. Lawrence and R. M. Warner, Jr., The Bell Sys. Tech. J., 389 (1960).
8. G. Dearnaley and J. C. Lewis, Nucl. Inst. and Meth. 25, 237 (1964).
9. Charles Kittel, Introduction to Solid State Physics (John Wiley and Sons, New York, 1956).
10. Mendel Sachs, Solid State Theory (McGraw Hill, New York, 1963).
11. Crawford Dunlap, An Introduction to Semiconductors (John Wiley and Sons, New York, 1957).
12. F. J. Morin and J. P. Maita, Phys. Rev. 94, 1525 (1954).
13. W. Shockley, Electrons and Holes in Semiconductors (D. Van Nostrand, Princeton, N. J., 1953), 1st ed., Chap. 7.
14. M. Shashkov and I. P. Akimchenko, Soviet Phys. Doklady 4, 115 (1959).
15. E. M. Conwell, Proc. IRE 46, 1281 (L958).
16. Richard Bube, Photoconductivity of Solids (John Wiley and Sons, New York, 1960), 1st ed., Chap. 3.
17. E. M. Conwell, Proc. IRE 40, 1331 (1952).
18. E. M. Conwell and V. F. Weisskopf, Phys. Ref. 77, 388 (1950).
19. G. W. Ludwig and R. L. Watters, Phys. Rev. 101, 1699 (1956).

20. M. B. Prince, Phys. Rev. 92, 681 (1953).
21. M. B. Prince, Phys. Rev. 93, 1204 (1964).
22. G. Backenstoss, Phys. Rev. 108, 1416 (1957).
23. W. R. Runyan, Silicon Semiconductor Technology (McGraw-Hill, New York, 1965).
24. R. H. Kingston, J. Appl. Phys. 27, 101 (1956).
25. J. Bardeen, Phys. Rev. 71, 649 (1947).
26. W. H. Brattain and J. Bardeen, The Bell Sys. Tech. J. 32, 1 (1953).
27. G. Bemski, Proc. IRE 46, 990 (1958).
28. R. N. Hall, Phys. Rev. 83, 228 (1951).
29. W. Shockley and W. T. Read, Jr., Phys. Rev. 87, 835 (1952).
30. R. N. Hall, Phys. Rev. 87, 387 (1952).
31. J. R. Haynes and W. Shockley, Phys. Rev. 75, 691 (1949).
32. John Crank, The Mathematics of Diffusions (Clarendon Press, Oxford, England, 1956).
33. J. M. Taylor, Semiconductor Particle Detectors (Washington Butterworths, Washington, D. C., 1963).
34. J. P. Maita, J. Phys. Chem. Solids 4, 1546 (1958).
35. C. S. Fuller and J. A. Ditzenberger, Phys. Rev. 91, 193 (1953).
36. G. Backenstoss, The Bell Sys. Tech. J., 37 (3), 699 (1958).
37. K. G. McKay and K. B. McAfee, Phys. Rev. 91, 1079 (1953).
38. K. G. McKay, Phys. Rev. 94, 877 (1954).
39. R. L. Pritchard, G. E. Research Lab. Report No. 57-RL-1817 (1957).
40. H. Lawrence and R. M. Warner, Jr., The Bell Sys. Tech J. 39, 394 (1960).
41. G. L. Miller, W. M. Gibson, and P. F. Donovan, Annual Rev. of N. Sc. 12, 194 (1962).
42. J. L. Blankenship and C. J. Barkowski, I. R. E. Trans. on N. Sc. 7, 181 (1960).
43. W. H. Fonger, Noise in Electrical Devices (John Wiley and Sons, New York, 1957).
44. A. Van Der Ziel, Fluctuation Phenomena in Semiconductors (Butterworths, London, England, 1959).

CHAPTER 3

THE THEORY, FABRICATION AND PROPERTIES OF A LITHIUM DRIFTED SEMICONDUCTOR NUCLEAR PARTICLE DETECTOR WITH A LARGE SENSITIVE VOLUME

By Patrick Harrold Hunt

I. INTRODUCTION

The interaction of energetic particles and x-rays with solids have been used extensively to study the properties of these radiations. Only during the last two decades has the direct measurement of ionization in solids been a practical means of studying the incident particles. It has long been recognized that many advantages would be obtained if these measurements could be made in solids. These include (1) increase in sensitivity, i.e., a larger number of ions produced by the same energy particle as a result of the lower ionization energy in solids than in gases, (2) greater stopping power for penetrating radiation, and (3) little or no loss of energy by the incident particle in entering the detector, i.e., windowless operation.

The early work was carried out with diamond and the alkali halide crystals because of their insulating properties and relatively high purity. This early work was disappointing because trapping and recombination effects prevented efficient charge collection.[1,2,3]

In the early 1950's, McKay and McAfee[4,5] using hyper-pure germanium and silicon produced by the zone refining process and fabricating reversed-biased diode structures were able to produce a device capable of withstanding high electric fields at room temperature without excessive noise. The serious trapping and recombination problems associated with other materials were found to be absent in germanium and silicon. However, the thin depletion depths obtained resulted in a very poor counting geometry.

Since the depletion depth in a reversed-biased diode is proportioned to the square root of the resistivity and voltage, very high resistivity material capable of withstanding high voltages is required.

Due to the higher intrinsic resistivity of silicon as compared with germanium at room temperature (250,000 Ω-cm as compared with 60 Ω-cm), silicon is usually used. Commercially available silicon crystals have a maximum resistivity of the order of 1,000-10,000 Ω-cm. This limit is due to the unfavorable segregation coefficient of boron ($k = 0.8$)[6] which means boron is not readily removed from silicon crystals by multiple zone passes.

In order to achieve very high resistivities, the lithium drift process as developed by Pell[7] is used. Lithium atoms are drifted into a 'P' type silicon crystal (~ 100 Ω-cm) and compensate the excess acceptors present to form an intrinsic region in the crystal. The depth of this intrinsic region is controlled by the time and temperature of drift.

If a bias voltage is now applied across this intrinsic region, a very wide depletion depth can be obtained. An energetic charged particle entering this depletion layer breaks the co-valent bonds between the silicon atoms liberating electron hole pairs. Since both the electrons and holes are mobile, they move in opposite directions under the applied field until they reach the electrodes or until they recombine.

This flow of charge across the depletion region results in a voltage pulse in the auxiliary equipment connected across the detector. This charge pulse is proportional to the energy absorbed from the incident charged particle provided the average energy required to create an electron hole pair is independent of the energy and/or type of ionizing radiation.

The work included in this thesis discusses the theory of the depletion depth and the lithium drift process, and also proposes a theory for the charge collection efficiency of the detectors built. The experimental method of fabricating the detectors is given in some detail. Finally the experiment results obtained with the detectors are compared with the theory.

II. THEORY

If an N-type donor is diffused into a P-type semiconducting crystal, a P-N junction is formed inside the crystal. A field exists across the junction due to the electrons in the heavily doped N-type material diffusing into the relatively low concentration P-type material, and the holes from the P-type region diffusing into the N-type region. This results in a potential barrier, V_o, which prevents further flow of electrons and holes. A space charge region or depletion depth is formed, made up on one side of donors without a corresponding number of electrons and on the other by acceptors without holes. The space charge region must contain an equal number of positive donors and negative acceptors to maintain electrical neutrality. Since the concentration of the donors is large compared with the acceptors, the space charge region is much wider on the P-side of the junction than on the N-side.

The space charge width may be increased by reverse biasing the junction causing the electrons and holes to diffuse further away from each other.

Figure 1 shows a schematic of a P-N junction under reverse bias together with the associated depletion region.

Depletion Depth Theory For An Abrupt Junction

Poisson's equation for the depletion region may be written

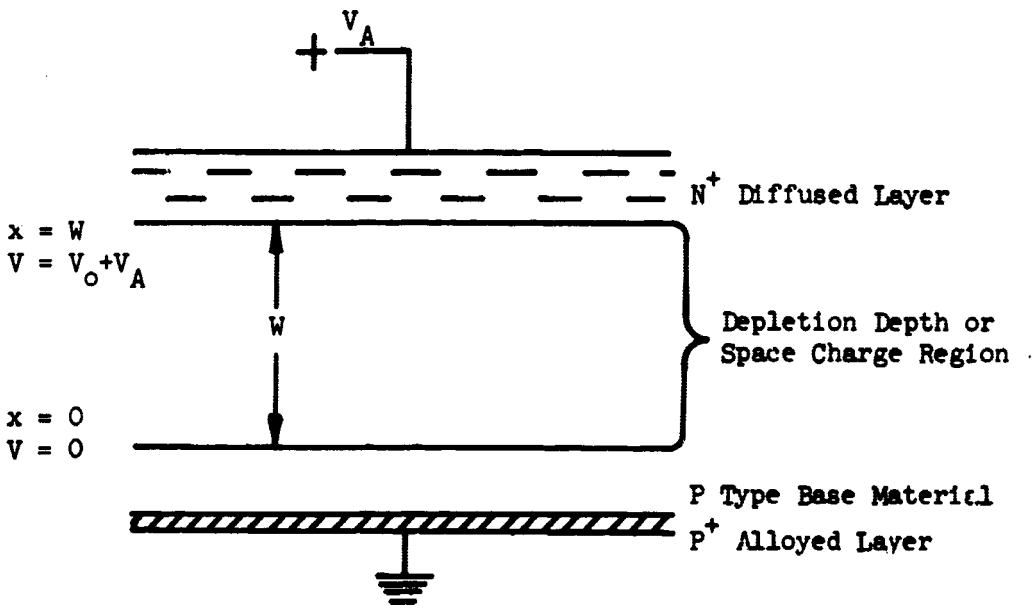

Fig. 1. Schematic Of A P-N Junction Under Reverse Bias.

$$\frac{\partial^2 V}{\partial X^2} = \frac{N_A q}{\epsilon} \qquad (1)$$

if N_A is constant

Where N_A is the acceptor density of the P-type material, q is the magnitude of the electronic charge and ϵ permittivity of silicon. The sign in the equation is positive since the charge on an ionized acceptor is negative. Integration of this equation yields

$$\frac{\partial V}{\partial X} = \frac{N_A q}{\epsilon} x + K_1 \qquad (2)$$

$$V = \frac{N_A q}{2\epsilon} x^2 + K_1 x + K_2 \qquad (3)$$

Assuming all the applied voltage is dropped across the depletion region, we may arbitrarily set the voltage to be zero at $X = 0$.

$$V = 0 \text{ at } X = 0 \qquad (4)$$

Also the field must be zero at this point i.e.

$$\frac{\partial V}{\partial X} = 0 \text{ at } X = 0 \qquad (5)$$

Substituting equations (4) and (5) into equations (1) and (2) gives

$$K_1 = K_2 = 0$$

or

$$V_x = \frac{N_A q X^2}{2\epsilon} \tag{6}$$

Thus at X = W

$$V_o + V_A = \frac{N_A q W^2}{2\epsilon} \tag{7}$$

where V_A is the applied voltage.

The resistivity 'ρ' of the P-type material is given by

$$\rho = \frac{1}{N_A q \mu_p} \tag{8}$$

or

$$N_A q = \frac{1}{\rho \mu_p} \tag{9}$$

substituting (9) into (7) one obtains

$$W = \sqrt{2\epsilon\rho\mu_p(V_o + V_A)} \tag{10}$$

The reversed biased diode acts as a parallel plate condenser of a capacity C where

$$C = \frac{\epsilon A}{W} \tag{11}$$

and A is the area of the junction.

Substituting equation (10) into (11)

$$C = A\sqrt{\frac{\epsilon}{2\rho\mu_p(V_o+V_A)}} \tag{12}$$

Under these conditions for P-type material the widths of the space charge region is given by

$$W = \sqrt{10^{-9}\rho(V_o+V_A)} \tag{13}$$

on substituting the appropriate values of μ_p and ϵ. In practice the built in potential barrier V_o is small (< 1 volt) and may be neglected for a large applied bias, hence

$$W = \sqrt{10^{-9}\rho V_A} \tag{14}$$

If carriers are generated within the space charge region, for example, by an energetic charged particle interacting with the valence electrons and lifting them into the conduction band, these carriers will be swept out of the space charge region by the applied field and result in a pulse of charge in any circuit connected across the junction.

Commercially available high purity silicon contains at least 0.1 to 0.2 parts per billion of boron after vacuum float zone refining. This is equivalent to a resistivity of approximately 2000 Ω-cm. Using this resistivity and an applied bias of 2000 volts it is readily seen that the width of the space charge region is only 0.6 mm. This

width would be useless for attempting to completely absorb very high energy (200 Mev) protons, since in all practical cases the beam diameter is normally at least 1 mm and a large proportion of the protons which did enter the sensitive region would be scattered out of the region and their full energy loss not recorded by the detector. Detectors having a greater space charge width may be made by drifting lithium into the silicon.

The Lithium Drift Process

In order to obtain space charge regions with very much greater depth Pell developed the lithium drift process whereby the P-type regions in the device's could be compensated to a much higher resistivity with ionised lithium atoms.

Theory Of The Lithium Drift Process

The theory of the lithium drift process was developed by Pell[7] as a means of studying the drift-diffusion process.

The Li^+ ion acts as a donor in P-type silicon, the latter being produced by the addition of boron during crystal growth. If it is assumed (a) that the acceptor impurity boron is distributed uniformly throughout the silicon at a level of N_A atoms/c.c. (b) that a p-n junction is formed at a distance $X = C$ in the material by the diffusion of lithium from a surface source of N_o atoms/c.c. ($N_o \gg N_A$) into the silicon, reaching a depth at which the number of diffused donors is equal to the number of acceptors present, or when

$$N_A = N_D = No\ \mathrm{erfc}\left[C/2(D_o t_o)^{\frac{1}{2}} \right]^2 \qquad (15)$$

as shown in Fig. 2.

Assuming D_o is independent of concentration, and the lithium does not interact with the other impurities present.

If a reverse bias is now applied to this N-P junction, an electrostatic field (E) will be present in the depletion region extending a short distance in both directions from X = C, The field will exert a force on the positively charged Li^+ ions tending to move them from the lithium rich side of the junction to the lithium deficient side. Provided the temperature is high enough to give the lithium ions sufficient mobility, μ, this movement or drift will occur in a reasonable time.

The number of Li^+ ions pe. cm^2 moved across the junction in time, t, will be given by

$$N = E\mu N_A t \qquad (16)$$

since the field exists only in the region where $N_A \approx N_D$.

In this case the Li^+ concentration will decrease for $x < C$ and increase for $x > C$. The Li^+ concentration cannot, however, fall below N_A for $x < C$ because the excess acceptors in such a region would change the depletion layer, increasing the field on the excess Li^+ side and decreasing it on the opposite side, causing the Li^+ to flow into the deficit region until the deficit disappears.

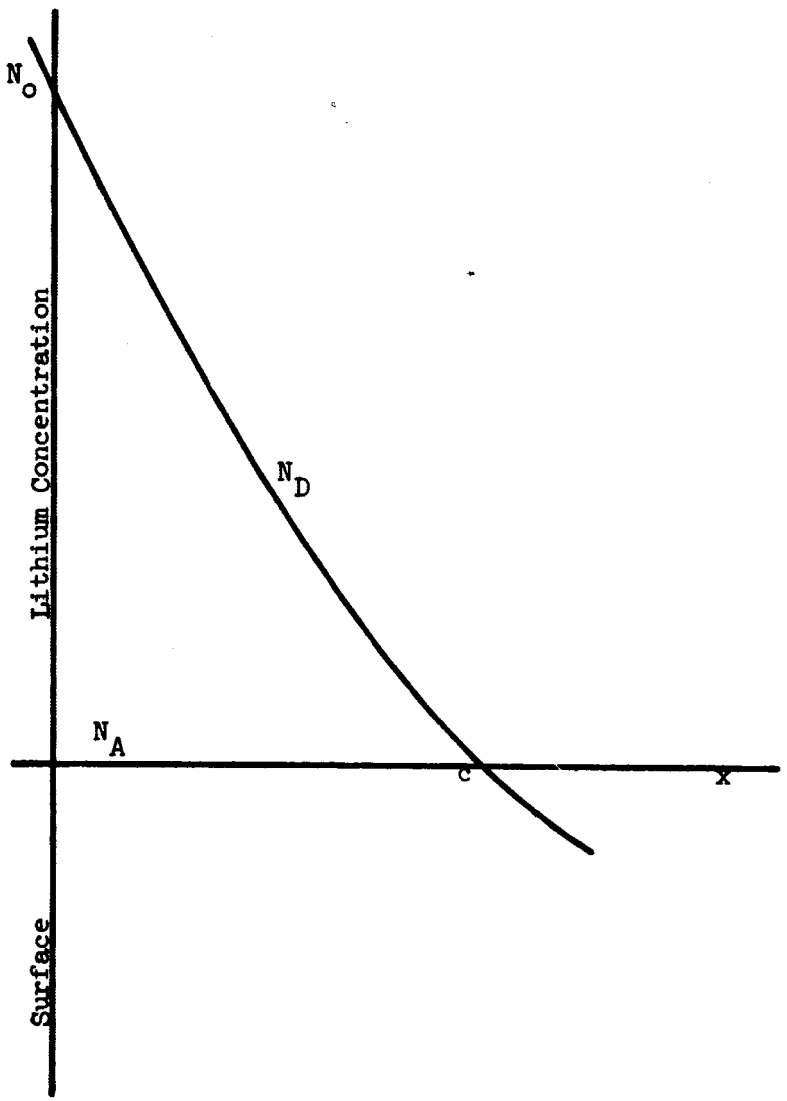

Fig. 2. Showing The Lithium Concentration Profile After Diffusion.

From similar reasoning, the Li^+ concentration cannot rise above N_A for $x < C$. As the value of N_D tends toward N_A for $x < C$ and rises toward N_A at $x > C$, an intrinsic region is produced extending the region in which the field E is present. This is shown in Fig. 3.

If it is assumed the abrupt change in N_D at the points $X = a$ and $X = b$ is vertical, then the amount of lithium drifted in time, t, is represented by the shaded area and is given by

$$\int_o^t E\mu N_A dt = \int_a^c N_D dx - (c-a)N_A$$

$$= (b-c)N_A - \int_c^b N_D dx \qquad (17)$$

Substituting the value of N_D from equation (15)

$$\int_o^t E\mu N_A dt = \int_a^c N_o \operatorname{erfc}\left[x/2(D_o t_o)^{\frac{1}{2}}\right] dx - (c-a)N_A \qquad (18)$$

Integrating by parts

$$\int_o^t E\mu N_A dt = \left[N_o x \operatorname{erfc}(x/2(D_o t_o)^{\frac{1}{2}}\right]_a^c - \frac{1}{2(D_o t_o)^{\frac{1}{2}}} \times$$

$$\int_a^c N_o\left(\frac{-2}{\sqrt{\pi}} e^{\frac{-x^2}{4 D_o t_o}}\right) x dx - (c-a) N_A \qquad (19)$$

This reduces to

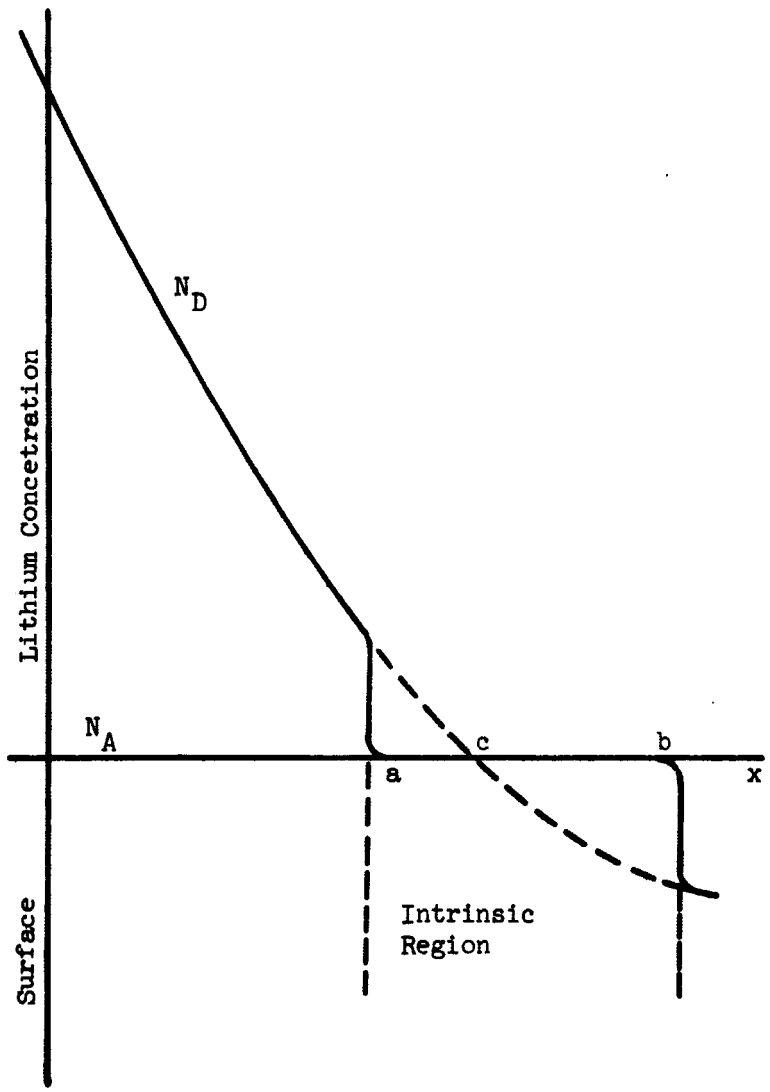

Fig. 3. Showing The Lithium Concentration Profile After Diffusion And Drifting.

$$\int_o^t E\mu N_A dt = N_o c \operatorname{erfc}(c/2(D_o t_o)^{\frac{1}{2}} - N_o a \operatorname{erfc}(a/2(D_o t_o)^{\frac{1}{2}}) + \frac{No}{\sqrt{\pi}} 2(D_o t_o)^{\frac{1}{2}} \left[e^{-\frac{a^2}{4 D_o t_o}} - e^{-\frac{c^2}{4 D_o t_o}} \right] - (c-a)N_A \tag{20}$$

If one considers the drifting process for a long time at constant applied voltage, then the intrinsic region moves back little into the steep region of N_D at $x < C$ and primarily grows in the region of $x > C$ where the accepter concentration is N_A which is very much less than N_D in the region of $x < C$. Defining

$$L = \frac{2 D_o t_o}{c} \tag{21}$$

For long periods of drift one can make the following approximations and assumptions

$$c = a \tag{22}$$

$$W = b - a \gg L \tag{23}$$

$$b - c \gg c - a \gg L \tag{24}$$

The asymototic series for the erfc of large argument is[8]

$$\operatorname{erfc}(x) \sim \frac{e^{-x^2}}{x\sqrt{\pi}} \left[1 - \frac{1}{2x^2} + \frac{1.3}{(2x^2)^3} \cdots \right] \tag{25}$$

Using this series to the second term in equation (20)

$$\int_o^t E\mu N_A \, dt \approx \frac{N_o}{c\sqrt{\pi}} C \exp\left[\frac{-c^2}{4D_o t_o}\right] \cdot 2(D_o t_o)^{\frac{1}{2}}\left[1 - \frac{4D_o t_o}{2c^2}\right]$$

$$- \frac{N_o a}{a\sqrt{\pi}} \exp\left[\frac{-a^2}{4D_o t_o}\right] \cdot 2(D_o t_o)^{\frac{1}{2}}\left[1 - \frac{4D_o t_o}{2a^2}\right]$$

$$+ \frac{N_o}{\sqrt{\pi}} 2(D_o t_o)^{\frac{1}{2}}\left[e^{\frac{-a^2}{4D_o t_o}} - e^{\frac{c^2}{4D_o t_o}}\right] - (c-a) N_A \qquad (26)$$

From equations (15) and (25)

$$N_A = \frac{N_o}{c\sqrt{\pi}} \exp\left(\frac{c^2}{4D_o t_o}\right) \cdot 2(D_o t_o)^{\frac{1}{2}}\left[1 - \frac{4D_o t_o}{2c^2}\right] \qquad (27)$$

Dividing equation (26) by (27) and rearranging terms this reduces to

$$\int_o^t E\mu N_A \, dt = \frac{c \cdot L}{c-L}\left[\frac{c^2}{a^2} e^{\frac{c^2-a^2}{4D_o t_o}} - 1\right] + a - c \qquad (28)$$

combining equations (22) and (24)

$$o \gg L \qquad (29)$$

and (28) reduces to

$$\int_o^t E\mu N_A dt = L\left[\frac{c^2}{a^2} \exp\left(\frac{c^2-a^2}{4D_o t_o}\right) - 1\right] + a-c \qquad (30)$$

Similarly the second equality of equation (17) reduces to

$$\int_o^t E\mu dt = b - c - L\left[1 - \frac{c^2}{b^2} \exp \frac{c^2-b^2}{4D_o t_o} \right] \qquad (31)$$

Since for the conditions under consideration $b - c \gg L$ (24) the exponential in (31) tends to zero and equation (31) reduces to

$$\int_o^t E\mu dt = b - c - L \qquad (32)$$

and approximating E by $\frac{V}{W}$

$$\int_o^t \frac{V}{W} \mu dt \approx b - c - L \qquad (33)$$

Combining equations (30) and (33)

$$L\left[\frac{c^2}{a^2} \exp \left(\frac{c^2-a^2}{4D_o t_o} \right) - 1 \right] + a - \phi = b - \phi - L.$$

or

$$b - a = W = L \frac{c^2}{a^2} \exp \frac{c^2-a^2}{4D_o t_o}$$

i.e. $$\frac{W}{L} = \frac{c^2}{a^2} \exp \frac{c^2-a^2}{4D_o t_o} \qquad (34)$$

but from (21)

$$L = \frac{2D_o t_o}{C}$$

$$\frac{W}{L} = \frac{c^2}{a^2} \exp \frac{(c-a).(c+a)}{2\,L\,c} \tag{35}$$

but since $c \approx a$ from (22)

$$\frac{W}{L} \approx \exp \left(\frac{c-a}{L}\right) \tag{36}$$

or

$$c = A + L \ell n \frac{W}{L} \tag{37}$$

Substituting (37) into (33)

$$\int_o^t \frac{V}{W} \mu dt = b - a - L \ell n \frac{W}{L} - L$$

But

$$b - a = W \quad (23)$$

$$\int_o^t \frac{\mu V}{W} dt = W - L - L \ell n \frac{W}{L} \tag{38}$$

Differentiating equation (38) with respect to 't'

$$\frac{\mu V}{W} = 1 - \frac{L}{W} \frac{dW}{dt} \tag{39}$$

or

$$\frac{dW}{dt} = \frac{\mu V}{W-L} \tag{40}$$

Integrating (40)

$$W^2 - 2LW = 2\mu V t + \text{constant} \qquad (41)$$

The integration constant must be determined experimentally. The integral is only approximate when integrated over short time intervals and when $E \neq \frac{V}{W}$, but holds for long time periods. When $L \ll W$, the square of the junction width should be proportioned to time. Pell has demonstrated that this indeed is the case.

Collection Characteristics Of The Detector

Consider a group of electron hole pairs liberated by a charged particle at distance, d, from the grounded side of the space charge region. If one assumes that the charges are all liberated simultaneously (i.e. the charged particle is stopped in zero time, or at least a time small compared with the time for the electrons and holes to drift across the depletion region), that the electrons liberated remain free for a time T_e before capture and that T_e is independent of the field E, then the range of the electrons is given by

$$\lambda_e = \mu_e E T_e \qquad (42)$$

Fig. 4. shows the electron-hole pairs liberated in the depletion layer. The symbol μ_e is defined as the mobility of the electrons, or velocity of drift in a unit field.

If we assume that, for an electron in the free state, the probability of capture is $\frac{dt}{T_e}$, and that at time t there are n electrons and at time t + dt there are n - dn electrons, then,

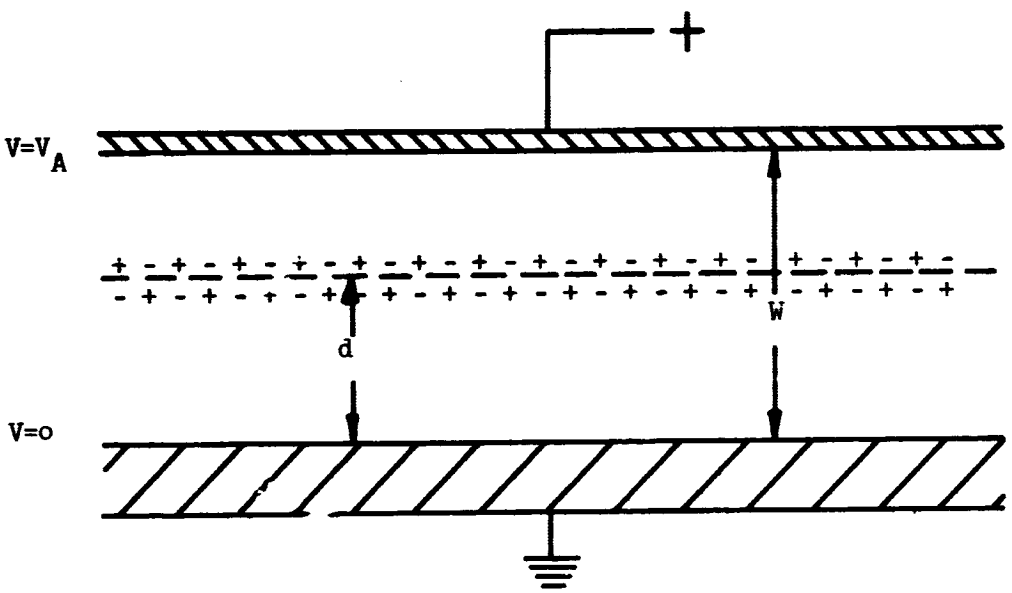

Fig. 4. Liberation Of Electron-Hole Pairs In The Depletion Layer

$$- dn = n \frac{dt}{T_e} \tag{43}$$

$$\int_{n_o}^{n} \frac{dn}{n} = - \int_{o}^{t} \frac{dt}{T_e} \tag{44}$$

where n_o is the number of electrons released at time t = 0 or

$$\left[\log_e n \right]_{n_o}^{n} = - \frac{1}{T} \left[t \right]_{o}^{t} \tag{45}$$

$$\log_e \frac{n}{n_o} = \frac{-t}{T_e} \tag{46}$$

or

$$n = n_o \, e^{\frac{-t}{T_e}} \tag{47}$$

If the n_o electrons are released at a distance W - d from the anode, then after travelling a distance X there will remain n where

$$n = n_o \, e^{\frac{-t}{T_e}}$$

$$= n_o \, e^{\frac{-X}{\mu_e E T_e}} = n_o \, e^{\frac{-X}{\lambda_e}} \tag{48}$$

Since

$$t = \frac{X}{\mu_e E} \quad \text{and where } \lambda_e = \mu_e \, E \, T_e$$

Thus the number of electrons which end their path in the range dx is

$$\frac{-dn}{dX} \, dX = \frac{n_o}{\lambda_e} \, e^{\frac{-x}{\lambda_e}} \, dn$$

The total distance drifted by the n_o particles is made up of two terms, the first is the distance drifted by particles which do not reach the anode, which is

$$\int_o^{W-d} x\frac{dn}{dx}\,dx = \frac{n_o'}{\lambda_e}\int_o^{W-d} xe^{-x/\lambda_e} \tag{49}$$

which reduces to

$$\int_o^{W-d} x\frac{dn}{dx}\,dx = n_o\left[\ \lambda_e\ (\ 1-e^{\frac{-W-d}{\lambda_e}}\ ) -(W-d)e^{-(W-d)/\lambda_e}\ \right] \tag{50}$$

and the second is the distance drifted by the $n_o e^{\frac{-W-d}{\lambda_e}}$ particles which do reach the anode, which is

$$n_o e^{\frac{-W-d}{\lambda_e}}\ (W-d) \tag{51}$$

Taking the sum of (50) and (51) and dividing by n_o to get the average distance travelled by the electrons, we find

$$\bar{x} = \lambda_e\ (1 - e^{\frac{-W-d}{\lambda_e}}\ ) \tag{52}$$

Thus the amount of charge observed by the detector due to the electrons is

$$Q_e = n_o\, e^{\frac{\bar{x}}{W}} \tag{53}$$

or substituting (52) into (53)

$$Q_e = \frac{n_o e}{W} \cdot \lambda_e \left[1 - e^{\frac{-W-d}{\lambda_e}} \right] \tag{54}$$

By similar reasoning the amount of charge observed by the detector due to the holes is

$$Q_p = \frac{n_o e}{W} \cdot \lambda_p \left[1 - e^{\frac{-d}{\lambda_p}} \right] \tag{55}$$

or the total charge collected by the detector is

$$Q_T = \frac{n_o e}{W} \lambda_e \left[1 - e^{\frac{-W-d}{\lambda_e}} \right] + \lambda_p \left[1 - e^{\frac{-d}{\lambda_p}} \right] \tag{56}$$

The times for the holes to reach the cathode is given by

$$\tau_h = \frac{d}{\mu_p E} \tag{57}$$

and the time for the electrons to reach the anode is given by

$$\tau_e = \frac{W - d}{\mu_e E} \tag{58}$$

The fastest collection time is obviously when $\tau_e = \tau_h$, i.e. when

$$\frac{d}{\mu_p E} = \frac{W - d}{\mu_e E} \tag{59}$$

or

$$\frac{\mu_p}{\mu_e} = \frac{d}{W - d} \tag{60}$$

For high resistivity silicon

$$\frac{\mu_p}{\mu_e} = \frac{1}{3} \quad (61)$$

or

$$d = \frac{W}{4} \quad (62)$$

Thus in the general case the shape of the voltage pulse will be shown in Fig. 5 if the decay constant of the associated circuitary is long compared with T_e and T_h.

In practice, however, the charged particle forms a very localized high density of electron-hole pairs or plasma[10] so dense that the electric field cannot penetrate it. Only the carriers located at the outside of the plasma are in a region of field and subject to drift. With increasing time, however, the field eats into the distribution and erodes it away at the edges, thus the plasma effect would serve to increase the collection time of the carriers beyond the simple transit time in the original field. An indication of an increase in collection time which may be attributed to this effect has been observed in fission fragment counting. The delay in separation of the interpenetrating clouds of holes and electrons may also increase the likelihood of loss of holes and electrons through recombination processes i.e. decrease T_e and T_h.

The plasma effect will result in a smoothing out and lengthening of the collection time and consequently the charge time curve will look as shown in Fig. 6.

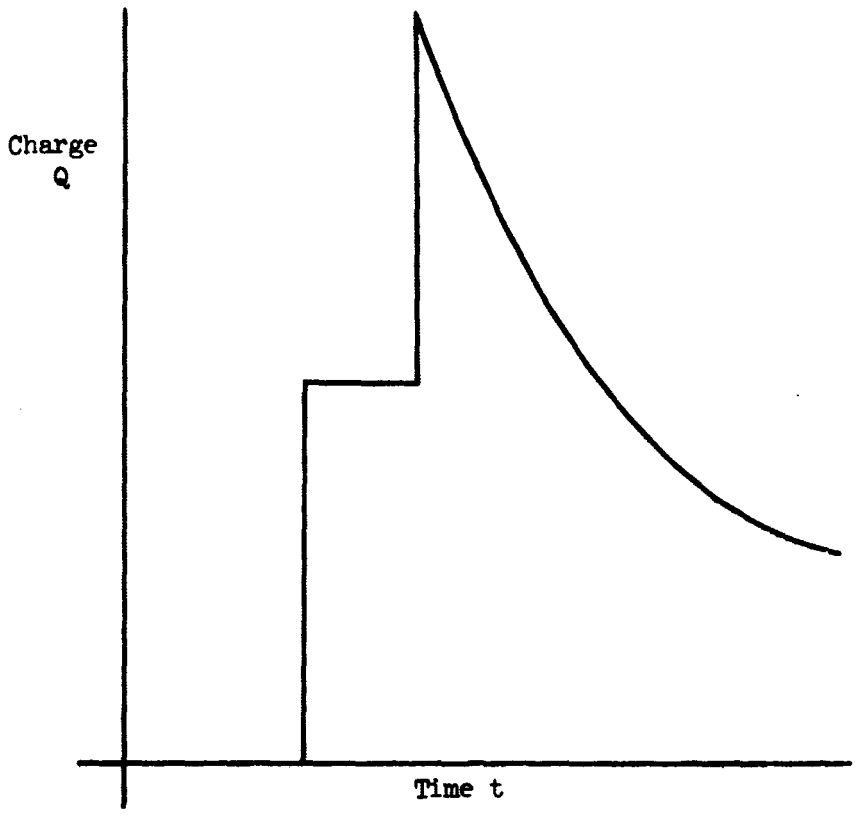

Fig. 5. "Ideal" Pulse Shape With No Interactions Between Electrons And Holes.

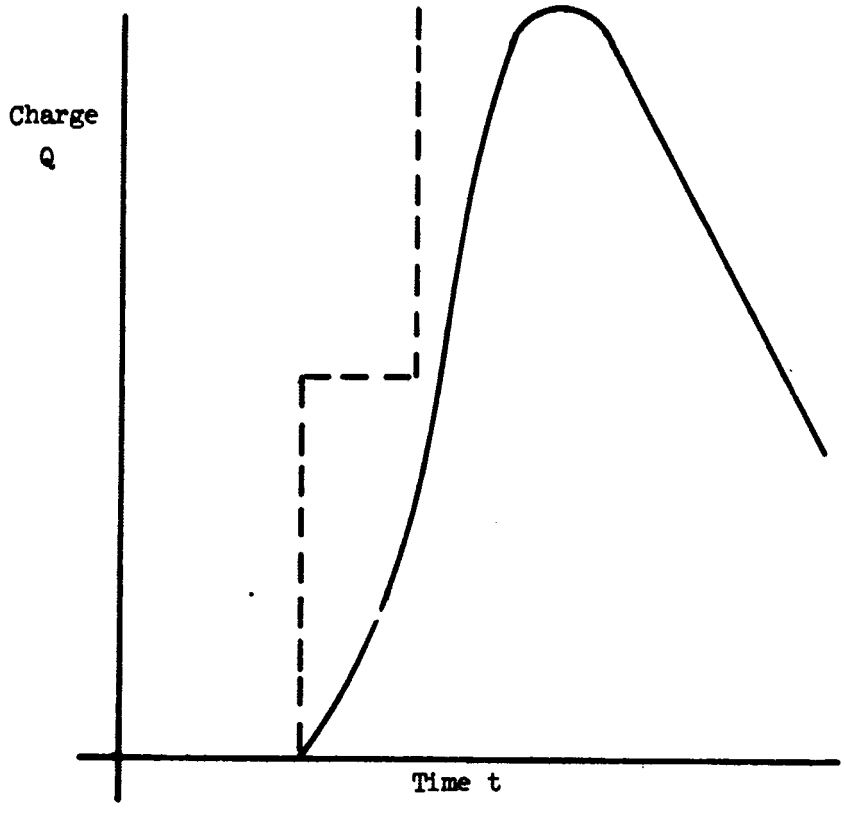

Fig. 6. Actual Pulse Shape With Interaction Between Electrons And Holes.

For a radiation detector with 0.5 cm depletion region and 2000 volt bias, the shortest collection time occurs when

$$d = \frac{W}{4}$$

or

$$d = 0.125 \text{ cms}$$

as is given by

$$T = \frac{0.125 \times 0.5}{500 \times 2000} \quad \frac{\text{CMS} \quad \text{CMS}}{\text{CM}^2 \text{ VOLT}^{-1} \text{ SEC}^{-1} \text{ VOLT}}$$

$$= 62.5 \times 10^{-9} \text{ secs}$$

$$= 62.5 \text{ nanosecs.}$$

The theory proposed assumes the mobility of the holes and electrons is constant at high fields. In practice the electron mobility in silicon appears to be constant up to 2500V/CM and the hole mobility up to 7500 V/CM[11,12]. For higher fields the mobility is proportional to $E^{-\frac{1}{2}}$ up to a few times 10^4 V/CM[13]. Thus in the example above, the electron mobility would in fact be lower than that assumed which would result in a longer collection time.

In the event that the electron and holes have a very long lifetime compared with the time it takes them to cover the space charge region i.e.

$$\lambda_e \text{ and } \lambda_p \gg W$$

Then equation (56) reduces to

$$Q_T = \frac{n_o e}{W} W - d + d \tag{63}$$

$$Q_T = n_o e \tag{64}$$

or the charge collected is independent of the position of liberation of the carriers.

Noise And The Limit Of Energy Resolution

In an ideal situation a charged particle of a given energy could give rise to a unique pulse in the detector, which when fed to a multichannel analyser, would store in one discreet channel. Thus if a mono-energetic beam of particles fell on the detector, pulses would only be observed in one channel in the analyser, and all other channels would be empty.

In practice this ideal situation is never achieved and a monoenergetic beam of particles is stored in several channels forming a peak in the analyser, with, in generals, all channels below the peak containing some counts. The reasons for this are discussed briefly below.

(1) Statistical Limitations

As the ionisation process which takes place in the detector is a cascade one, the final set of events which produce the ion pairs commensurate with the particle energy will be independent of one another and consequently there will be some fluctuation in the number

of ion pairs produced for particles with a given energy.

It can be shown[14] that

$$\frac{\sigma}{\bar{q}} = \frac{\omega^{\frac{1}{2}}}{W} \tag{65}$$

where σ is the standard deviation in the number of ion pairs produced, $\bar{q}$ is the average collected. ω is the mean energy per ion pair and W the particle energy. Thus the resolution will improve as the mean energy/ion pair decreases and as the energy of the incedent particle increases.

(2) Scattering

The charged particle may be scattered out of the detector sensitive region at any time during its course through the detector. The only charge collected by the detector will be that due to the energy loss of the particle in the sensitive region, this will show up as a pulse in the analyser at a lower channel number than that when all the particle energy is lost in the sensitive volume of the detector.

(3) Incomplete Charge Collection

There will be some fluctuation in the number of charges that reach the electrodes depending on where in the body of the detector they were liberated. Equation (56) shows that Q is directly related to 'd' except in the case of infinite carrier lifetime.

In addition, fluctuations will occur due to recombination in the region of the particle track after the charges have moved such a short distance that their contribution to the signal is negligible.

In the region of the plasma where no field exists, it is conceivable that the charges will recombine without moving at all in the direction of the electrodes.

(4) Noise

Electrical noise is present in all circuits even at room temperature. Four types of noise are prevalent in semiconductor devices.

(i) Thermal or Johnson noise which is caused by variations in the spatial distribution of carriers due to thermal diffusion.

(ii) Current or Shot noise due to statistical fluctuations in the number of carriers leading to changes in resistivity.

(iii) Generation - Recombination noise due the generation and recombination of carriers in the bulk material which traverse only part of the distance between the electrodes and so contribute current pulses which are shorter than those due to carriers which traverse the specimen completely.

(iv) Excess noise is as the name implies, current noise which is over and above the noise attributed to shot noise and generation and recombination noise.

Excess noise is associated in an unpredictable way with the nature of the contacts to the device as well as to the surface condition of the device.

Dearnaley and Northrup[14] show that for thermal noise, shot noise and generation-recombination noise the mean square noise voltage is inversely proportional to the device capacitance or some power of it.

Since the device capacitance is inversely proportional to

the applied bias, Equation (16), we see in general that as the applied bias is increased the noise level increases.

Thus as the field is increased to obtain faster pulses and higher charge collection efficiency the noise level also increases. Since a limit is reached in the rise time of the pulses and in the charge collection efficiency due to the mobility of the carriers decreasing above a certain field strength, a point is reached where the noise is increasing and the rise time of the pulses and the charge collection efficiency are decreasing.

In order to specify the resolution of a detector, so that the effect of the above variable are taken into consideration it has become standard practice to plot out the pulse height spectrum obtained from the detector when bombarded with monoenergetic particles and measure the full width of this distribution at its half maximum value. This is known as FWHM and is normally expressed as an energy.

III. PREPARATION OF THE DETECTOR

The experimental techniques used in fabricating the detectors were in general those described by Snow[15], but with some modifications. Use was also made of the nomographs of Blankenship and Borkowski[16] in calculating the depletion depth for various drift times and temperatures.

Silicon Crystal Preparation

Fairly stringent requirements are necessary on the starting material for the detector. As seen in theory, for good collection characteristics, a high carrier lifetime and high mobility together with a reasonably high resistivity are necessary. Factors which affect the lifetime are

(1) Heavy metal impurties which act as recombination centers[17].

(2) Dislocations and similar faults which also act as recombination centers[18]. In order to produce a silicon crystal with the best possible electrical characteristics a silicon rod was float-zone refined in vacuum five times. The heavy metals which adversely affect lifetime (notably gold and copper) have very low segregation coefficients[6] and consequently are readily removed from the silicon during the successive zone passes.

By processing in vacuum the N-type impurities, which have a relatively high segregation coefficient and consequently are not easily removed by multiple zone passes, are removed from the melt by

evaporation[19]. At the end of the five vacuum passes the rod was removed from the equipment and its resistivity measured, and was found to be in the range 450-500 Ω-cm P-type. This rod was then carefully cleaned in C.P. 5[1] etch rinsed thoroughly in deionised water and dried in an air oven at 200°C. The rod was then placed in a float-zone machine under an argon atmosphere and a silicon single crystal grown of Lopex[2] quality. The resistivity was again measured and found to be unchanged and in addition the minority carrier lifetime was measured by the photo conductive decay technique and found to be over 1000 μsecs.

This crystal was then cut into two slabs 15 cms long and 1 cm deep using a 30 mil thick diamond blade on a Do-All saw. The slabs of silicon were then cleaned by ultrasonically rinsing in trichloroethylene and deionised water, and then by boiling in H_2SO_4, HNO_3, and distilled water[15].

A thin film of aluminum was evaporated on the larger of the two flat faces and alloyed into the silicon at 600°C in a hydrogen atmosphere.

The Lithium Diffusion Process and Drift Process

A film of Lithium in oil suspension[3] was painted onto the

---

[1] CP comprises 1 part H.F., 1.5 parts HNO_3, 1 part CH_3COOH.

[2] Lopex is a trade name of Texas Instruments Inc. signifying silicon crystals with an oxygen content of less than 10^{16} ATOMS/CC and an etch pit count (for dislocations) of less than 500/SQ-CM.

[3] Obtained from the Lithium Corporation of America.

smaller flat face of the silicon slab to within approximately 1/16" of the edge.

The slab of silicon with the Lithium coated face uppermost was placed on a hot plate maintained at 400°C and covered with a Bell jar through which dry N_2 was flowing. The slab was kept on the hot plate for 5 minutes in order to allow the Lithium to diffuse from the Lithium in oil suspension into the silicon.

After the bars had cooled to room temperature the sheet resistance was measured and found to be 3.6 Ω/square. Previously samples of silicon of the same resistivity had been diffused under identical conditions, and lapped and stained to locate the position of the P-N junction. A measurement of the junction depth on these pilot samples gave a junction depth of 1.0 mm. From a knowledge of the junction depth and sheet resistance the surface concentration of the Lithium could be calculated at 10^{20} atoms/sq.cm which is more than adequate to compensate the P-type bulk material since if N_s is the surface concentration of the Li in atoms/sq. cm required to compensate the bulk material, N_A the acceptor concentration of the bulk material in atoms/c.c. and L the depth required for compensation in cms

$$N_S = N_A \times L \tag{66}$$

In our case $N_A \Xi 3.3 \times 10^{13}$ atoms/c.c. and L is 1 cm, thus N_S must be at least 3.3×10^{13} atoms/sq.cm.

In order to prepare the bar for drifting, the faces of the bar were masked with a 5:3 mixture of piecin and beeswax, the masking compound covering the Lithium diffused surface to within 1/16" of the edge of the Lithium diffused area.

The bar was then etched four times in a solution of 3 parts HNO_3; 1 part HF (analar grade) for five minutes, fresh solution being used for each etch.

The procedure for etching was found to remove approximately 30 mils from the silicon surface and kept the masking compound on the silicon surface. If longer etching times were used it was found the etch solution became warm and tended to "float" the masking compound off the silicon surface allowing the etch to attack the aluminum alloyed area and the Lithium diffused area.

After etching the masking compound was removed by placing the bar in boiling trichloroethylene for five minutes in three different solutions. The beaker and bar being thoroughly rinsed in cold trichloroethylene between each boiling.

After the final boil the bar was removed from the beaker with teflon coated tongs, wrapped in soft absorbent paper to dry and allowed to cool to room temperature. Fig. 7 is schematic of the detector shape at this time and Fig. 8 is a cross sectional view showing the various regions in the detector.

Once the detector was dry it was placed, Lithium diffused face uppermost, on a hot plate maintained at 130°C and covered with a teflon lined steel box. Access through the box was provided for

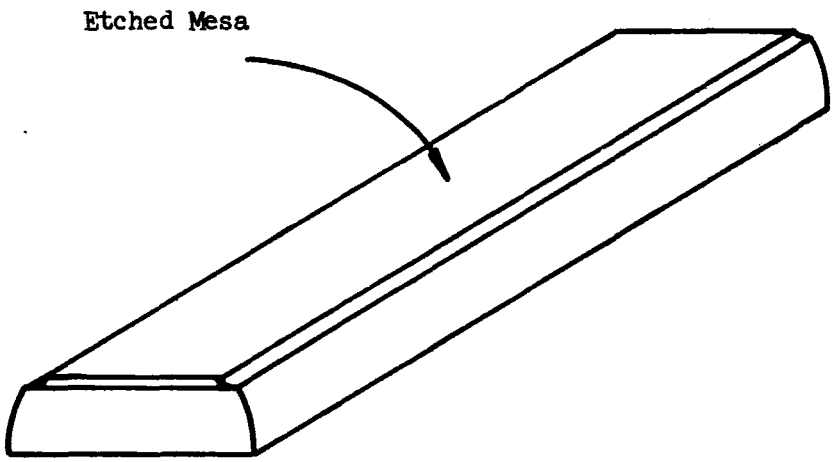

Fig. 7. The Silicon Slab after Diffusion and Etching.

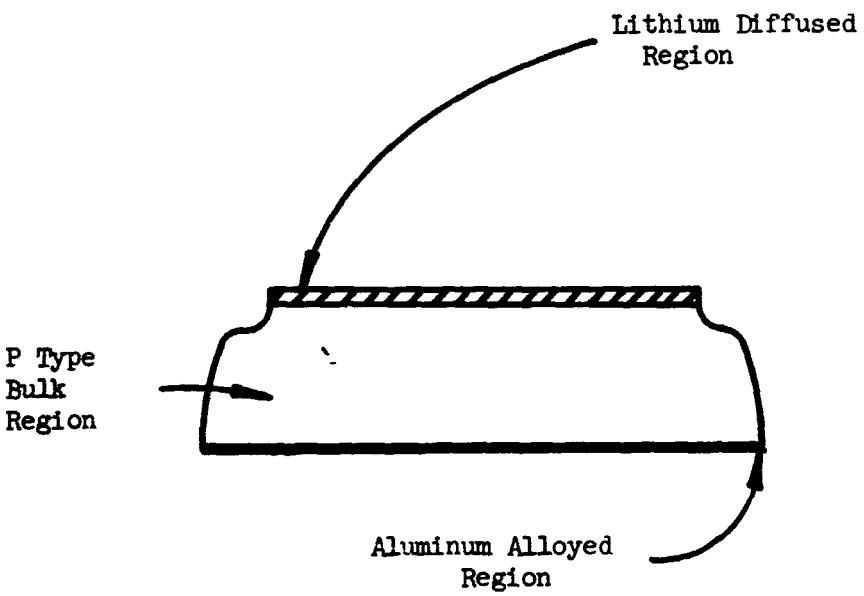

Fig. 8. End View of the Silicon Slab Showing the Various Layers.

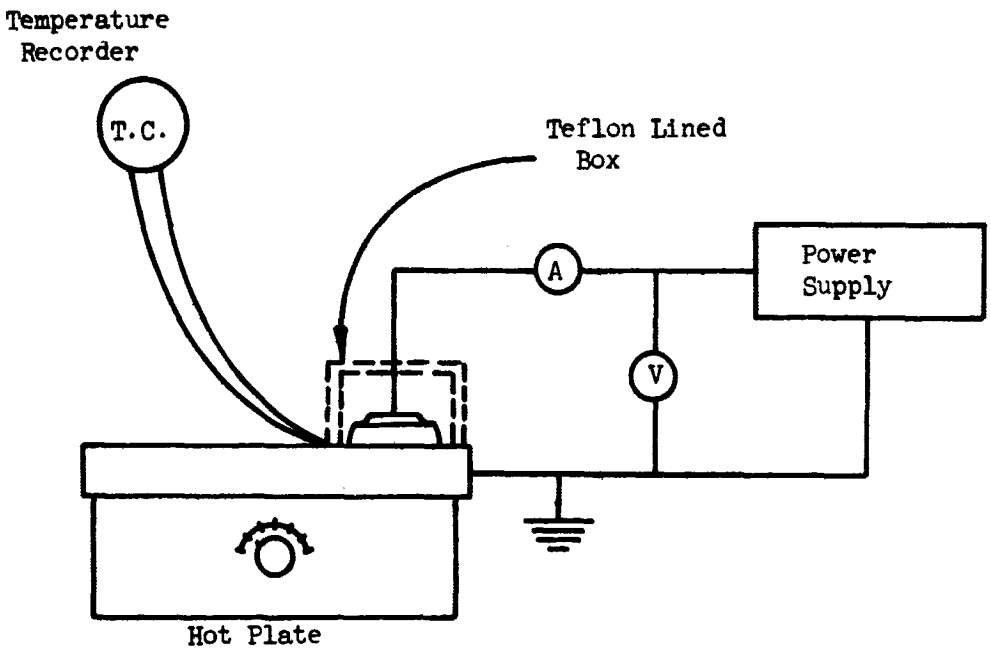

Fig. 9. Schematic Of The Drifting Equipment

a probe which could make a pressure contact to the Lithium diffused surface. The probe was connected to a high voltage D.C. power supply which had facilities for automatic voltage control and automatic current limitation. A Cu-Fe thermocouple was clamped to the top of the hot plate adjacent to the silicon slab and connected to a direct reading temperature meter. A schematic of the equipment is shown in Fig. 9.

The system was allowed to come to equilibrium then a positive D.C. potential of 340 volts applied to the probe. The bar was allowed to drift twelve days and four hours under these conditions, the current voltage and temperature being periodically checked during this time.

Using the nomograph of Blankenship and Borkowski, this is equivalent to a depletion depth of 7 mm.

The slab of drifted silicon was then taken and cut into a rectangular shape. The width being governed by the width of the mesa. For the detectors under consideration this width was 1.5 cms. After cutting, the dimensions of the detectors were 1.0 cm deep × 1.25 cms wide × 14.0 cms long.

The rectangular bar was cleaned, masked and lightly etched as described previously in order that the surfaces should be clean and free from contaminants. Once dry, all exposed surfaces except the aluminum alloy and Lithium diffused surfaces were coated with A thin layer of non conducting Epoxy[4] in order to maintain the

---

[4] No. 2500 resin and No. 21 hardener from Epoxy Products Inc., Irvington, New Jersey.

surface cleanliness.

The aluminum alloyed surface was mounted on a brass strip by means of a conducting Epoxy[5] and the strip in turn mounted on a B.N.C. fitting. Conducting Epoxy was spread over the top of the Lithium diffused surface and a thin copper wire connected from it to the center electrode of the B.N.C. fitting. Fig. 10 is a schematic of the completed detector.

---

[5]E-Solder 3021 Silver Epoxy from Epoxy Products Inc., Irvington, New Jersey.

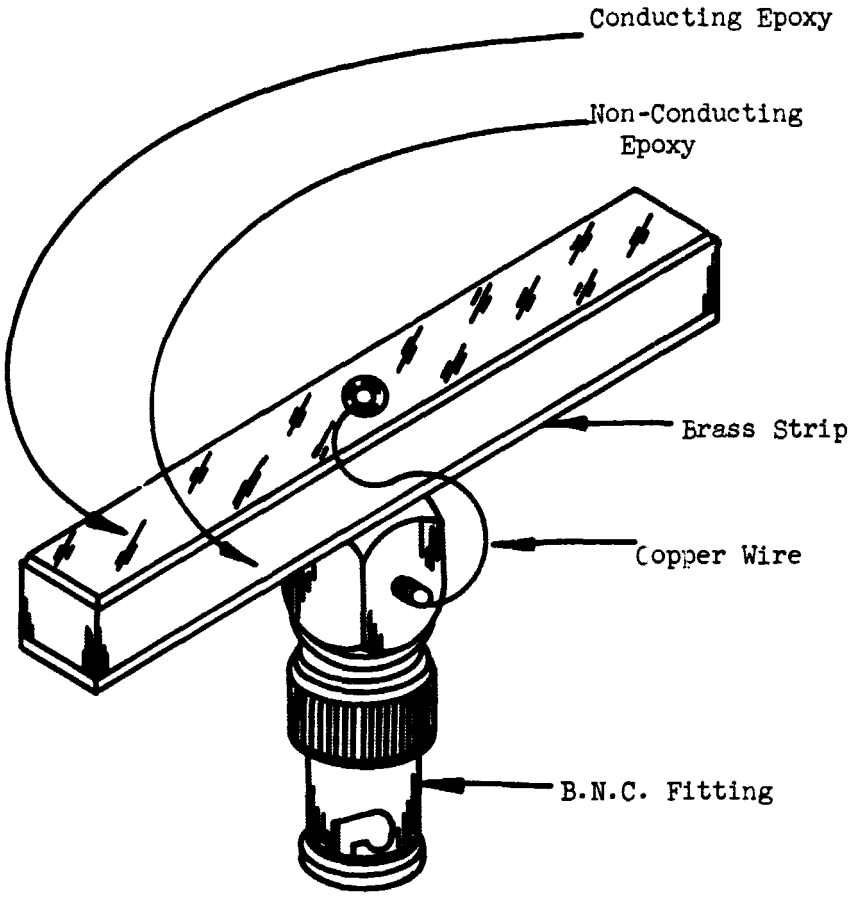

Fig. 10. The Assembled Detector

IV. ELECTRICAL MEASUREMENTS ON DETECTORS

Capacity Measurements

The capacity of the detectors at various bias voltages up to 600 V was measured using a General Radio L.C.R. Bridge. The bridge was first of all calibrated using a Tektronix Inc. S-30 Delta Standards capacity box and the stray capacity of the various adaptors used to connect the detector to the bridge were then measured. Finally the capacity of the detector as a function of bias voltage was obtained. The stray capacitance readings were substracted from the observed readings to obtain the true capacity of the depletion region.

Fig. 11 is a plot of capacitance against $V^{-\frac{1}{2}}$ which shows a very good straight line as predicted by theory (cf equation (12)).

Table 1 shows the values of the resistivity of this intrinsic region and the depletion depth calculated from the capacity measurements. The average of this resistivity was used to calculate the depletion depth and capacities for bias voltages above 600 volts.

Leakage Measurements

The diode characteristics of the detectors were measured on a Tektronix Type 575 Transistor Curve Tracer. The results for one of the detectors is shown in Fig. 12.

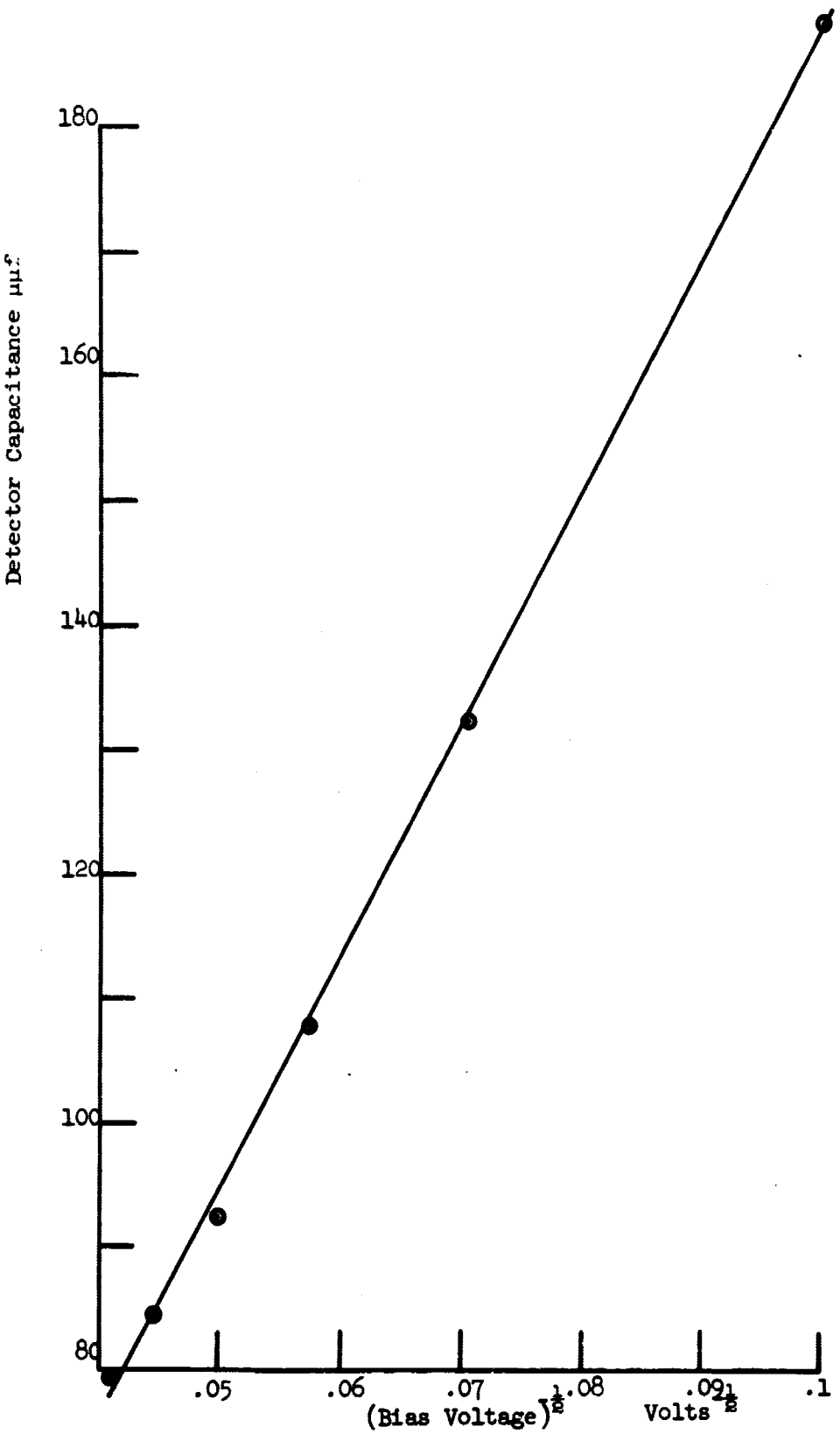

Fig. 11. The Detector Capacitance as a Function of the Reciprocal of the Square Root of the Bias Voltage.

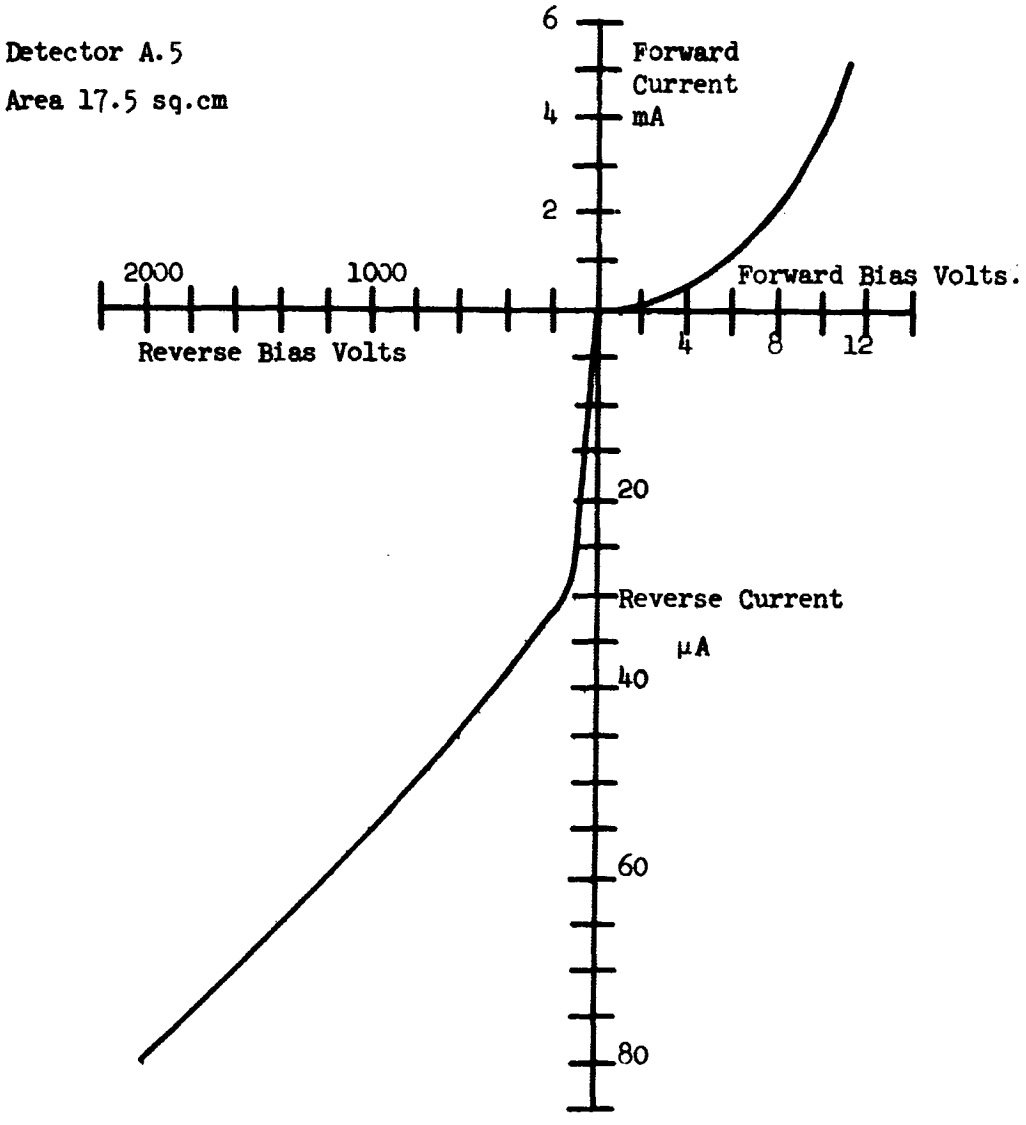

Fig. 12. The Diode Characteristics Of the Detector.

TABLE 1

DETECTOR CAPACITANCE, CALCULATED RESISTIVITY AND DEPLETION DEPTH AS A FUNCTION OF REVERSE BIAS VOLTAGE.

Detector Capacitance μμf	Bias Voltage Volts	Calculated Resistivity Ω-cm	Depletion Depth cms
188	100	3.93×10^4	.099
132.5	200	3.96×10^4	.140
108.0	300	3.96×10^4	.172
92.5	400	4.06×10^4	.201
84.5	500	3.90×10^4	.220
79.5	600	3.67×10^4	.234
61.9	800	3.91×10^4[a]	.300
55.4	1000	3.91×10^4	.336
46.8	1400	3.91×10^4	.397
45.3	1500	3.91×10^4	.410
42.5	1700	3.91×10^4	.437
39.2	2000	3.91×10^4	.474
35.0	2500	3.91×10^4	.531

[a] The average value of the calculated resistivity for voltages up to 600 volts was used to calculate the detector capacitance and depletion depth for voltage above six hundred volts.

V. USE OF THE DETECTORS

The detectors were used at Uppsala University in Sweden where 185.6 Mev protons were obtainable from the cyclotron, as part of a N.A.S.A. program to study the stopping power of different materials at various proton energies. In addition measurements were made on the detectors, to study their properties, which are reported below.

Fig. 13 shows a schematic of the experimental arrangement used. The detector was mounted in a light-tight box and connected to a Tennelic Model 1008 pre-amplifier, and the amplifier output fed to a R.I.D.L. multi-channel analyser. A Tektronix Type 545 oscilloscope was connected in the circuit in order that the voltage pulses from the preamplifier could be observed. The multichannel analyser was connected to an automatic typewriter and tape-recorder, so that the information contained in the analyser could be printed out or stored for later analysis. The system was calibrated using a pulse generator. The voltage pulses from the pulse generator were measured on an oscilloscope and fed to the preamplifier and the channel of the multichannel analyser observed in which the known voltage pulses stored. Knowing the input capacitance of the preamplifier it was possible to obtain a relationship between channel number and charge.

Fig. 14 shows the calibration curve obtained.

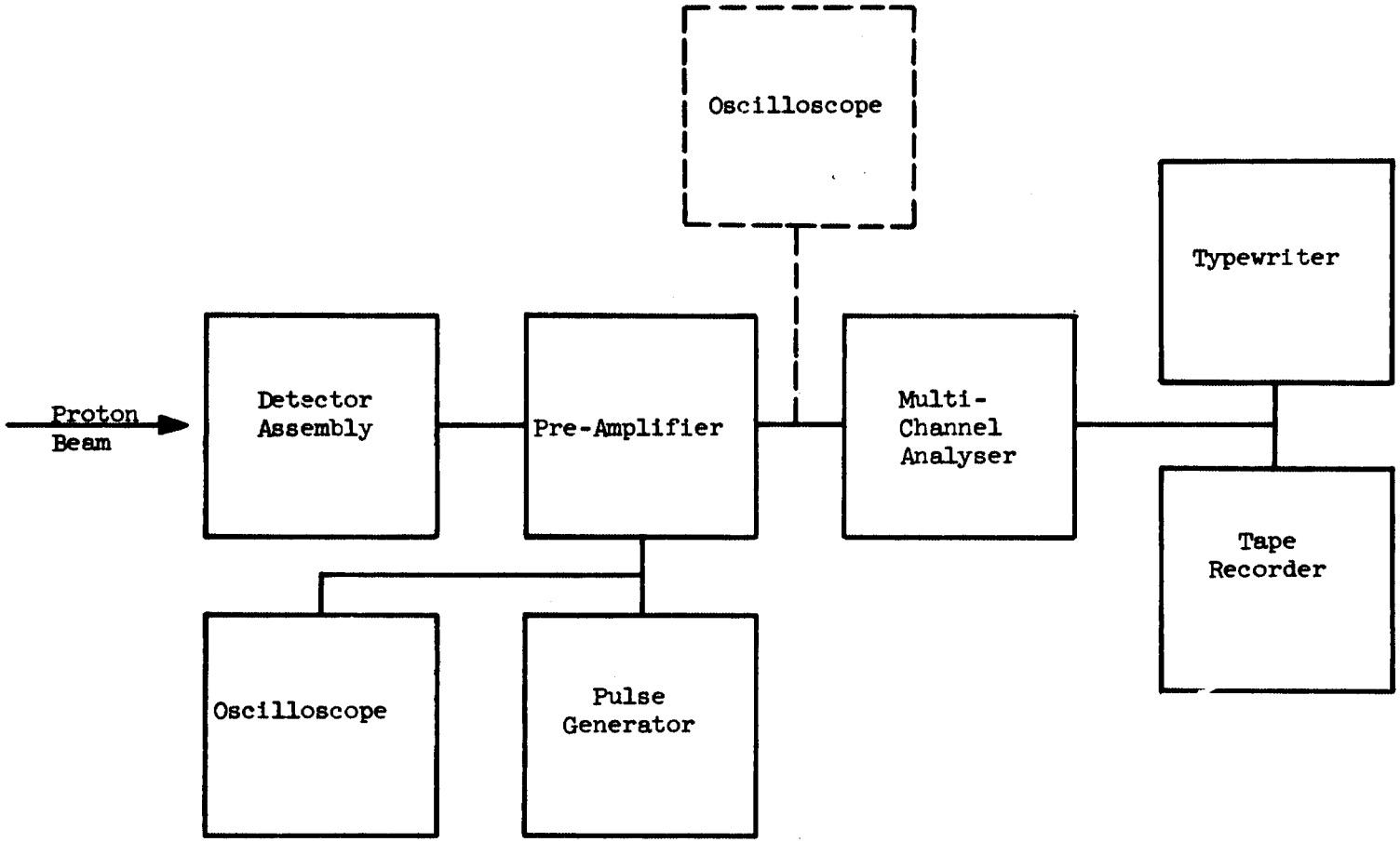

Fig. 13. Block Diagram Of The Equipment Used For The Bombardment Measurements

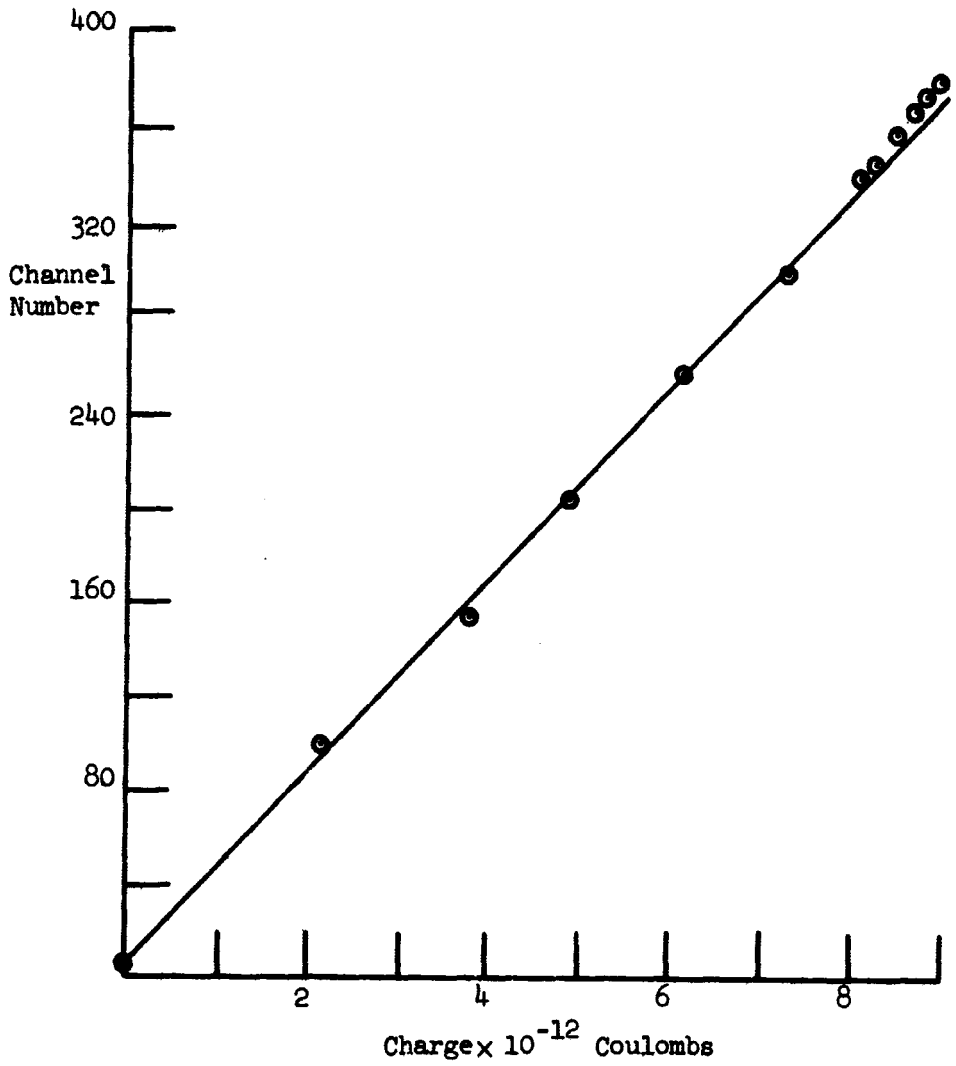

Fig. 14. Calibration Curve For The Multi-Channel Analyser.

The diameter of the proton beam was measured by using a Poloroid type 57 3000 speed film and found to be 1 mm. The detector was then carefully aligned in the beam, such that the beam entered the side of the detector perpendicular to its length and perpendicular to the direction of the applied field. Measurements were made at 1 mm intervals up the side of the detectors, so that the proton beam entered the detector at various distances from the bottom of the depletion region. Knowing the channel number in which the pulses stored, the charge collected for each beam position could be calculated. The proton energy loss in the 1.25 cm path length of silicon was 11.24 Mev[20].

In addition to the side measurements, the beam was totally absorbed along the detector length, and the charge collected for various bias voltages obtained.

In all cases the data from the multichannel analyser was analysed by a computer to obtain the stored channel number to the nearest one hundredth channel.

VI. RESULTS

1. Electrical Properties of the Detectors

The capacitance of the detectors built varied as the reciprical of the square root of the applied reverse bias voltage. This was predicted by theory (equation 12) and a plot of the results is shown in Fig. 11. The diode characteristics of the detectors is amply demonstrated by Fig. 12, showing a very low leakage current at high reverse bias.

2. Carrier Lifetime and Depletion Depth Measurements from Proton Bombardment Experiments.

The results obtained from the side bombardment of the detectors with protons gave a depletion depth or sensitive depth of ~ 5 mm. If the protons were allowed to strike the detector above or below this depth the count rate observed dropped to a very low level indicating most of the protons were striking the detector outside the sensitive volume. Bearing in mind the 1 mm beam diameter used the measurement of the depletion depth from the bombardment data is in close agreement with the 0.474 cms predicted from the capacity measurements at the operating voltage of 2000 volts.

The measurement of the electron and hole lifetimes depends on a knwoledge of 'p', the energy necessary to create an electron - hole pair. This is normally taken as 3.49 ev/ion

pair[15], however Tarrillion[21] has shown that 'p' is not constant but depends on the proton energy. The results obtained in this work also shows that 'p' varies with the energy lost in the detector. Assuming 100% charge collection when the beam hits the detector in the position which gives the maximum charge collection in both cases, values of 'p' ranging between 3.36 and 3.425 ev/ion pair were obtained for complete absorption of the 185.6 Mev proton beam, compared with values of 3.73 to 4.0 ev/ion pair when only 11.24 Mev was lost in the detector from the side bombardment measurements. Fig. 15 shows a plot of the various values of 'p' against the fraction of the proton energy lost in the detector.

Fig. 16 shows the results obtained with the side bombardment measurements. The results are for two detectors at three positions along the length of each detector. A value of 'p' of 3.49 ev/ion pair was assumed to obtain the charge ratio (the ratio of charge collected to charge liberated). The line drawn in each case is for the value of the charge ratio ($Q_T/n_o e$) calculated from equation (56). Assuming that T_e = 0.1μsecs and T_p = 1.0μsecs. These were the order of lifetime values that best fitted the results.

For the measurements when the 185.6 Mev protons were completely absorbed along the length of the detector careful alignment of the detector was made so that the maximum signal output was obtained when using the 2000 volt bias. A study was then made of the charge collected as a function of bias voltage with the beam entering the detector at a fixed position below the top of the depletion layer. This distance was assumed to be 1.25 mm's, in agreement

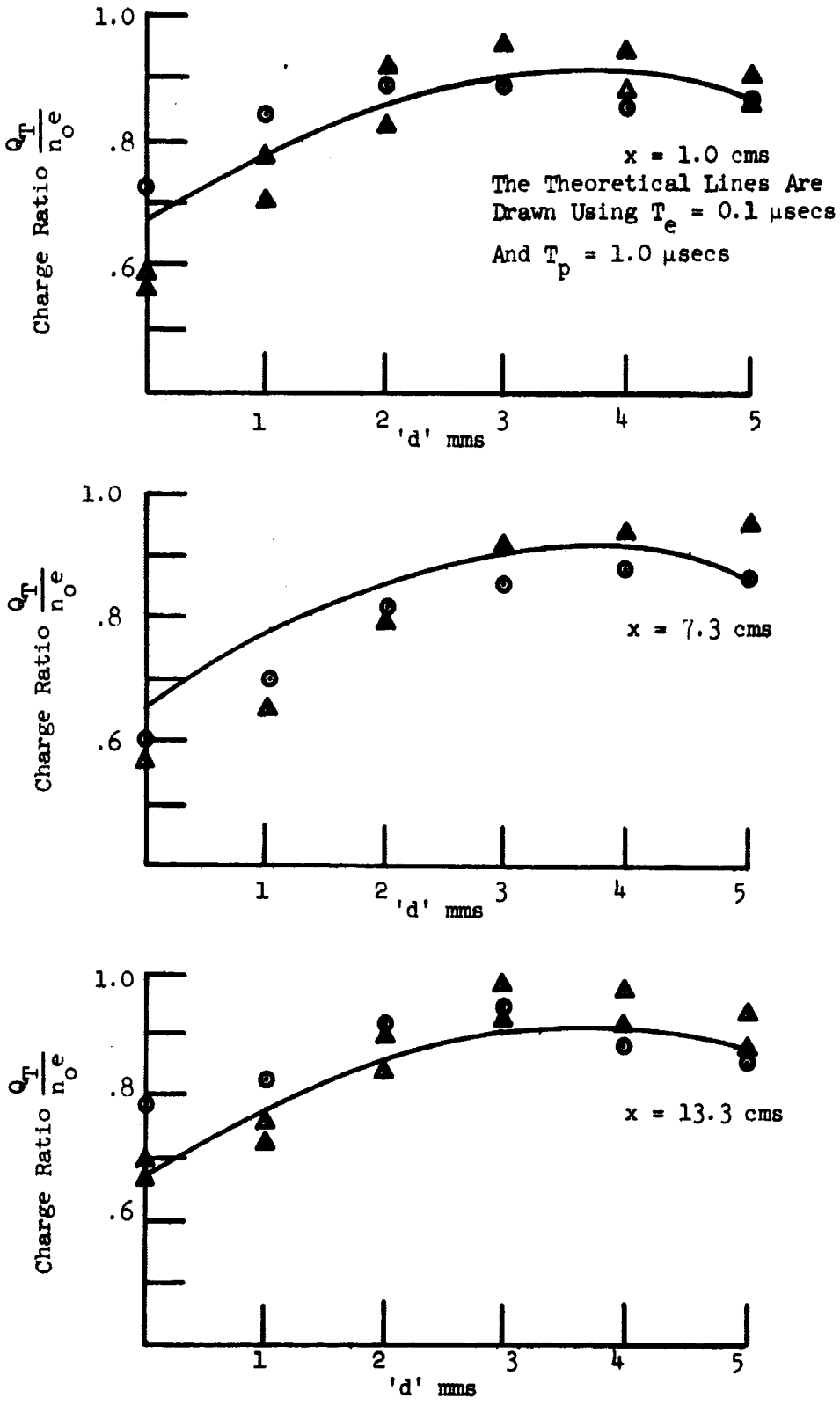

Fig. 16. Experimental Results From Side Bombardment Measurements On Two Different Detectors At Three Different Positions.

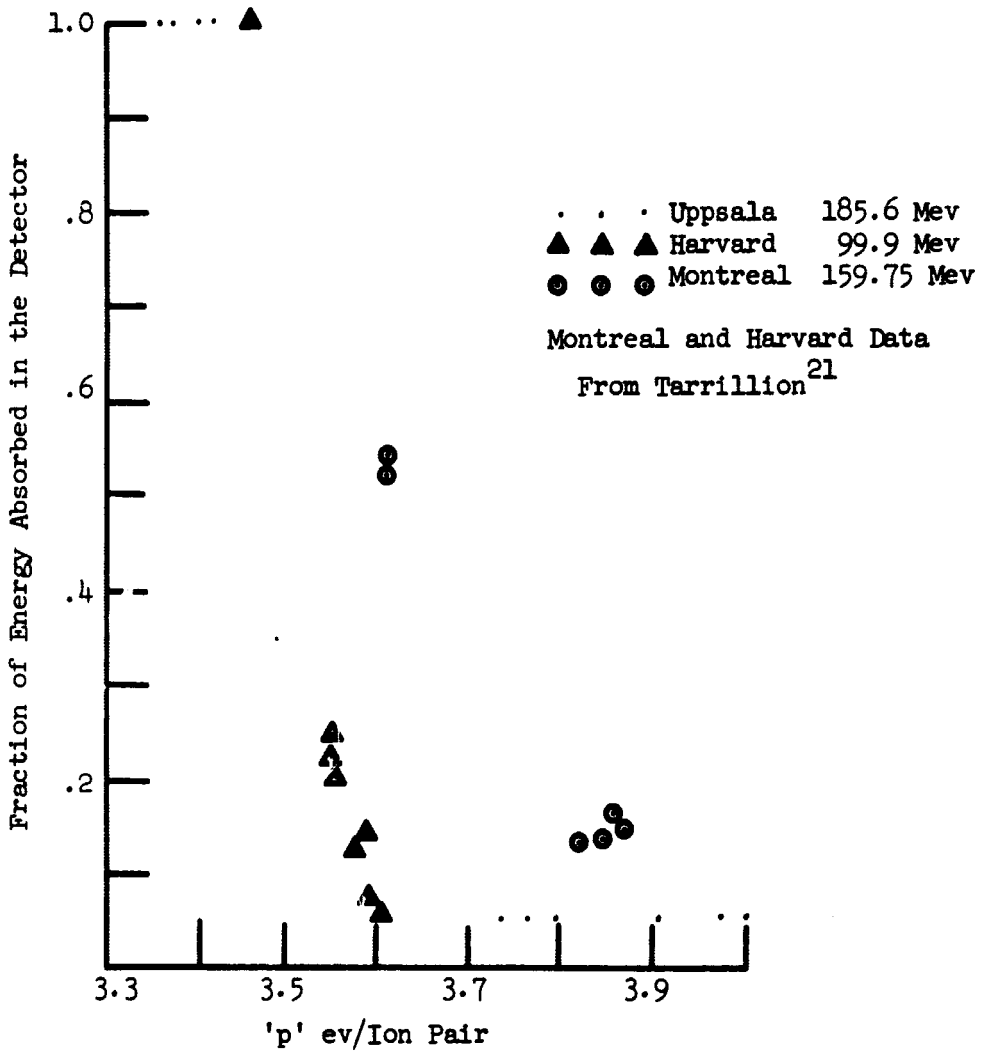

Fig. 15. Plot of the Various Values of the Energy Required for Electron-Hole Pair Formation as a Function of the Fraction of the Energy Absorbed in Various Detectors.

with the maximum charge collection position from the side bombardment measurements.

Fig. 17 shows the charge ratio as function of applied voltage for the end bombardment measurements. In this case a value of 'p' of 3.16 ev/ion pair was assumed to obtain the theoretical line shown. The value of 3.49 ev/ion pair for 'p' was not used in this case as more charge was collected than could have been liberated with that assumption. The value of 'p' used was obtained on the basis of a charge ratio of 0.92 for the 2000 volt bias condition, again in agreement with results observed from the side bombardment measurement.

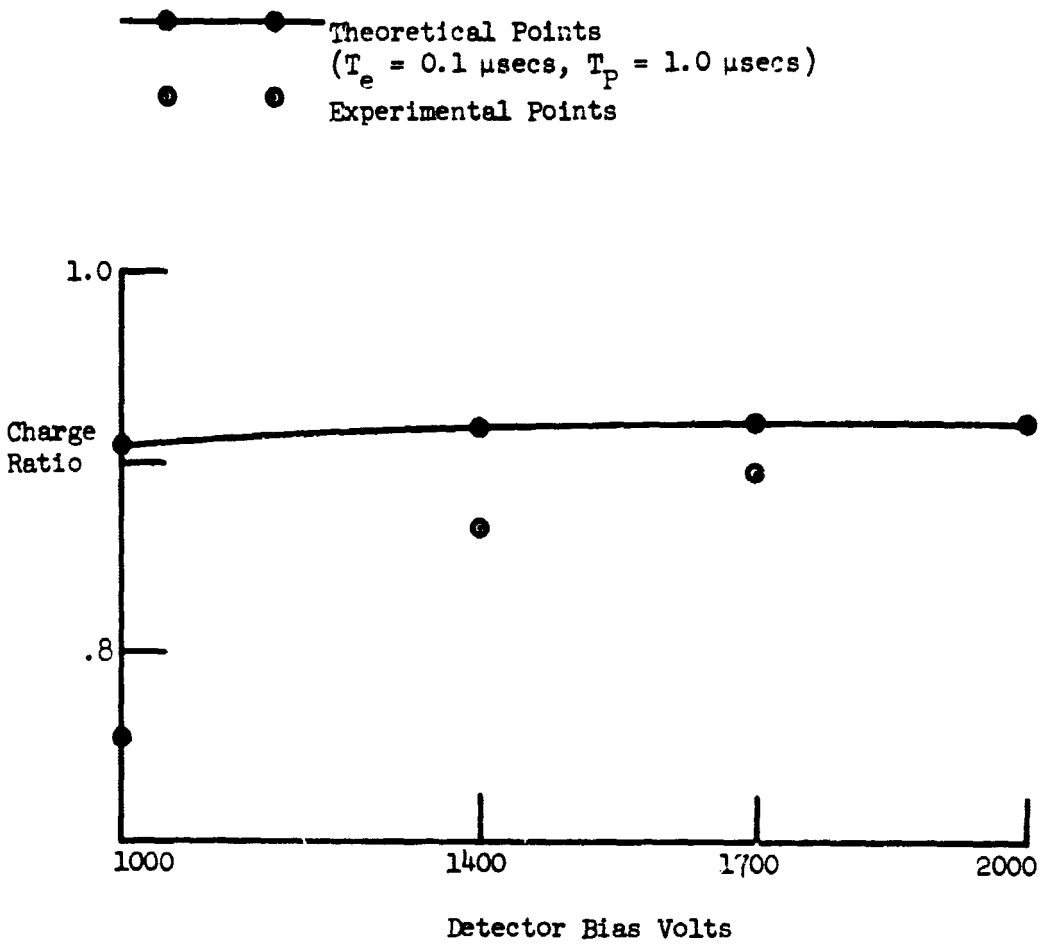

Fig. 17. Experimental Results Showing the Charge Ratio $\frac{Q_T}{n_o e}$ as a Function of Bias Voltage For Complete Absorption.

VII. DISCUSSION

The accepted theory as regards the depletion depth as a function of reverse bias for an abrupt junction (Equation 14) was shown to be applicable in the case of the Lithium drifted reverse biased diode. (Fig. 11) The Lithium drift process as developed by Pell[7] was shown to work quite well, but depletion depths as calculated by the nomograph of Blankenship and Borkowski were not observed for the conditions used. The results show that the compensation of the excess acceptors in the starting material is not complete at room temperature when the drift is carried out at 130°C. The calculated room temperature resistivity of 3.91×10^4 Ω-cm for the 'I' region of the detectors is approximately an order of magnitude lower than the room temperature intrinsic resistivity of 2.5×10^5 Ω-cm.

The 130°C drift temperature was chosen to give a reasonable drift time to obtain a 1 cm depletion on the basis of the nomograph. Better compensation would have been obtained if the Lithium drift had been carried out at a lower temperature or at least the temperature lowered for the last portion of the drift. Finally if the detectors could be stored at room temperature under high reverse bias for an extended period of time before use more perfect compensation could be obtained.

The model proposed for the charge collection characteristics

of the detectors has been substantiated by the experimental data. Fairly good agreement between theory and experiment is obtained on the basis of an electron lifetime of 0.1 μsecs, and a hole lifetime of 1.0 μsecs. These are very low values for the lifetimes of the electrons and holes considering the quality of the silicon used to fabricate the detectors. These low values can be explained by the formation of a very high density of holes and electrons along the track of the proton. The holes and electrons form a plasma which is so dense that the electric field cannot reach to the center of it immediately. With increasing time, however, the field extends into the plasma moving the carriers towards the electrode. During the time it takes the field to extend into the plasma, the electron and holes are in very close proximity and can easily recombine if an appropriate recombination center is available.

As can be seen from Fig. 17, the agreement between actual charge ratio and theoretical charge ratio as a function of bias voltage for complete absorption is not very good. However, as the bias voltage is decreased so is the depletion depth, and consequently the probability of the proton being scattered out of the sensitive volume is increased. This will result in lower charge collection, since all the proton energy is not absorbed in the sensitive volume.

VIII. CONCLUSIONS

The results obtained show that silicon semiconductor radiation detectors can be built quite successfully using relatively inexpensive equipment and fairly simple processes.

Depletion depths of the order of 0.5 cm were obtained. Deeper depths than this are possible if the Lithium drifing is done at a lower temperature, and for a longer time.

For 185.6 Mev protons interacting in silicon, the plasma density is high and the carrier lifetimes in the detectors are low. Values of the order of 0.1 and 1.0 μsecs were required for the electron and hole lifetimes respectively to account for the observed data. This resulted in a maximum charge collection efficiency of 92% in the region from 1 to 1.25 mm below the anode. At the anode, the collection efficiency was 87%. In the region from 0.5 mm to 2.0 mm, the charge collection efficiency was above 90%. As one goes deeper below the anode from 2.0 mm to 3.0 mm, the charge collection efficiency drops from 90% to 85%. At 4.0 mm, the charge collection has dropped to 78%. At the bottom of the depletion region, 4.8 mm, the collection efficiency is 67%.

The energy 'p' necessary to create an electron hole pair in silicon is not constant but depends on the proton energy.

The accepted value of 3.49 ev/ion pair formation in a silicon radiation detector is compatible with the 0.1 μsecs and 1.0 secs

carrier lifetimes and a 92% charge collection efficiency, for a loss in energy of a proton from 185.6 Mev to 174.36 Mev in the detector. If the proton loses all the 185.6 Mev in the detector then the average energy to create an electron hole pair drops to 3.16 ev/ion pair.

BIBLIOGRAPHY

1. Hofstadter, R. Nucleonics, 4, 2 (1949).
2. Chynoweth, A. G. Am. J. Phys. 20, 218 (1952).
3. McKay, K. G. Phys Today. 6, 10 (1953).
4. McKay, K. G. Phy Rev. 76, 1537 (1949).
5. McKay, K. G. and McAfee, K. B., Phy Rev. 91, 1079 (1953).
6. Runyan, W. R. Silicon Semiconductor Technology. McGraw-Hill, New York, 1966, Chapter 6.
7. Pell, E. M. J. App. Phy. 31, 2 (1960).
8. Schelkunoff, S. A., Applied Mathematics for Engineers and Scientists. D. Van Nostrand Co., New York, 1948.
9. Runyan, W. R. Silicon Semiconductor Technology. McGraw-Hill New York, 1966, Chapter 8.
10. Brown, W. L. I.R.E. Trans Nuc. Sci., NS8, No. 1, 2 (1961).
11. Ryder, E. J.Phys. Rev. 90, 766 (1953).
12. Prior, A. C. J. Chem. Phy. Solids 12, 175 (1960).
13. Tove, P. A. and Falk, K.Nuc. Inst. Methods, 12, 278 (1961).
14. Dearnaley, G. and Northrop, D. C. Semiconductor Counters for Nuclear Radiations. John Wiley Inc., New York, 1963.
15. Snow, Bobby D. Masters Thesis at Southern Methodist University.
16. Blankenship, J. L. and Borkowski, C. J., I.R.E. Trans. Nuc. Sci. NS9, No. 3, 181 (1962).
17. Bemski, G. Proc. I.R.E. 46, 990 (1958).
18. Kurtz, A. D. Kulin, S. A. and Averbach, B. L. Phys. Rev 101, 1285 (1956).
19. Bradshaw, S. E. and Mlavsky, A. I. J. Elect. 2 134 (1956).
20. Crawford, George W. Private Communication.
21. Tarrillion, Robert J. Masters Thesis at Southern Methodist University.

CHAPTER 4

THEORY OF ELECTRON - HOLE PAIR GENERATION AND COLLECTION OF CHARGE IN SILICON DETECTORS

By Robert John Tarrillion

The primary advantage of semiconductor over scintillation and gas detectors in nuclear particle spectroscopy lies in the improved efficiency with which particle energy is converted into an electrical signal.[1] The pulse amplitude from the semiconductor detector is directly proportional to the energy lost by the charged particle in the depletion region, that is, one electron-hole pair is produced for every 3.5 ev (for silicon) of energy deposited[2] as opposed to 35 ev for a typical gas. For particles that are completely absorbed within the silicon detector the pulse amplitude is linearly proportional to the incident particle energy. The amplitude is nonlinear for charged particles that pass completely through the detector. The greater the energy of the particle the less the energy absorbed by the detector. Measurements of the mean energy required to generate electron-hole pairs in silicon by ionizing radiations have been reported.[3-15] The value of ϵ is important because of its extensive use in dosimetry measurements,[2,16] and in nuclear particle identifying systems.[17-28] It is clearly worthwhile to investigate a possible dependence of ϵ on the energy of the incident proton as well as the total energy absorbed in the detector.

THEORY

In order to fully discuss the complex phenomena associated with the energy required to produce an electron-hole pair in silicon, discussion of the theory will be divided into five parts. These include: (1) Energy-loss process in a semiconductor; (2) Energy required for electron - hole pair formation in a semiconductor; (3) Shockley's model for ϵ; (4) Energy resolution in a semiconductor detector; and (5) Noise in a semiconductor detector.

Energy-Loss Process In A Semiconductor

The principal mechanism for the energy loss of charged nuclear particles passing through a solid is the ionization and excitation of the electrons of the solid owing to the interaction with the electromagnetic field of the moving particle. The energetic electron - hole pairs, which are produced by the primary particle, interact with the valence band electrons, thereby leading to the generation of new electron-hole pairs. In semiconductors this intrinsic impact ionization was first observed in the breakdown of silicon p-n junctions.[3, 29-32] The existence of an energy gap in a semiconductor gives rise to a minimum energy that an electron must have to produce an electron - hole pair by impact ionization. The existence of a threshold level for pair production is well established[3] and is illustrated in Figure I. On the other hand, according to Shockley's

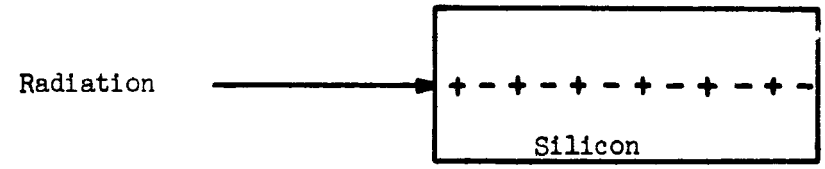

(a) Particle interaction in silicon.

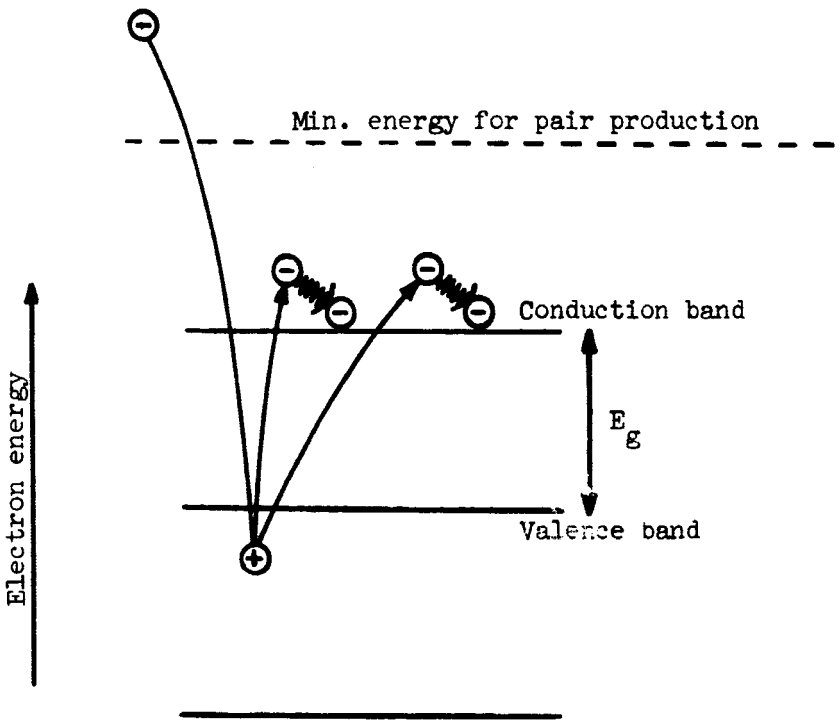

(b) Electron-hole pair production by impact ionization processes.

Fig. I. Formation of electron-hole pairs in silicon.

model,[33] instead of generating new electron - hole pairs, the electron (or hole) could begin at energies appreciably greater than the threshold energy, lose energy gradually by emitting phonons, and end up below the threshold energy without producing pairs. Shockley[33,34] has calculated the magnitude of this competing energy loss process (new electron - hole pair generation versus phonon emission) in silicon and the effect that it has in making the average energy deposited in the crystal per ion pair generated higher than the threshold energy for impact ionization. Shockley's model will be treated in more detail later on in the theory section.

In summary, the energetic particles incident on a semiconductor produce phonons and electron - hole pairs through a branching process, the mechanism of which is shown in FigureII.[35] An electron or hole created by the energetic particle can lose energy in two fundamentally different ways:

a. Creation of an electron - hole pair. The available energy (primary electron energy minus band-gap energy loss) is randomly shared by the degraded primary electron and the pair. The electron and the hole are assumed to share equally the energy given to the pair.

b. Phonon losses to the crystal lattice. These phonons arise from electrons having energies both above and below the band-gap energy.

Theoretically, the relative yield[35] of electron - hole pairs in semiconductors is defined by the ionization threshold energy E_{th} divided by the average energy per electron - hole pair ϵ

$$Y = \frac{E_{th}}{\epsilon} \qquad (1)$$

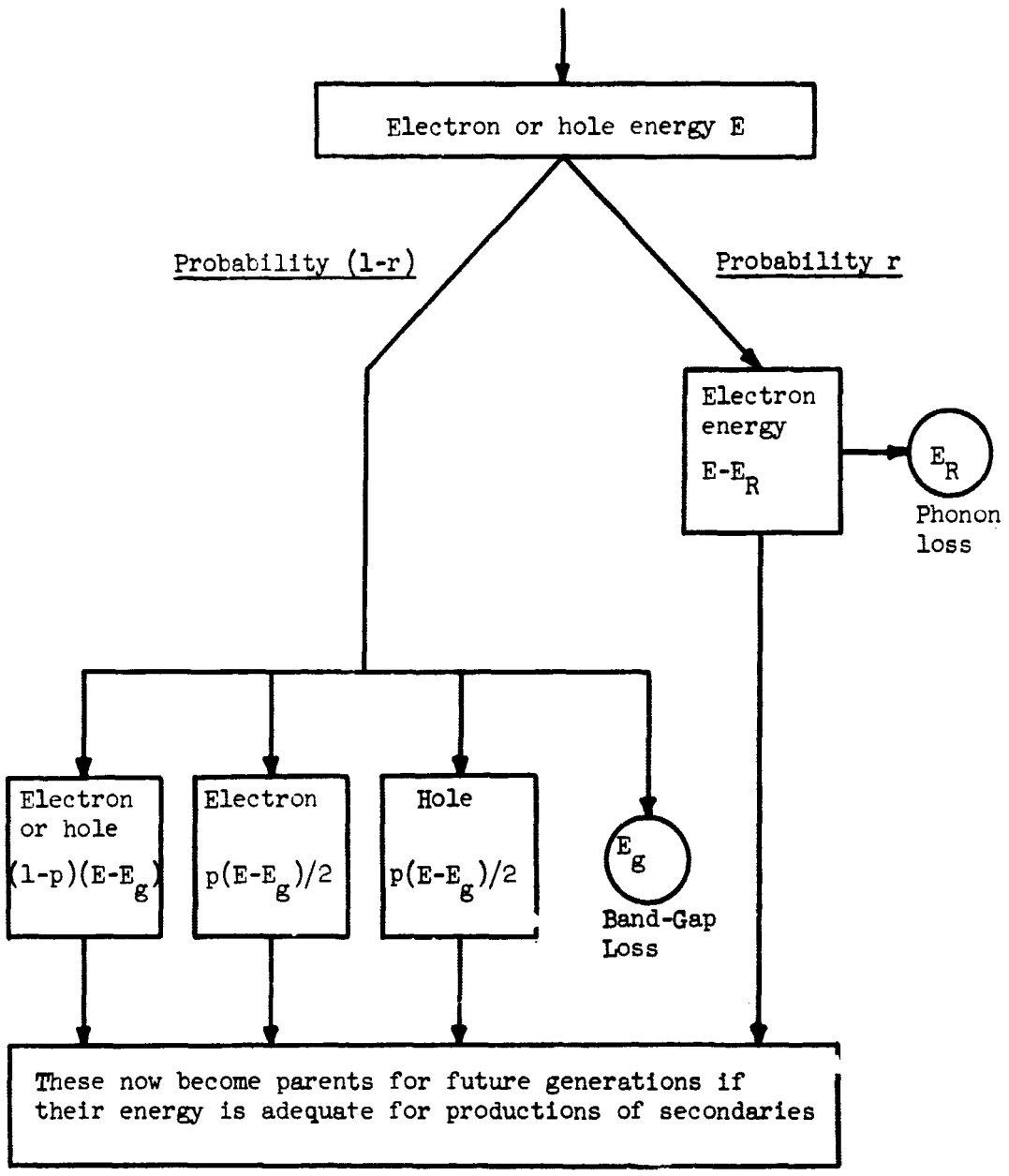

E_R = Raman phonon energy for the lattice,
E_g = Band-gap of the semiconductor, and
p = assumed random value from 0 to 1.

Fig. II Diagrammatic representation of the energy-loss process in a solid-state detector.

The statistical behavior of the energy - loss process is determined mainly at the end of the branching process, where most of the secondaries having an energy of just a few ionization - threshold units are generated.

Energy Required For Electron - Hole Pair Formation In A Semiconductor Detector

The track of the charged particle as it travels through the semiconductor will be essentially straight so that it creates a narrow cylinder of ionization in which the excited electrons and holes will rapidly lose their excess kinetic energy by impact ionization and phonon emission. The signal by which the particle will be detected and its energy measured is due to the separation of the electron - hole pairs around the particle track and their collection at the semiconductor electrodes as illustrated in Figure III.In order to observe the total charge created by the particle (a requirement for good spectroscopy), all the carriers must be swept out of the field region. The distance the carriers move can be characterized by their "Schubweg", λ_t, which is given by[36]

$$\lambda_t = \mu\phi\tau \qquad (2)$$

where μ is the carrier mobility, ϕ the electric field and τ the effective carrier lifetime. The collection time in an N.I.P. detector is strongly dependent on bias. Assuming a uniform field across the depletion region ($\phi = V/W$) and complete charge collection, we set $\lambda_t = W$ and $t_c = \tau$ in eq. (2) and obtain the approximate expression for the collection time in an N.I.P. detector:[37,38]

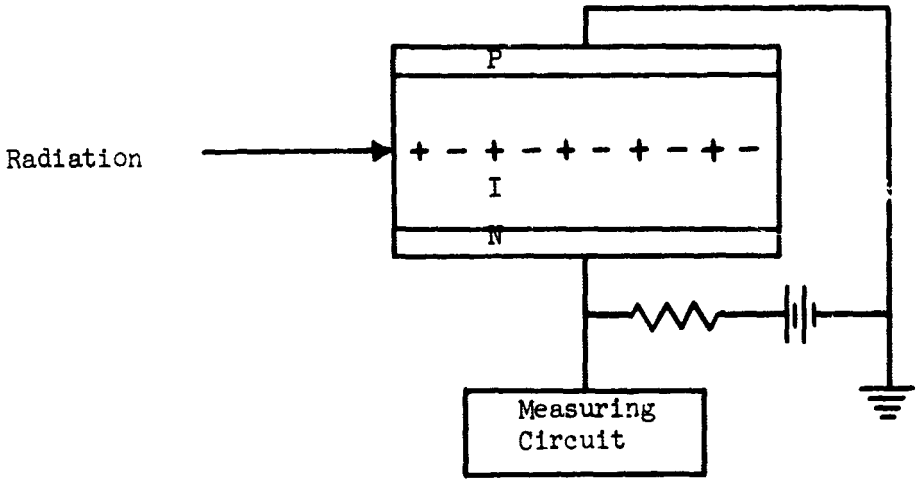

(a) Semiconductor detector with voltage applied. An incident charged particle creates electron-hole pairs.

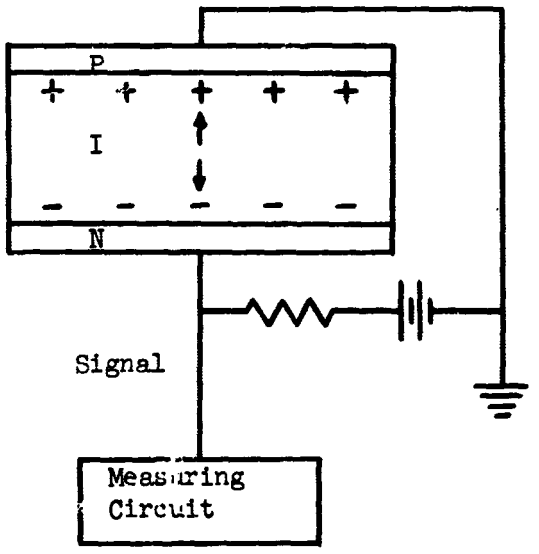

(b) The motion of the charged carriers induces charge on the electrodes, thereby producing an external signal.

Fig. III. Creation and collection of electron-hole pairs in a semiconductor detector.

$$W = \mu_p \frac{V t_c}{W}$$

that is,

$$t_c = \frac{W^2}{\mu_p V} \qquad (3)$$

where t_c = collection time (sec),

μ_p = hole mobility (cm^2 $volt^{-1}$ sec^{-1}),

W = depletion depth of detector (cm), and

V = applied voltage.

For W = 4 mm and a bias of 100 volts, eq. (3) gives t_c = 4 μsec for silicon. This is an upper limit for the charge separation process, and observed charge collection times are often much shorter. A long collection time may cause charge loss by recombination and may also prevent optimum adjustment of system parameters to give good energy resolution. In eq. (3), no allowance is made for the ambipolar effect,[39] which is important in the detection of fission fragments, nor is any allowance made for the reduced carrier mobility[40] in a high field.

For an understanding of the way in which the signal in an external circuit builds up as the electrons and holes are swept toward the electrodes it is necessary to consider the displacement currents due to the movements of individual charges. Each electron contributes a current $e\bar{v}/W$ when moving with a velocity $\bar{v}$ in the counter, inducing an identical current in the external circuit. This current ends abruptly when the electron is trapped or reaches an electrode. The signal is made up of square current pulses from both electron and holes, and any electron causes a charge to flow in the external circuit integrated over the total path of the carrier,

that is,

$$q = \int_0^{\frac{\lambda}{\bar{v}}} \frac{e\bar{v}}{W}\, dt \qquad (4)$$

If the carrier traverses the counter completely in however many stages, the limits of integration are zero and $W/\bar{v}$, so that the integral reduces to e. But if the carrier drift length λ is less than the specimen dimension, W, than the charge flowing in the external circuit is reduced proportionately to $e\lambda/W$. The total charge, $q_{tot.}$, is simply the sum of contributions given by equation (4) for all the charged particles.

The defining relationship for the charge collection efficiency, n, is given by

$$q_c = nq_g \qquad (5)$$

where q_c is the charge collected and q_g is the charge generated. With the assumptions of equal lifetime - mobility products for holes and electrons and a uniform electric field in the detector, we have the expression[13]

$$n = \frac{\mu\tau\phi}{W}\left[1 - e^{-(W/\mu\tau\phi)}\right] \qquad (6)$$

where μ = carrier mobility,

τ = carrier lifetime,

ϕ = electric field internal to the detector, and

W = active width of the detector.

Under sufficiently high electric field we may use a McClaurin expansion on equation (6). Hence, equation (6) becomes

$$n = \frac{\frac{\mu\tau\phi}{W}\left[e^{\frac{W}{\mu\tau\phi}} - 1\right]}{e^{\frac{W}{\mu\tau\phi}}}$$

$$n = \frac{\frac{\mu\tau\phi}{W}\left\{1 + \frac{W}{\mu\tau\phi} + \frac{1}{2}\left[\frac{W}{\mu\tau\phi}\right]^2 + \frac{1}{6}\left[\frac{W}{\mu\tau\phi}\right]^3 + \cdots - 1\right\}}{1 + \frac{W}{\mu\tau\phi} + \frac{1}{2}\left[\frac{W}{\mu\tau\phi}\right]^2 + \frac{1}{6}\left[\frac{W}{\mu\tau\phi}\right]^3 + \cdots}$$

$$n = \frac{1 + \frac{1}{2}\frac{W}{\mu\tau\phi} + \frac{1}{6}\left[\frac{W}{\mu\tau\phi}\right]^2 + \cdots}{1 + \frac{W}{\mu\tau\phi} + \frac{1}{2}\left[\frac{W}{\mu\tau\phi}\right]^2 + \cdots}$$

$$n \approx \frac{1}{1 + \frac{1}{2}\frac{W}{\mu\tau\phi}} \approx \frac{1}{1 + \frac{W}{\frac{2\mu\tau}{\phi}}}$$

$$n \approx \frac{1}{1 + \frac{\text{constant}}{\phi}} \qquad (7)$$

From equations (5) and (7) we see that we may plot $1/q_c$ versus $1/\phi$ and determine the true amount of change generated. Such plots are amply displayed in the literature.[12,13,41,42]

Instead of the charge collection efficiency, n, it is more appropriate to talk of ϵ, the average energy per ionized electron - hole pair, which is defined by the relation[43]

$$q = Ne = \frac{Ee}{\epsilon} \qquad (8)$$

that is, $$\epsilon = \frac{E}{N} = \frac{Ee}{q} \qquad (9)$$

where q = charge of pulse created by the absorption of the proton (or particle) energy E,

N = average number of ion pairs created by the absorption of proton energy E,

e = electronic charge = 1.60206×10^{-19} coulomb,

E = energy lost by the incident proton in the active region of the detector, and

ϵ = average energy in ev per ion pair.

Also, we have the expression[43]

$$\vartheta = \frac{Q}{C} \tag{10}$$

where ϑ = voltage pulse created by the incident proton (or particle) in the detector,

Q = total charge liberated by the proton in the active region of the detector, and

C = detector capacitance and external shunt capacities.

In terms of the electronic measuring circut, equation (10) can be written as

$$Vv = \frac{qA}{C} \tag{11}$$

where V = channel of the multichannel analyser in which the pulse is stored,

v = voltage per channel = 0.02045 volts, and

A = amplification factor of the electronic system

Substituting the value of q from equation (8) into equation (11) and solving for ϵ, we obtain

$$Vv = \frac{Ee}{\epsilon} \frac{A}{C}$$

that is, $\epsilon = \frac{eE\Lambda}{vVC}$ (12)

Shockley's Model For ϵ

A fairly simple model which explains several phonomena regarding ϵ has been developed by Shockley[33] and has led to new understanding of this subject. The earlier models had proposed that the most likely fate of an electron with energy just above the threshold energy was to create an electron - hole pair. Shockley's model states that electrons can begin at energies appreciably greater than the threshold energy, lose energy gradually by emitting phonons, and end up below the threshold energy without producing pairs. He also contradicted the earlier models by stating that when an electron - hole pair is created, the residual kinetic energy is shared more or less equally between the electron and the hole rather than being given entirely to one of the carriers. In particular, Shockley was interested in determining that energy which an electron must have for it to have an equal chance of producing an electron - hole pair or losing energy by phonon emission.[34] We will now consider some details of Shockley's model for ϵ.

For carriers in fields so high that secondary ionization processes are significant it is probable that the dominant scattering by phonons involves the phonons of the highest frequency.[30,40] The highest energy phonons are those in which the two face-centered cubic sub-lattices of the diamond structure are vibrating in opposite directions. The wave vector for this vibration has zero length and corresponds to the center of the Brillouin zone. The vibration is three-fold degenerate. This vibration has been referred to as the "Raman" vibration for the crystal. The energy

of a quantum at this frequency is denoted by E_R. Values of E_R have been determined by neutron diffraction for silicon by Palevsky et al.[44] The value for silicon is

$$E_R = 0.063 \pm 0.003 \text{ ev} \tag{13}$$

For non-vanishing vectors in the Brillouin zone, the energy decreases, falling to about 0.7 E_R at the edge of the zone. In the model treated here, the energy of the high-frequency phonons is taken as constant and equal to E_R. All collisions are considered to produce energy losses, which is a good approximation for silicon at room temperature with $kT < E_R/2$ so that the high-frequency modes are not excited. E_R is one of the four parameters of the model but since it is independently determined it is not an adjustable constant. The three adjustable constants are:

E_i = threshold energy measured from the band edge for a carrier above which it may produce a hole - electron pair,

L_R = the mean-free-path between scattering by "Raman" modes, and

$r = L_i/L_R$ where L_i is the mean-free-path between ionizations for a carrier with energy greater than E_i.

From the definition of r it follows that an electron with energy greater than E_i generates on the average r phonons per ionization.

When a high-energy particle such as a proton, B-ray, or even a fission fragment enters a silicon crystal, the high-energy particle dissipates its energy in the production of pairs of high-energy holes and high-energy electrons, which in turn can produce pairs in an energy cascade process.

The incident energy can be accounted for in three ways. Every pair-producing impact ionization consumes an amount of energy E_i from the kinetic energy of the system of carriers. In addition, in general, rE_R of energy is also converted to phonon energy before the ionization is produced. (It should be noted that most of the pairs are probably produced by carriers whose energy is only a few times E_i). After a carrier has been produced and no longer ionizes, it will have kinetic energy of motion, denoted by E_f, and called the final energy which it dissipates to phonons. It is evident that E_f will be of the order of magnitude of E_i since if a carrier is created just below energy E_i it will not be able to ionize and must dissipate E_i as heat. The same statement applies to a carrier which has reached E_i just after producing a hole - electron pair. In terms of the final energy E_f the energy to produce a pair is

$$\epsilon = 2E_f + E_i + rE_R \tag{14}$$

If we assume that the carriers as finally produced are equally likely to be anywhere in the Brillouin zone with energy less than E_i, then for parabolic energy surfaces, the average E_f for the volume in question is[45]

$$\langle E_f \rangle = \int_0^{E_i} Eg(E)\, dE \tag{15}$$

The total density of states, $g(e)$, is from free electron theory[45]

$$g(e) = \frac{8\pi v}{h^3} (2m^3)^{\frac{1}{2}} E^{\frac{1}{2}} \tag{16}$$

where v = volume in momentum space,

m = mass of the electron,

E = energy of the electron, and

h = Boltzman constant.

Substituting equation (16) into equation (15) and integrating, we obtain:

$$\langle E_f \rangle = \frac{8\pi v}{h^3} (2m^3)^{\frac{1}{2}} \int_0^{E_i} E^{\frac{3}{2}} \, dE$$

$$\langle E_f \rangle = \frac{2}{5} \frac{8\pi v}{h^3} (2m^3)^{\frac{1}{2}} \left[E^{\frac{5}{2}} \right]_0^{E_i}$$

$$\langle E_f \rangle = \frac{16\pi v}{5h^3} (2m^3)^{\frac{1}{2}} E_i^{\frac{5}{2}} \qquad (17)$$

The charge-carrier concentration, N, is given by[45]

$$N = \frac{16\pi (2m^3)^{\frac{1}{2}}}{3h^3} E_i^{\frac{3}{2}}$$

or

$$3N = \frac{16\pi (2m^3)^{\frac{1}{2}}}{h^3} E_i^{\frac{3}{2}} \qquad (18)$$

Substituting equation (18) into equation (17), we have

$$\langle E_f \rangle = \frac{3}{5} N v E_i \qquad (19)$$

Equation (19) gives the average kinetic energy for N carriers in a volume v. Hence, the average final kinetic energy of one carrier will be

$$E_f = \frac{3}{5} E_i \qquad (20)$$

By use of equation (20), we can write equation (14) in the form

$$\epsilon = a\left[\frac{3}{5} E_i\right] + E_i + rE_R$$

i.e. $$\epsilon = 1.2E_i + E_i + rE_R$$

or $$\epsilon = 2.21E_i + rE_R \qquad (21)$$

Using the values:[33]

$$E_i = 1.1 \text{ ev}, \; r = 17.5, \; E_R = 0.063 \text{ ev}, \text{ in equation (21)},$$

Shockley's model gives

$$\epsilon = 3.52 \text{ ev/ion pair.} \qquad (22)$$

Energy Resolution In Semiconductor Detectors

An ideal detector for particle spectrometry would be one in which particles of equal energy always produce signals of the same amplitude, but in practice this never quite happens. This can conveniently be expressed as the standard deviation in the set of measurements, σ; the smaller σ the better is the counter as a spectrometer. The standard deviation will be made up of a number of independent contributions, some fundamental, and others a function of the way in which the counter is constructed and used. The most fundamental contribution to the standard deviation is that due to fluctuations in N, the number of ion pairs produced by a particle, and this

is the standard against which other contributions can be judged. The signal in this discussion is q, the charge collected at the electrodes of the detector after the absorption of a single particle. When the charge collection is perfect the charge collected after any one event is given by equation (8)

$$q = Ne = \frac{Ee}{\epsilon} \tag{8}$$

But because the process of ionization described earlier is a cascade one, the final set of events which produce N ion pairs are independent of one another. Therefore, the standard deviation[46] in N is $\sqrt{N}$, i.e.

$$\sigma = e\sqrt{N} \tag{23}$$

It is convenient to define the energy resolution of the counter for this type of particle as σ/q so that due to this particular cause the resolution is from equations (8) and (23),

$$\frac{\sigma}{q} = \frac{1}{\sqrt{N}} \tag{24}$$

or, expressing N in terms of the particle energy E and the mean energy per ion pair ϵ, we have

$$\frac{\sigma}{q} = \frac{1}{\sqrt{E/\epsilon}} = \left[\frac{\epsilon}{E}\right]^{\frac{1}{2}} \tag{25}$$

It is obvious from equation (25) that the resolution will improve as the

particle energy increases, and as the mean energy per ion pair decreases. Both changes increase the total number of ion pairs produced.

Two alternative methods[46] of specifying the resolution of a counter are in common use. The first method considers the energy of a particle which would produce a signal equal to the standard deviation, i.e. $\frac{\sigma\epsilon}{e}$. Using equations (23) and (8), we obtain

$$v = e\left[\frac{E}{\epsilon}\right]^{\frac{1}{2}}$$

or,
$$\frac{\sigma\epsilon}{e} = (\epsilon E)^{\frac{1}{2}} \qquad (26)$$

The second, and more commonly used, method considers a quantity which is measured experimentally by plotting the pulse height spectrum obtained from the counter under bombardment by monoenergetic particles and measuring the full width of this distribution at its half maximum values (FWHM). This can again be expressed either as an energy or as a ratio or percentage. These quantities are related to those previously defined by the actual shape of the pulse height spectrum, and where this is Gaussian the FWHM is 2.35 times the resolution defined from the standard deviation.

As a matter of principle the resolutions defined above should be multiplied by the Fano factor F which expresses the degree to which the ionization events producing an average of N ion pairs are correlated.[35] The Fano factor for silicon is not, as yet, well established, but it is thought that the Fano factor is unlikely to be noticeably different from unity. For minimum ionizing particles, or especially thin counters, there

will be a worsening of the resolution due to the Landau effect.[47] This is applicable wherever the number of high energy secondaries generated by the primary particle is small, or in other words, where the actual energy deposited in the counter suffers statistical fluctuations.

Failure of all the charge to reach the electrodes can affect the resolution of the counter in three quite different ways. In the first place charge carriers may recombine in the particle track after moving distances so small that their contribution to the signal is negligible. A second cause of line broadening occurs when some of the charge leaving the particle track fails to reach the electrodes. However, these two causes of line broadening have less effect on the loss of resolution than that due to statistical fluctuations in the ionization.

The third, and by far the most important, effect of incomplete charge collection arises from geometrical causes when particles are absorbed at random in the body of a crystal. Northrop and Simpson[48,46] have treated this case by considering the geometrical position of the incident particle track in relation to the two charge collecting electrodes of the detector. The conclusion of their geometrical analysis shows that if good energy resolution is to be obtained both carriers must be collected with high efficiency and the worse possible case arises when one charge carrier is completely collected but the other makes no contribution to the signal. Therefore, whenever possible, counters with incomplete charge collection should be used with particles incident parallel to the electric field, that is, perpendicular to the junctions of the detector. This is equivalent to

making the distance between the incident particle track and the collecting electrodes a constant for any one particle energy and reduces the loss of resolution due to geometrical causes. Also, for good energy resolution the maximum electrode separation in a semiconductor counter should be about one centimeter, for reasons which will emerge later. The problem of making a counter with one dimension greater than one centimeter is easily solved by having the particles incident perpendicular to the electric field, that is, parallel to the detector junctions, and making one of the electrode dimensions the large one. However, other considerations may require different geometrical constructions or arrangements.

Noise In Semiconductor Detectors

Various kinds of electrical noise in the measuring circuit can also superimpose fluctuations on the signals and thereby contribute to the resolution of the detector. All these kinds of noise arise fundamentally because the detector is not a perfect dielectric; it contains electrons and holes in thermal equilibrium with the lattice in addition to any carriers generated by incident radiation. Certain basic limitations on the bandwidth through which both signal and noise can be observed are set by the circuit which is used to apply the necessary field to the detector. The circuit shown in Figure IV is the barest minimum which can perform this function and allow measurement of what is happening in the detector.[46] R_d and C_d are the resistance and capacitance of the detector, shown in parallel with the stray circuit capacitances C_s. R_L is the load resistor.

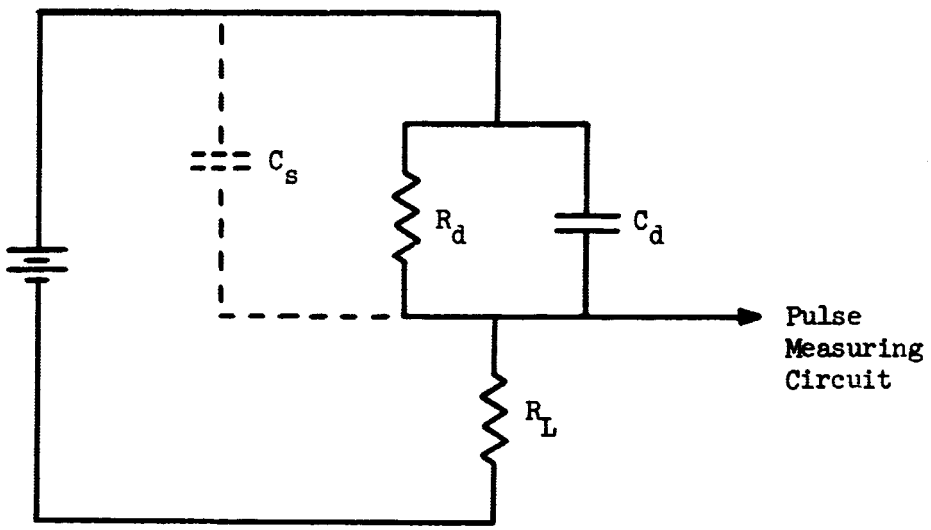

(a) The effective circuit of a counter.

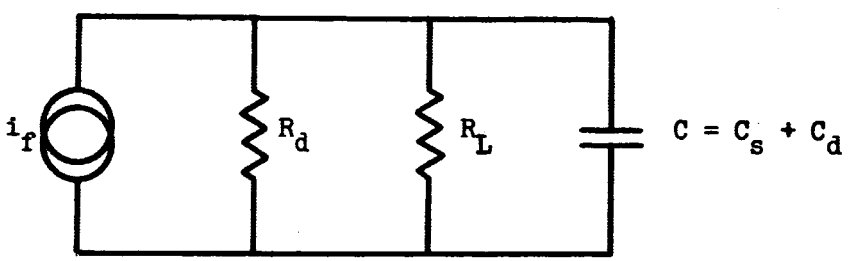

(b) The equivalent thermal noise circuit.

Fig. IV. The effective circuit for determining the thermal noise of a semiconductor detector.

It is convenient to define

$$C = C_d + C_s \tag{27}$$

and

$$R = \frac{R_L R_d}{R_L + R_d} \tag{28}$$

and the circuit time constant,

$$\tau = CR \tag{29}$$

Normally τ will be made greater than the charge collection time t_c for both carriers. The observed voltage across the load resistor R_L will then decay according to the equation

$$V = \frac{Ne}{C} \cdot \exp\ (-t/\tau) \tag{30}$$

where Ne is the total charge collected. For efficient charge collection τ is made much shorter than τ_o, the dielectric relazation time, which is given by[49]

$$\tau_o = \rho K \xi_o = C_d R_d \tag{31}$$

where ρ = resistivity of the detector depletion region,

K = dielectric constant, and

ξ_o = free space permittivity,

Comparison of equations (29) and (31) shows that R_L must be less than R_d in order for $\tau \ll \tau_o$.

Noise is conveniently expressed as the energy of an ionizing particle which would produce a signal equal to the r.m.s. noise. This definition is consistent with the earlier use of the standard deviation of pulse height, so that the overall resolution of any detector can be found by adding the squares of all the various contributions and taking the square root of the sum.

The thermal noise, or Johnson noise, shows up as a fluctuating voltage across the parallel combination of resistors and capacitors of Figure IV. Its r.m.s. value, in the frequency interval df, is expressed as[46,50]

$$\overline{V_f^2} = \overline{i_f^2} \left|\frac{1}{Y}\right|^2 = \overline{i_f^2} \left|\frac{1}{g_d+g_L+j\omega C}\right|^2$$

$$\overline{V_f^2} = 4kT\,(g_d+g_L)df \left|\frac{1}{g_d+g_L+j\omega C}\right|^2 \qquad (32)$$

where $\overline{V_f^2}$ = thermal r.m.s. noise voltage,

$\overline{i_f^2}$ = thermal r.m.s. noise current,

Y = admittance of combination of R_d, R_L and C,

$g_d = \frac{1}{R_d}$ = admittance,

$g_L = \frac{1}{R_L}$ = admittance,

k = Boltzmann's constant, and

T = temperature in degrees Kelvin.

The integrated r.m.s. voltage seen by the measuring circuit, for the frequency band, is from equation (32)

$$\overline{V^2} = 4KT\,(g_d+g_L) \int_o^\infty \frac{df}{(g_d+g_L)^2 + \omega^2C^2} \tag{33}$$

Let $$a = \frac{g_d+g_L}{2\pi C} \tag{34}$$

and $$f = a \tan\theta \tag{35}$$

Substituting equations (34) and (35) into equations (33), we obtain

$$\overline{V^2} = 4kT\,(2\pi C)\,a \int_o^{\frac{\pi}{2}} \frac{a\sec^2\theta d\theta}{4a^2\pi^2C^2 + 4\pi^2C^2a^2\tan^2\theta}$$

$$= \frac{4kT(2\pi C)a^2}{4a^2\pi^2C^2} \int_o^{\frac{\pi}{2}} \frac{\sec^2\theta d\theta}{1+\tan^2\theta}$$

$$= \frac{2kT}{\pi C} \int_o^{\frac{\pi}{2}} d\theta = \frac{2kT}{\pi C}\,\frac{\pi}{2}$$

i.e. $$\overline{V^2} = \frac{kT}{C} \tag{36}$$

The number of ion pairs necessary to produce a signal $(\overline{V^2})^{\frac{1}{2}}$ is, using equations (8) and (36),

$$\Delta N = \frac{q}{e} = \frac{1}{e}\,C(\overline{V^2})^{\frac{1}{2}} = \frac{1}{e}\,C\,(\frac{kT}{C})^{\frac{1}{2}}$$

that is, $$\Delta N = \frac{1}{e}\,(kTC)^{\frac{1}{2}} \tag{37}$$

and the energy of a particle necessary to give this number of ion pairs,

using equations (9) and (37), is

$$\Delta E = \epsilon \Delta N = \epsilon \frac{1}{e} (kTC)^{\frac{1}{2}}$$

i.e.
$$\Delta E = \frac{\epsilon}{e} (kTC)^{\frac{1}{2}} \qquad (38)$$

Current noise arises when a field is applied to the detector. The resulting current is made up of discrete movements of electrons and holes which may be introduced and withdrawn at electrodes or trapped, recombined or generated thermally within the detector. Any process which interrupts the movement of carriers destroys the continuity of the current, and constitutes an additional source of noise in the counter. The three types of current noise are

(1) Shot noise, which occurs in a system most clearly exemplified by an electron beam where each carrier crosses continuously from one electrode to another and all electrons have the same transit time.

(2) Generation-Recombination noise, which results from the generation and recombination of pairs of carriers at points in the bulk of the semiconductor material. The current pulses are shorter than those due to electrons and holes which traverse the detector region completely.

(3) Flicker noise, often called 1/f noise, believed to originate at the surface and is dependent on the surface leakage and the contact resistance of the detector.

Hansen and Goulding,[38,39,51] with their guard-ring detectors, found only two sources of current noise which were really significant. These are

tube shot noise and detector leakage noise. Hansen and Goulding give the following equation for the effect of the current noise in a detector-amplifier measuring system on the energy resolution.

$$\overline{(\Delta E)^2} = \left[0.02 \frac{C_T^2}{g_m \tau} + 0.16 \tau i_L \right] (\text{kev})^2 \qquad (39)$$

where $\overline{(\Delta E)^2}$ = mean square noise level in terms of the standard deviation,

C_T = total input capacitance (detector, tube, strays) in pf,

g_m = mutual conductance of the amplifier input in mA/V,

τ = amplifier time constant in micro-sec, and

i_L = detector leakage current in nanoamperes.

An important consideration from a noise standpoint is the increase in thermal noise due to the application of high electric fields to the semiconductor detector. When the electric field exceeds a certain limit the thermal noise begins to increase and the carrier mobilities are reduced. The cause of this phenomenon is as follows: As the electric field is increased, conduction electrons absorb energy from the applied field and this energy appears as extra kinetic energy. The scattering processes normally remove this energy gained from the field and convert it into thermal energy of the crystal lattice. When the rate at which the electrons gain energy from the field exceeds the rate at which the scattering processes can transfer the kinetic energy from the electrons to the lattice, then the electrons are no longer in thermal equilibrium with the lattice.

Shockley[40] called such carriers "hot" and found that the new velocity distribution function was approximately a Boltzmann distribution with an effective temperature T_e greater than the lattice temperature. Thermal noise derives from the velocity distribution of the charge carriers, and, therefore, T_e should be used in equation (38) for high electric fields, giving

$$\Delta E = \frac{\epsilon}{e} (kT_e C)^{\frac{1}{2}} \tag{40}$$

Shockley's calculated value of T_e is

$$T_e = \left[\frac{3\pi}{32}\right]^{\frac{1}{2}} \frac{\mu\phi}{v_s} T \text{ for } \mu\phi \gg v_s \tag{41}$$

where v_s is the velocity of sound in the semiconductor. For silicon, if we substitute $v_s = 7 \times 10^5$ cm/sec and $\mu = 1200$ $cm^2 volt^{-1} sec^{-1}$ into equation (41), we find that a ϕ of approximately 600 volt cm^{-1} will make $\mu\phi$ comparable with v_s. When the applied field approaches this value thermal noise will begin to increase and the mobility of the carriers will begin to decrease. It is often attractive to increase the electric field applied to the counter to obtain faster pulses (see equation 3) and higher charge collection efficiencies (see equation 7) but obviously a point is reached when the noise is increasing rapidly with applied field and the collection of charge is hardly improving at all.

In summary, we can express the effect (broadening) on the energy resolution by the thermal and current noise by the use of equations (38) and (39). We obtain

$$\overline{(\Delta E)^2} = \left[\frac{\epsilon^2}{e} \frac{kT}{e} C + 0.02 \frac{C_T^2}{g_m \tau} + 0.16 \tau i_L \right] (kev)^2 \qquad (42)$$

For silicon, if we substitute $\epsilon = 3.6$ ev and $\frac{kT}{e} = 0.026$ volt into equation (42), we obtain

$$\overline{(\Delta E)^2} = \left[2.105 C + 0.02 \frac{C_T}{g_m \tau} + 0.16 \tau i_L \right] (kev)^2 \qquad (43)$$

Using the FWHM terminology, equation (43) becomes

$$\overline{(\Delta E_{FWHM})^2} = (2.35)^2 \left[2.105C + 0.02 \frac{C_T^2}{g_m \tau} + 0.16 \tau i_L \right] (kev)^2 \qquad (44)$$

BIBLIOGRAPHY

1. F. S. Goulding, IEEE Transactions on Nuclear Science, NS-11, No. 3, 177, June, 1964.

2. G. W. Grew, IEEE Transactions on Nuclear Science, NS-12, No. 1, Feb. 1965.

3. K. G. McKay and K. B. McAffee, Phys. Rev. 91. 1079 (1953).

4. V. S. Vavilov, J. Phys. Chem. Solids 8, 223 (1958).

5. W. D. Davis, J. Appl. Physics 29, 231 (1958).

6. J. M. McKenzie and D. A. Bromley, Bull. Am. Phys. Soc.4, 422 (1959).

7. W. L. Buys, Nucl. Inst. and Meth. 42, 329 (1966).

8. V. A. J. VanLint, H. Roth and E. G. Wikner, Bull. of Am. Phys. Soc. 4, 457 (1959).

9. M. L. Halbert and J. L. Blankenship, Nucl. Inst. and Meth. 8, 106 (1960).

10. L. Koch, J. Messier and J. Valin, IRE Transactions on Nuclear Science, NS-8 (1961).

11. E. Baldinger, W. Czaja and J. Gutmann, Helv. Phys. Acta. 35, 559 (1962).

12. C. Bussolati and A. Fiorentini, Phys. Rev. 136, 6A, A1756 (1964).

13. F. E. Emergy and T. A. Rabson, Phys. Rev. 140, 6A, A2089 (1965).

14. B. D. Snow, Thesis, Southern Methodist Univ., (1966).

15. J. J. Smithrick and I. T. Myers, NASA TN D-3694 (1966).

16. H. E. Wegner and C. Erginsoy, IEEE Trans. on Nucl. Sci., NS-12, No. 1, 240, Feb. 1965.

17. H. E. Wegner, IRE Transactions, NS-8, 103, Jan. 1961.

18. F. S. Goulding, et al, IEEE Trans. on Nucl. Sci., NS-11, No. 3, 388, June 1964.

19. C. N. Inskeep, IRE Trans. On Nucl. Sci., NS-9, No. 3, 167, June, 1962.

20. T. C. Madden and W. M. Gibson, IEEE Trans. on Nucl. Sci., NS-11, No. 3, 254, June, 1964.

21. E. R. Parkinson and D. Bodansky, Nucl. Instr. and Meth., 35, No. 2, 347, (1965).

22. N. Cindro, Nucl. Inst. and Meth., 13, No. 1, 99, Aug., 1961.

23. E. M. Pell, J. Appl. Phys., 31, No. 2, 291, (1960).

24. J. H. Elliott, Nuclear Inst. and Meth., 12, 60 (1961).

25. H. M. Mann and J. W. Haslett, Argonne National Laboratory Report ANL - 6455, 23 (1961).

26. J. L. Blankenship and C. J. Borkowski, IRE Trans on Nucl. Sci., NS-9, No. 3, 181, June, 1962.

27. N. A. Bailey, et al, Rev. Sci. Instr., 32 (5), 865 (1961).

28. E. J. Ludwig, Rev. Sci. Instr., 36, No. 8, 1175 (Aug., 1965).

29. K. G. McKay, Phys. Rev. 94, 877 (1954).

30. P. A. Wolff, Phys. Rev. 95, 1415 (1954).

31. S. L. Miller, Phys. Rev. 105, 1246 (1957).

32. A. G. Chynoweth and K. G. McKay, Phys. Rev. 108, 29 (1957).

33. W. Shockley, Solid-State Electronics, 2, 35 (1961).

34. A. G. Chynoweth, Proceedings of Asheville Conference, NAS-NRC Publication, 871, 95 (1961).

35. S. O. W. Antman, D. A. Landis and R. H. Pehl, Nucl. Instr. and Meth., 40, 272 (1966).

36. J. W. Mayer, Natl. Acad. Sci. Report, NAS-NSS 32, Publ. 871, 1 (1961)

37. J. M. Taylor, Semiconductor Particle Detectors (Washington Butterworths, Washington, D. C., 1963). 1st. ed., Chaps. 4,6,7.

38. F. S. Goulding IEEE Trans. on Nucl. Sci., NS-11, No. 3, 177 (June, 1964).

39. G. L. Miller, W. L. Brown, P. F. Donovan and J. M. Mackintosh, Proceedings of Seventh Scintillation Counter Symposium, IRE, NS-7, Nos. 2 and 3, 185 (Sept. 1960).

40. W. Shockley, Bell System Tech. J., 30, 990 (1951).

41. E. Baldinger and W. Czaja, Nucl. Instr. Methods 10, 237 (1961).

42. G. Fabri, E. Gatti and V. Svelto, Phys. Rev. 131, 134 (1963).

43. R. Takaki, M. Perkins and A. Tuzzolino, IRE Transactions, NS-8, 64 (Jan. 1961).

44. H. Palevsky, D. J. Hughes, W. Kley and E. Tunkelo, Phys. Rev. Letters 2, 258 (1959).

45. M. Sachs, Solid State Theory (McGraw-Hill, New York, 1963), 1st ed., pp. 159-163.

46. G. Dearnaley and D. C. Northrop, Semiconductor Counters For Nuclear Radiations (John Wiley and Sons, New York, 1963), 1st ed., pp. 83-89.

47. L. Landau, J. Phys. U.S.S.R., 8, 201 (1944).

48. D. C. Northrop and O. Simpson, Proc. Phys. Soc., 80, 262 (1962).

49. J. A. Stratton, Electromagnetic Theory (McGraw-Hill, New York, 1941), 1st ed., p. 15.

50. J. J. Freeman, Principles Of Noise, (John Wiley and Sons, New York, 1958), 1st ed., pp. 116, 117.

51. W. Hansen and F. S. Goulding, NAS, Publication 871, p. 202 (1961).

CHAPTER 5

"THIN" DETECTOR MEASUREMENTS OF ENERGY REQUIRED FOR ELECTRON - HOLE PAIR GENERATION IN SILICON

By Robert J. Tarrillion, Danny R. Dixon,
Patrick H. Hunt and George W. Crawford

Lithium-drifted NIP detectors of about 1, 2 and 3 cm. lengths were bombarded with 99.9, 159.75 and 185.6 MeV monoenergetic protons. The proton beam was passed through the active region of the detector parallel to the diffused junctions and perpendicular to the applied electric field. The detector was operated with a reverse bias which was adjusted to obtain full collection of all the electron - hole pairs created and yet was not high enough to cause cascading.

With the proton beam turned off, the electronic system was charge calibrated and checked for linearity of response. This calibration was performed with precision pulse generators which sent known voltage pulses into the input of the pre-amplifier via a known precision capacitor, C_c. The histogram of the number of pulses stored versus the channel number was recorded. The most probable channel, V, was calculated to the nearest one hundreth of a channel number using the procedure given in Chapter 1, Part 68-3 of this report, for each voltage pulse. For a given amplification setting, the calibration was repeated using different pulse generators. Examples of the calibration results are as follows:

TABLE 1

SAMPLE DATA FOR CHARGE CALIBRATION OF THE ELECTRONIC SYSTEM FOR PROTON EXPERIMENTS

For 99.9 MeV Protons		For 159.75 MeV Protons		For 185.6 MeV Protons	
Charge in picocoulombs (± 0.006)	Analyser Channel (± 0.05)	Charge in picocoulombs (± 0.006)	Analyser Channel (± 0.05)	Charge in picocoulombs (± 0.01)	Analyser Channel (± 0.05)
0.275	12.75	0.132	5.80	0.550	26.81
0.550	25.50	0.264	11.60	1.100	53.63
0.825	38.50	0.550	24.18	2.440	104.25
1.100	51.00	1.100	48.32	3.652	154.38
1.375	63.75	1.540	67.66	4.840	206.05
1.650	76.50	1.760	77.33	6.028	254.50
1.925	89.25	2.200	96.67	7.128	299.20
2.200	102.00	2.640	116.00	7.678	322.74
2.475	114.75	3.300	145.00	8.140	344.54
2.750	127.50	3.850	169.15	8.360	354.54
3.300	152.95	4.400	193.32	8.580	364.10
4.400	204.10	5.500	241.64	8.844	376.59
5.500	255.25	6.050	265.80	8.954	381.77

In each case, the voltage pulse from the pulse generator was introduced to the Tennelec 100 B low-noise preamplifier through a carefully calibrated capacitor. The internal 1.1 picofarad capacitor was used at all except the 185.6 MeV measurements. As shown in Figure 1, this capacitor was so low compared to the capacitance of the detector (from 30 to 64 picofarads) and the input and stray capacitances of the preamplifier (15,000 pf minimum), that the charge which appears at the input of the preamplifier is equal to the charge which is created across the capacitor, C_c, by the pulse generator[1]. The charge corresponding to the measured proton peak was found by interpolating between bracketing pulse generator voltage pulses, i.e., known charge input stored and recorded at the time and under the same conditions as the data point being analysed.

The average energy per ionized electron-hole pair, ϵ, is equal to the energy, E, lost by the incident proton in the active region of the detector, divided by the average number of ion pairs created by the proton in losing the energy via the ionization process as it traverses the silicon. This total charge, q, collected from the detector for each proton was recorded as a count in a channel of the multichannel analyser. (Note: RIDL Model 24-1 multichannel analyzer was used for all measurements except those made using 185.6 MeV. For this energy, a RIDL 400-channel analyzer was used.)

A typical histogram is presented in Figure 2. The spectrum is that obtained using a 3.050 cm silicon detector being traversed by 99.9 MeV protons. The entire spectrum includes the proton peak and six pulse generator peaks. The proton peak is superimposed on the curve created by the computer program, Figure 3, to find the most probable channel number to be associated with this histogram. This most probable channel number is obtained by setting the first derivative of the curve chosen as the best fit to zero and locating the peak to the nearest ± 0.05 of a channel. The experimental energy resolution expressed in terms of the full-width-half-maximum (FWHM) was determined for each histogram. Typical results are given in Table 2.

TABLE 2

RESOLUTION EXPRESSED IN TERMS OF THE FWHM FOR THE 159.75 MEV PROTON EXPERIMENTS

Detector Length (cm)	Channel Number V (±.05)	FWHM in Channels	FWHM (%)	Average FWHM (%)	Electronic Noise Contribution to FWHM (%)
1.009	19.77	3.64	18.40	17.3	0.80
1.093	21.52	3.48	16.15		2.02
1.980	39.88	4.68	11.72	16.4	0.57
2.076	41.79	8.80	21.06		1.60
3.050	63.52	5.65	8.89		1.61
3.070	64.21	5.55	8.64	8.34	2.43
3.100	64.78	4.85	7.49		0.21

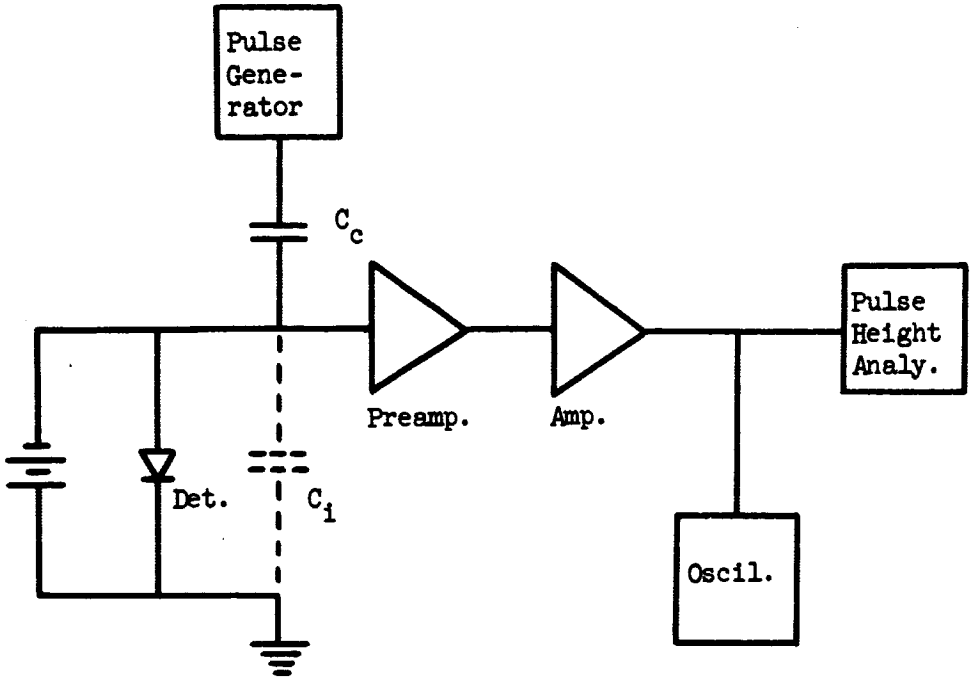

(a) Schematic of experimental equipment.

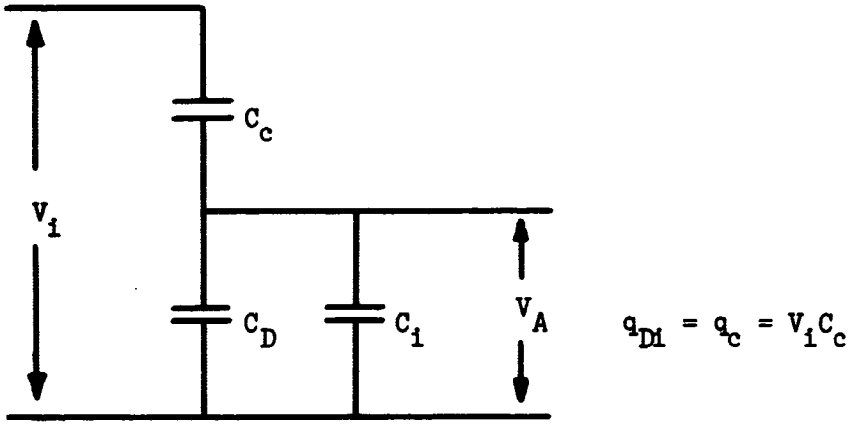

(b) Circuit for determining the calibration charge which enters the amplifier system.

Fig. 1. Schematic of the experimental equipment and the charge calibration technique.

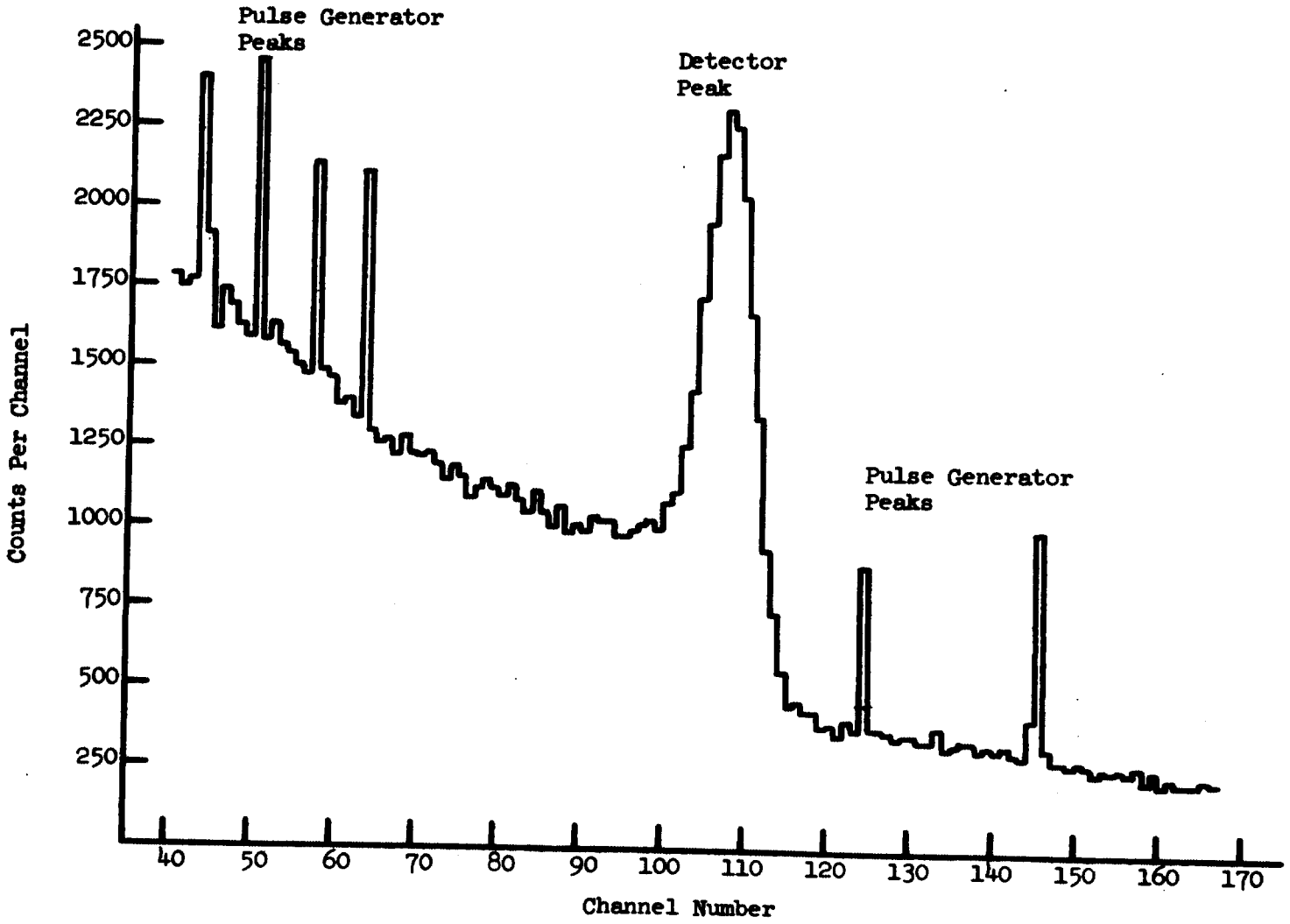

Fig. 2. Entire pulse height spectrum for the 3.050 cm detector using 99.9 Mev protons.

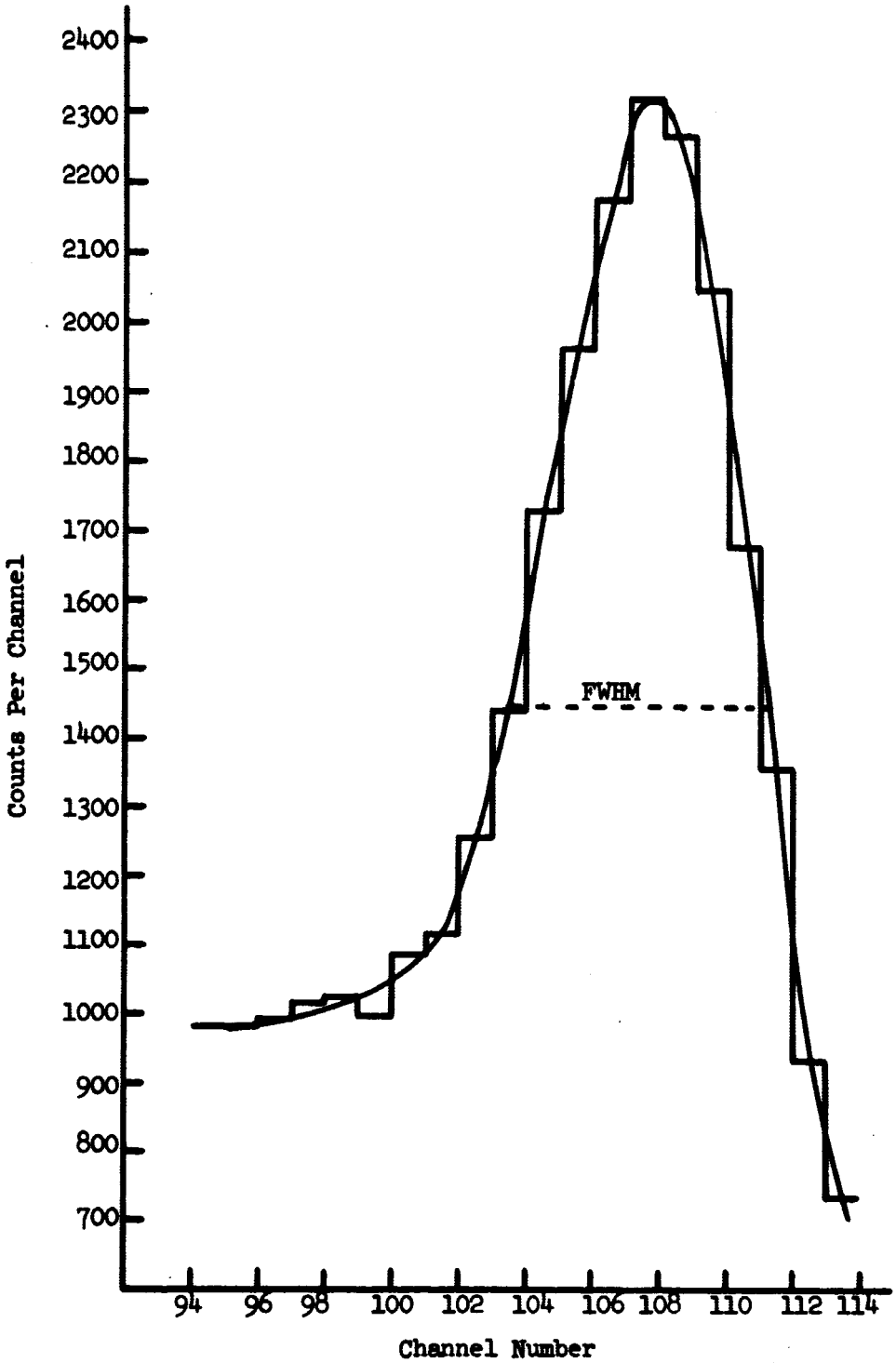

Fig. 3. Pulse height spectrum of the detector peak for the 3.050 cm detector using 99.9 Mev protons.

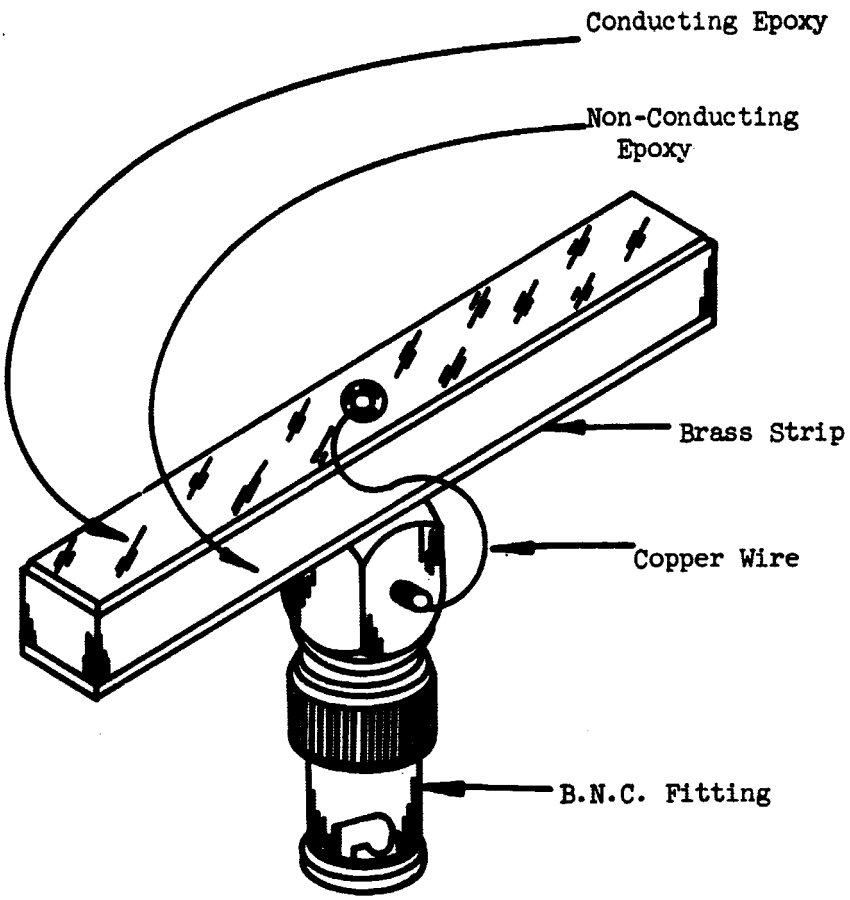

Fig. 4. The Assembled Detector

The fifteen different lithium-drifted silicon NIP detectors used in these experiments had a rectangular volume and were shaped similar to the 3 cm detector shown in Figure 4. Each had a width of about 0.5 cm. The depth of the depletion layer varied from 1.5 to 3 mm. Four detectors were about 1 cm in length, seven were about 2 cm in length, and four were about 3 cm inlength. A General Radio Impedance Bridge, Type No. 1650-A, was used to measure the capacitance, C_D, of each detector at the bias voltage used in each experimental run. A Tektronix Transistor Curve Tracer, Model 575, was used to measure the leakage current, i_L, at the operating bias voltage. Representative values are given in Table 3.

TABLE 3

DETECTOR CAPACITANCE AND LEAKAGE AT THE DETECTOR OPERATING BIAS

Detector Length (cm)	Detector Bias (volts)	C_D (pf)	i_L (uA)
0.9504	300.	18.5	5.5
1.009	300.	30.0	4.
1.980	1000.	14.0	15.
2.076	1200.	45.0	130.
3.100	200.	30.0	5.
3.110	300.	23.5	5.

Both the detector and the electronic measuring system noises cause broadening of the peak. Their undesirable contibutions are discussed in detail in Chapter 4 of this volume. The Tennelec Model 100 B preamplifier specifications give the measured relationship between the detector capacity and the corresponding electronic noise contribution for an amplifier time constant of 1 microsecond. A plot of this relationship for the range of interest is shown in Figure 5. Calculated values of this broadening are given in Table 2. It is apparent that the noise does not appreciably change the location of the most probable channel number.

Each proton, as it penetrates the silicon bar, loses its energy in small but definite amounts. Thus no two protons have exactly the same collision histories in traveling the length of the detector. These histories vary in total path traveled and in actual energy lost. A more detailed study of these fluctuations of energy loss is given in Tarrillion's thesis.[1]. In Vavilov's [2,3] treatment of the fluctuations of the energy loss in semiconductor detectors, the dimensionless parameter κ was introduced as

$$\kappa = 0.15\ (SZ\ z^2)\ (1-\beta^2)/A\beta^4 \qquad (1)$$

where S = the thickness of the detector in gm/cm^2,

Z = the atomic number of the detector material,

A = the atomic weight of the detector material,

z = the charge on the incident particle, and

β = speed of incident particle divided by speed of light in vacuum.

The parameter κ may be thought of as a measure of the ratio of the total energy loss to the maximum possible energy loss in a single collision. For $\kappa \ll 1$, the energy loss fluctuaions are large. For $\kappa \gg 1$, the fluctuations are negligible. Values for κ for silicon were calculated for several proton energies and are given in Table 4. For equal energy losses, a remarkable difference exists between the κ values of the totally and partially absorbed energies. For partial absorption the energy loss fluctuations decrease as the silicon detector length increases.

TABLE 4

VALUES OF κ FOR VARIOUS PROTON ENERGY LOSSES IN SILICON

Total Absorption of Incident Energy		Partial Absorption of Incident Energy			
		E = 99.9 MeV		E = 159.75 MeV	
E (MeV)	κ	ΔE (MeV)	κ	ΔE (MeV)	κ
8	29.5				
10	27.8			10	1.75
12	26.5				
14	25.6	14.5	4.24		
20	23.6			20	3.49
32	21.5			32	5.24
52	19.6	52.	12.7		

In order to determine the exact energy lost by the proton in traversing the detector, the charge calibration of the detector had to be translated into MeV. Knowing the original energy of the proton beam and using calibrated aluminum foils it was possible to calibrate the high energy region, i.e., from 99.9 down to 50 MeV, response of the detector. After calibration, a selected series of silicon absorbers were placed in turn in the beam and the corresponding decrease in energy of the incident beam measured. Thus one could compare the $E_o - E_i$ measurement of the energy lost by the protons in traversing a silicon absorber of known thickness to the calibrated measured ΔE from the most probable channel number of the peak.

A second method of determining the correct value for the energy loss in the detector required knowing the exact thickness of the detector, i.e., the protons entered one end of the detector perpendicular to the face of the end, remained in the active region of the detector traveling parallel to the collection plates above and below the active region, and emerged from the back end still in the active region until exit from the back face. Then using the PROSPER 3B Monte Carlo proton transport program descibed in Volume 68-2 of this report, calculate the histogram comparable to the measured histogram. From this histogram, using the value for the mean ionization potential and shell corrections measured and reported in Volume 68-3 of this report, calculate the most probable energy loss for each case. The combined methods gave a value for ΔE within $\pm$ 0.02 MeV.

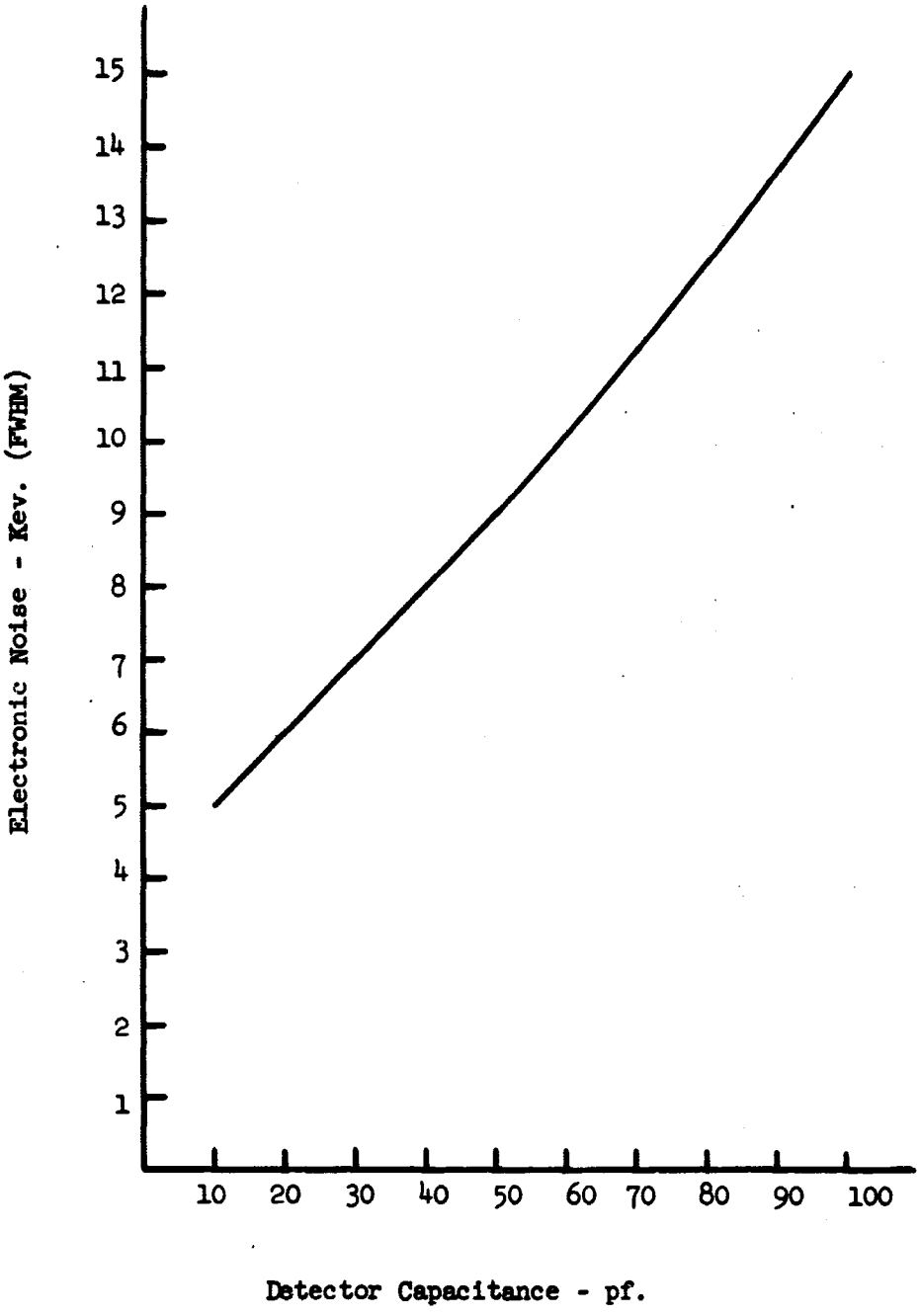

Fig. 5. Electronic noise as a function of detector capacitance for the Tennelec, Model 100 B, low-noise preamplifier.

The average energy per ionized electron-hole pair, ϵ, is defined by Equation 9 of chapter 4 of this volume as $\epsilon = Ee/q$. The most probable value for ϵ for each detector at each incident proton energy was calculated. The known errors were used to determine the maximum and minimum possible values for ϵ. These values are indicated as the * value with each measured result.

TABLE 5

VALUES OF ϵ OBTAINED FROM PARTIAL ABSORPTION OF 99.9, 159.75 and 185.6 MEV PROTONS USING SILICON DETECTORS OF VARIOUS LENGTHS

Detector Length (cm) ±0.001	E_o = 99.9 MeV ΔE (MeV) ±0.02	ϵ (eV per ion pair)	E_o = 159.75 MeV ΔE (MeV) ±0.02	ϵ (eV per ion pair)	E_o = 185.6 MeV ΔE (MeV) ±0.02	ϵ (eV per ion pair)
0.9504	13.65	3.848±0.034				
0.9507	13.65	3.817±0.055				
1.009	14.54	3.864±0.041	10.12	3.603±0.025		
1.093	15.85	3.854±0.039	10.99	3.595±0.023		
1.25					11.24	3.73 ±0.06[4]
1.980	30.48	3.673±0.045	20.28	3.579±0.016	18.18	3.592±0.045
2.076	32.22	3.670±0.035	21.30	3.588±0.016	19.08	3.585±0.051
3.050	52.26	3.614±0.025	32.07	3.554±0.013	28.56	3.562±0.025
3.070			32.38	3.550±0.013	28.75	3.554±0.025
3.100			32.68	3.551±0.013		
3.110	53.69	3.611±0.025				

The values for ϵ obtained for each group of detectors in the same length band, gave results nearly the same and clearly within experimental error overlap. However, in each of the three incident energies, the value for ϵ decreased with increasing path length. Thus the energy required to create an electron-hole pair is not a constant, but is a function of the incident energy of the proton and the value for κ. In chapter 6 of this volume, these values will be compared to those obtained from total absorption measurements.

ACKNOWLEDGMENTS

We are grateful to Professor The Svedberg, Dr. Borje Larsson and Dr. Bo Jung of the Gustaf Werner Institute, University of Uppsala, Uppsala, Sweden; to Dr. R. E. Bell of the Foster Radiation Laboratory, McGill University, Montreal, Canada; to Dr. A. M. Koehler of the Cyclotron Laboratory, Harvard University, Cambridge, Massachusetts for their support and interest in this experiment.

BIBLIOGRAPHY

1. Tarrillion, R. J. Masters Thesis at Southern Methodist University, (1967).
2. Vavivlov, P. V. Soviet Phys. JETP 5, 749 (1957).
3. Maccabee, H. D., Raju, M. R. and Tobias, C. A. IEEE Transactions on Nuclear Science, NS-13, No. 3, 176 (June, 1966).
4. Hunt, P. H. Masters Thesis at Southern Methodist University, (1967).

CHAPTER 6

THE ENERGY REQUIRED TO PRODUCE AN ELECTRON-HOLE PAIR IN SILICON BY PROTONS OF 8 TO 187 MEV ENERGY

by George W. Crawford, Stephen M. Curry and Danny R. Dixon

Introduction

The mean energy, ϵ, required to generate an electron-hole pair in silicon must be known in order to calculate the energy deposited by the penetrating ionizing particle from the measurement of the charge collected from the detector. This charge may be amplified and stored in a multichannel analyzer for nuclear physics measurements or collected in an electrometer for dosimetry measurements.

The average energy per electron-hole pair, ϵ, is defined by the relation:

$$E = \Delta E/N = \Delta Ee/q$$

where E= the energy lost by the incident proton in the active region of the detector

N= average number of ion pairs created by the absorption of the proton energy ΔE

e= charge on the electron

q= charge collected from the electron-hole pairs created by the proton in penetrating the detector.

The Shockley model[1,2] for ϵ is discussed in detail in Chapter 4 of this report. Using this model one obtains a value for ϵ of 3.52 eV/ion pair. This model does not include any possible variation of the value of ϵ with incident proton energy.

A systemmatic study has been made of the average energy required to produce electron-hole pairs in lithium drifted silicon detectors. In each case the entire path of the incident proton was in the sensitive region of the detector and the operating conditions were such that optimum charge collection was accomplished. Detectors of eight different sizes were used. In each group size from two to four matching detectors were employed to obtain each average value reported as data in Table 1.

Field trips were made to six different radiation facilities in order to obtain data covering the range of proton energies from 8 to 187 MeV. The listing of these facilities and the acknowledgments are given in Chapter 1 of this report.

TABLE 1

VALUES OF ϵ OBTAINED FROM TOTAL ABSORPTION

OF PROTONS IN SILICON DETECTORS

Detector Characteristics				Charge** (pico-coulombs) ±0.006	Incident Proton Energy (MeV)	ϵ (eV per ion pair)	Error in ϵ Measurement
Length mm	Width mm	Depth mm	Capacitance* (picofarads)				
5	5	0.61	3.2	.4505	9.90±.02	3.523	±.06
				.5406	11.91 "	3.533	±.05
				.6307	13.92 "	3.538	±.04
5	5	1.3	8.1	.4465	9.90 "	3.529	±.06
				.5409	11.91 "	3.530	±.05
				.6316	13.92 "	3.533	±.04
20	5	.62	7.6	.4505	9.90 "	3.526	±.06
				.5372	11 91 "	3.557	±.05
				.6256	13.92 "	3.567	±.04
10	10	1.6	6.4	.3552	7.78 "	3.511	±.07
				.4522	9.90 "	3.510	±.06
				.5426	11.91 "	3.519	±.05
				.6331	13.92 "	3.525	±.04
				.818	18. ±.05	3.527	±.04
				.960	21. "	3.507	±.03
				1.102	24. "	3.497	±.03
				1.235	27. "	3.505	±.03
				1.292	28.76±.10	3.569	±.02
				1.385	30.79 "	3.563	"
				1.497	32.71 "	3.502	"
				1.581	34.49 "	3.496	"
				1.656	36.2 "	3.504	"
31.5	5	1.7	9.8	.4522	9.91±.02	3.513	±.06
				.5406	11.91 "	3.532	±.05
				.6324	13.92 "	3.538	±.04
				1.280	28.33±.05	3.541	±.02
				1.644	36.2 ±.10	3.529	±.02
50	5	1.3	45.	.3542	7.78±.02	3.523	±.07
				.4513	9.90 "	3.519	±.06
				.496	10.91 "	3.524	±.06
				.543	11.92 "	3.520	±.05
				.637	13.92 "	3.527	±.04
				1.651	36.2 ±.10	3.515	±.02
				2.659	59.89 "	3.490	±.01
				3.164	69.87 "	3.540	"
				3.682	79.95 "	3.481	"
				4.091	89.91 "	3.523	"
				4.545	99.9 "	3.503	"

**Measured at most probable channel number of peak determined from proton peak histogram.

*At operating voltage

TABLE 1 (Continued)

Detector Characteristics				Charge **	Incident	ϵ	Error in
Length mm	Width mm	Depth mm	Capacitance * (picofarads)	(pico-coulombs) ±0.006	Proton Energy (MeV)	(eV per ion pair)	ϵ Measurement
115	10	5.8	90.	.4522	9.90±.02	3.510	±.06
				.5426	11.92 "	3.519	±.05
				.6350	13.92 "	3.514	±.04
				1.643	36.2 ±.10	3.525	±.02
				4.569	99.9 ±.10	3.505	±.01
				6.118	134.00±.15	3.515	±.01
				6.382	139.76 "	3.511	"
				6.670	146.07 "	3.511	"
				7.295	159.75 "	3.510	"
				7.779	163.55±.10	3.368	±.06
				8.423	178.34 "	3.430	"
				8.715	186.45 "	3.427	"
140.	12.5	4.7	39.2	7.267	159.75±.15	3.514	±.01
				7.505	157.6 "	3.364	±.06
				7.889	167.2 "	3.395	"
				8.287	176.5 "	3.410	"
				8.380	181.4 "	3.395	"
				8.685	185.6 "	3.424	"

TABLE 2

REPORTED VALUES OF ϵ FOR SILICON

Type of Silicon Detector	Lit. Ref.	Radiation Type	Energy (MeV)	Value of ϵ (ev/pair)
Surface Barrier	4	Electron	0.030	4.2 ± 0.6
N.I.P. Junction	10	Electron	0.279	3.53± 0.07
N.I.P. Junction	10	Electron	0.660	3.55± 0.1
Surface Barrier	12	Electron	0.365	3.79± 0.01
Lithium Drifted	13	Electron	1	3.79± 0.01
Gold Doped	6	Alpha	3.5	3.60± 0.15
NP Junction	3	Alpha	5	3.6 ± 0.3
Gold Doped	5	Alpha	5	3.6 ± 0.1
Diffused Junction	7	Alpha	4.82	3.58± 0.015
Diffused Junction	7	Alpha	5.80	3.58± 0.015
Surface Barrier	9	Alpha	5.3	3.50± 0.05
Surface Barrier	11	Alpha	5.3	3.52± 0.04
Surface Barrier	12	Alpha	5.48	3.61± 0.01
Lithium Drifted	13	Alpha	5.5	3.61± 0.01
Gold Doped	6	Proton	0.8	3.60± 0.15
Surface Barrier	14	Triton	4.78	3.58± 0.04

**Measured at most probable channel number of peak determined from proton peak histogram.

*At operating voltage

Experimental Procedure

Essentially the same experimental procedure was followed at each radiation facility. First a thorough test of the linearity of response and of the noise level conditions of the electronic system was made under operating conditions. A block diagram listing the equipment used is shown in Figure 2. This included establishment of a ground connection giving a minimum noise input to the system. Tests were made frequently during the experiment to insure the stability of the system.

A very careful alignment of the detector in the beam was vital to the success of the experiment. The mounting of the detector permitted both translational and rotational motion with respect to all three axes. Fine adjustments were continued until the proton beam entered one end (at the center of the sensitive region of the detector) and remained in this sensitive volume, traveling parallel to the length of the detector, until totally absorbed. This alignment produced both the maximum charge pulse and the sharpest peak histogram at the optimum bias voltage.

A series of histograms, each with the protons being totally absorbed in the sensitive volume of the detector, were taken as a function of bias voltage in order to find the optimum bias voltage. The example given of this adjustment in Figure 1 is that of total absorption of 187 MeV protons in a 140 X 12.5 X 4.7 mm detector. In his most difficult case, the detector was located at the exit of the magnetic spectrometer described in Chapter 5 of Volume 68-3 of this report[15]. Increasing the bias voltage from 1800 to 2000 volts increased the collected charge by 0.232 picocoulombs (11 channels) and sharpened the peak. A further increase to 2200 volts increased the pulse by only 0.02 picocoulombs (one channel) and decreased the FWHM from 8 to 7 channels or about $\frac{1}{2}$ MeV. Further increases in the bias voltage produced no change in the peak location or sharpness until a voltage of 2800 volts was reached. At this bias, the charge pulse increased and the peak broadened, indicating cascading in the charge collection process. The selected operating voltage was the lowest giving full collection with the sharpest peak.

The proper alignment was further evidenced by a 180° rotation of the detector. With the protons entering the other end of the detector essentially the same peak histogram was recorded.

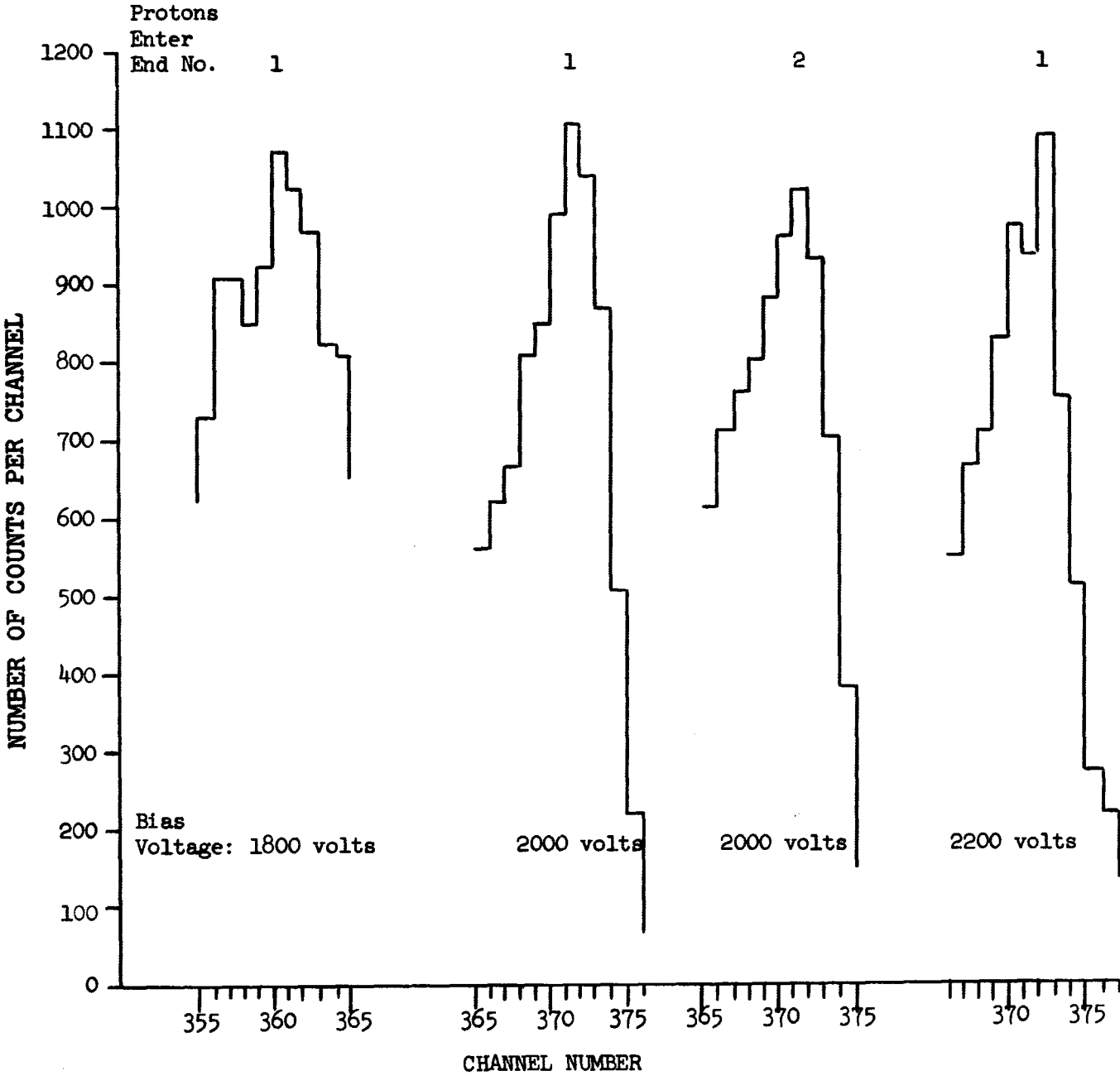

Figure 1. Proton Histograms of 187 MeV Protons Totally Absorbed in a 140 X 12.5 X 4.7 mm Silicon Detector at Various Bias Voltages.

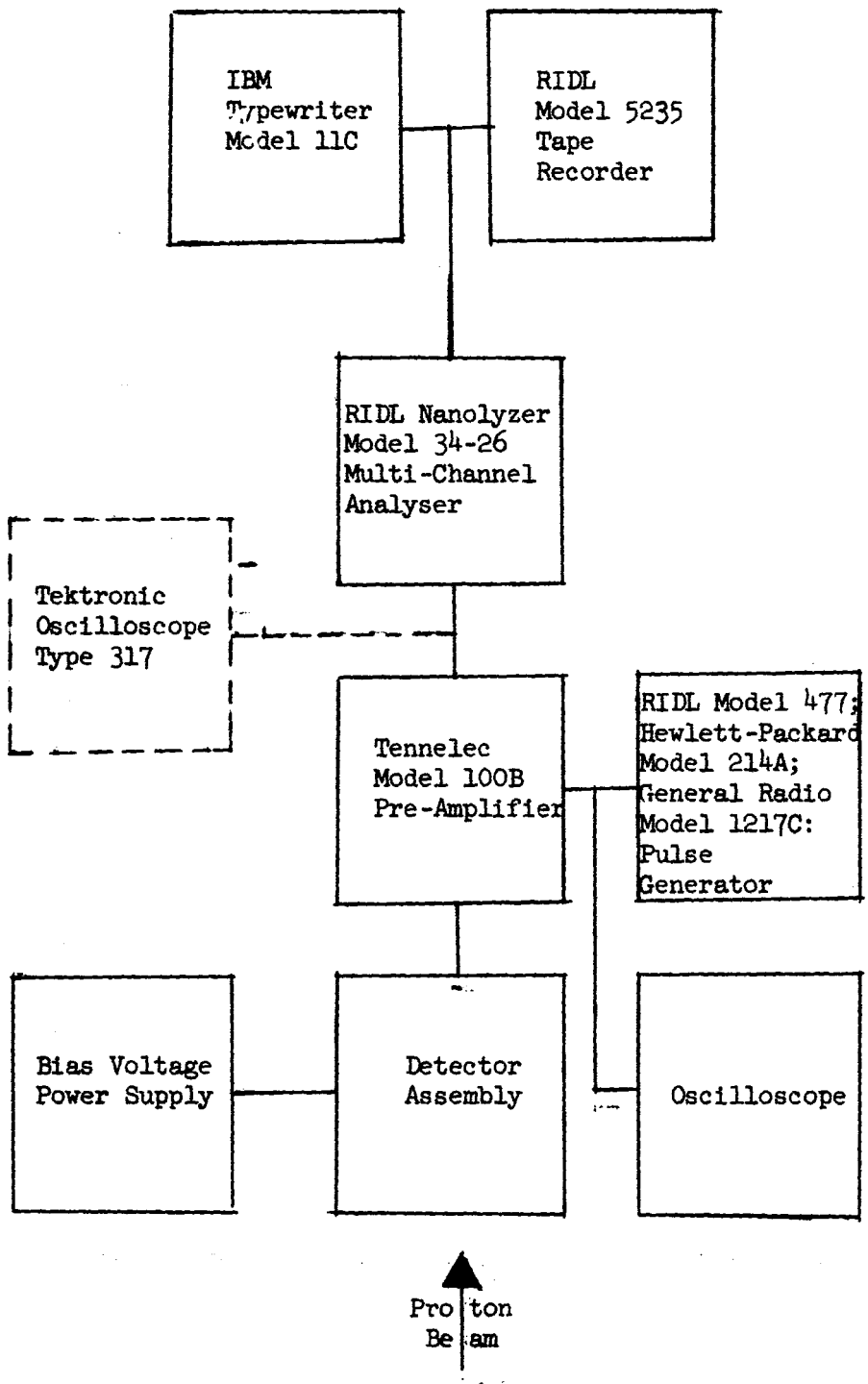

Figure 2. Block Diagram Of Equipment Used For ϵ Measurements

Precision pulse generators were used to measure the charge stored in the peak channel. The values listed in Table 1 are the average values of a number of measurements involving twin detectors and three or more pulse generators. More than one pulse generator was used for the value of charge at each peak. Three pulse generators belonging to SMU and at each facility, another pulse generator (belonging to that labratory) was used to measure the charge. The pulse generators were closely calibrated. Two or more measurements were made with the same detector at each energy. Also two or more measurements were made with a "twin" detector. The twin detectors were made at the same time and were as nearly identical as possible. The fabrication of the larger detectors is described in Chapters 2 and 3 of this report.

The proton energy associated with each full energy beam histogram was determined as accurately as possible at each facility using both the in-house full energy calibration value, calibrated aluminum foils, and range measurements in aluminum. At low energies, corrections were made for the "dead" layer on the end of the detector produced by the protective encapsulation material. At the University of Uppsala, the proton energies less than 187 MeV were measured using a magnetic spectrometer. The determination of the "correct" energy to use for a proton beam exiting from an absorber is reported in Chapter 4 of Volume 68-3[16].

Conclusions

1. For proton energies below 100 MeV, the average energy required to produce an electron - hole pair in silicon is 3.524 ±.005 eV in excellent agreement with Shockley's value[2].

2. This value is independent of both detector size and configuration.

3. At higher energies, the value decreases with increasing proton energy, averaging 3.508 eV at 160 MeV and 3.425 eV at 186 MeV.

4. When the proton undergoes partial absorption, the value for ϵ is a function both of E_o and ΔE with all measured values substantially higher than 3.524 eV, as reported in Chapter 5[17]. A loss of 20 MeV will produce about 5.67 million electron - hole pairs if from 20 to 0 MeV, about 5.27 million if from 100 to 80 MeV and about 5.58 if from 185 to 165 MeV. This 10% variation is significant both in dosimetry measurements and in identification of a particle of unknown energy.

ACKNOWLEDGMENTS

We are grateful to Professor The Svedberg, Dr. Borje Larsson and Dr. Bo Jung of the Gustaf Werner Institute, University of Uppsala, Uppsala, Sweden; to Dr. R. E. Bell of the Foster Radiation Laboratory, McGill University, Montreal, Canada; to Dr. A. M. Koehler of the Cyclotron Laboratory, Harvard University, Cambridge, Massachusetts; to Dr. Alexander Zucker and Dr. J. A. Auxier of the Oak Ridge National Laboratories, Oak Ridge, Tennessee; to Dr. Hans Bichsel of the Linear Accelerator Group, University of Southern California, Los Angeles, California; and to Dr. B. B. Kinsey, Dr. R. N. Little, and Mr. J. W. Jagger of the Accelerator Laboratory, The University of Texas, Austin, Texas for their support and interest in this experiment.

BIBLIOGRAPHY

1. W. Shockley, Solid-State Electronics, 2, 35 (1961).
2. W. Shockley, Bell System Tech. J., 30, 990 (1951).
3. K. G. McKay and K. B. McAffee, Phys. Rev. 91. 1079 (1953).
4. V. S. Vavilov, J. Phys. Chem. Solids 8, 223 (1958).
5. W. D. Davis, J. Appl. Physics 29, 231 (1958).
6. J. M. Mckenzie and D. A . Bromley, Bull Am. Phy. Soc. 4, 422 (1959).
7. W. L. Buys, Nucl. Inst. and Meth. 42, 329 (1966).
8. V. A. J. VanLint, H. Roth and E. G. Wikner, Bull. of Am Phys. Soc. 4, 457 (1959).
9. M. L. Halbert and J. L. Blankenship, Nucl. Inst. and Meth. 8, 106 (1960).
10. L. Koch, J. Messier and J. Valin, IRE Transactions on Nuclear Science, NS-8 (1961).
11. E. Baldinger, W. Czaja and J. Gutmann, Helv. Phys. Acta. 35, 559 (1962).
12. C. Bussolati and A. Fiorentini, Phys. Rev. 136, 6A, A1756 (1964).
13. F. E. Emergy and T. A. Rabson, Phys. Rev. 140, 6A, A2089 (1965).
14. J. J. Smithrick and I. T. Myers, NASA TN D-3694 (1966).
15. D. R. Dixon, et al, SMU Report 68-3, Chapter 5, 1968.
16. G. W. Crawford, et al, SMU Report 68-3 Chapter 4, 1968.
17. R. J. Tarrillion, et al, SMU Report 68-1, Chapter 5, 1968.

CHAPTER 7

INVESTIGATION OF THE EFFECTS OF HIGH MAGNETIC FIELDS ON SILICON RADIATION DETECTORS

by Stephen M. Curry and George W. Crawford

Abstract

A basic study of the effect of high magnetic fields on the charge collection characteristics of lithium-drifted silicon detectors has been made. The parameters studied included the strength of the magnetic field and its direction relative to the electric field of the biasing voltage. Specially constructed detectors were mounted on hinged bars, permitting measurements with the magnetic field either parallel or perpendicular to the biasing voltage. A collimated alpha source was mounted inside a vacuum chamber so that the alpha particles always traveled parallel to the magnetic field. The magnetic field strength was varied from zero to 66,000 gauss for each orientation of the detector. No changes in the collection characteristics were detected when collecting electron - hole pairs with the electric field parallel to the magnetic field. When collecting at right angles to the magnetic field, the total charge collected and stored in the multichannel analyser decreased with the increasing strength of magnetic field. This gave an "apparent" loss of alpha energy of 0.074 MeV per 10,000 gauss. Therefore $\Delta E = k H$, where $k = 7.4$ eV per gauss.

Introduction

The current study is one step in an effort to develop a nuclear detection and identification system which will use solid state detectors in a strong magnetic field to determine the charge, mass, and energy of each incident particle. The purpose of this research was to study the effect of a high intensity, steady-state magnetic field on the operating characteristics of lithium-drifted silicon detectors as a function of the size of the detector and of the relative orientation of the external magnetic field to the electric field produced by the detector bias voltage. The two orientations studied were with the magnetic and the electric fields (1) parallel, and (2) perpendicular.

Modification of Detectors

Specially constructed lithium-drifted silicon detectors were mounted on a flat copper bar. The bar was connected by a hinged mount to a BNC connector. Three sizes of detectors were so mounted: 5 X 5 X 3, 10 X 10 X 3 and 15 X 20 X 6 mm. One side and part of the top of each detector was freshly cleaned and etched before each series of runs to enable alpha particles to enter the sensitive volume of the detector without loss of energy. The charge pulse created by a given energy alpha particle in a given detector was the same whether the alpha entered from the top or the side.

A collimated alpha source was mounted inside a vacuum chamber so that the alpha particles would always travel parallel to the magnetic field with the chamber in the center of the SCAS magnet. Therefore, under operating conditions, the alpha particles traveled parallel to the magnetic field without loss of energy before entering the silicon detector. As the alpha particles penetrated the silicon detector, the electron - hole pairs created were collected at the electrodes of the detector and their movement was influenced by both fields.

In order for the alpha particles from the 241 Americum source to enter the detector without loss of energy, it was necessary to etch away any dead layer on the surface of the detector with a mixture of nitric and hydroflouric acids. A new dead layer was prevented from forming on the freshly etched surface by keeping the detector under bias in a vacuum.

The first step in the process was to use acetone to remove the thin coating of plastic which sealed the front surface of the silicon. A single drop of etching agent (nitric and hydroflouric acids in the ratio of one part HF to three parts of HNO_3) at room temperature was applied to the center of the clean face of the detector with a glass stirring rod. The drop was left for two minutes and then washed off. A second drop was applied, left for two minutes and washed off, producing a shallow cavity in the face of the detector, approximately 5 mm in diameter. The detector was mounted in the vacuum chamber. The alpha source was located 6 cm from the detector oriented so that the alpha particles traveled perpendicular to the face (side) of the detector. A mask was placed over the detector so that the

collimated beam of alpha particles entered the detector only at the center of the etched spot. To switch from the parallel field to the perpendicular field orientation, the detector on its hinged mount was rotated 90°.

Experimental Procedure

The vacuum chamber containing the detector and alpha source was placed in the solenoid of the high magnetic field facility at the Southwest Center for Advanced Studies (SCAS). It was positioned so that the detector was located at the center of the solenoid. The SCAS magnet is a no-ferrous, water cooled solenoid capable of sustaining a steady, uniform magnetic field as high as 80 kilogauss.

The Tennelec Model TC 150 pre-amplifier was located vertically above and centered on the axis of the magnetic. It was attached to the detector by means of a short coaxial cable. A Tennelec Model TC 200 linear amplifier amplified each charge pulse from the detector and shaped it for storage in the RIDL Nanolyzer Model 36-24 multichannel analyzer. Both typed and magnetic tape recorders were made of each spectra. Precision pulse generators were used to maintain calibration.

The vacuum chamber was shielded from electrical noise. The vacuum level maintained was low enough so that the alpha particles reached the surface of the detector without loss of energy. Cold traps were used to eliminate contamination.

Each unit used was carefully located and frequently checked to insure that increasing the magnetic field did not alter its performance. Every precaution was taken to insure that if a change occurred, it could be proven to be an effect within the silicon detector and not associated with the equipment. Tests were conducted to insure that the magnetic field in the word area was not affecting the amplifiers, analyzer, pulse generators, or any other parts of the electronic system. Data was taken using the 241 Am alpha source, with detector bias voltages ranging from 50 to 300 volts and magnetic fields from zero to 66 kilogauss, and with the biasing electric field both parallel and perpendicular to the applied magnetic field.

Observations and Results

The significant observations and results of this study are summarized below:

1. No change was measured in the peak channel as a function of magnetic field strength, when the detector was mounted with the direction of the biasing electric field parallel to that of the magnetic field.

2. A systematic decrease in the peak channel as a function of increasing magnetic field strength was measured when the detector was mounted with the biasing electric field perpendicular to the magnetic field. This shift in peak energy was found to follow the linear relation $\Delta E = KH$, where K has the value 7.4 eV/gauss for alpha particles primarily of energy 5.47 Mev from the 241 Am source. (For 241 Am, alpha energies and percentages are 5.476, 84.3%; 5.433, 13.6%; 5.739, 1.4%; 5.535, 0.42%; 5.503, 0.24%; 5.314, 0.015%.)

3. A progressive decrease in counting rate with increasing magnetic field was also observed for both orientations of the fileds. A similar quenching was reported by Yockey and Baily (1).

4. Detector response as a function of bias voltage with a high magnetic field did not vary significantly from the response in the absence of the magnetic field.

5. The effect measured was not a function of the detector sensitive volume.

Conclusions

The effect of the magnetic field on the position of the peak in the energy spectrum in the case where the electric and magnetic fields are perpendicular is as expected on the basis of a simplified model of charge collection process in the depletion layer of the detector. The electrons and holes move in a periodic potential with superimposed electric and magnetic fields. The action of the external fields alone is such as to cause a rotational motion of the charge carriers about a guiding center which moves in a direction mutually perpendicular to both the electric and magnetic fields. The collection of charge is thereby inhibited, since the mean time for collection then becomes longer than the lifetime of some of the carriers as the magnetic field increases. The addition of the periodic potential to the model complicates the picture, but should not effect the essential nature of the process. The reason for the decreased counting rate, which was observed in both orientations, is not yet apparent.

ACKNOWLEDGMENT

This research was supported by ARPA Grant No. DAHC15-67-G2 and DSS Washington.

REFERENCE

1. H.P. Yockey and N.A. Baily, Applied Physics Letters, 6, 163, (1965).